Engineered Interfaces for Liquid Crystal Technology

A Thesis

Submitted to the Faculty

of

Drexel University

by

Hemang J. Shah

in partial fulfillment of the

requirements for the degree

of

Doctor of Philosophy

August 2007

Acknowledgments

During my five years at Drexel, I have worked on many projects mainly out of curiosity and the desire to develop applications. My advisor, Dr. Adam K. Fontecchio, has always encouraged and guided me to turn the ideas into reality. He has been an excellent mentor and a good friend. Thanks, Adam!

All of my committee members have given me invaluable feedback and have helped refine my work. They have been always available for discussions and have given excellent direction to my work. I could not have found a better group of professors to guide me. Thank you Dr. N. John DiNardo, Dr. Yury Gogotsi, Dr. Gary Friedman, and Dr. Timothy Kuzweg.

I have been fortunate to have excellent colleagues who have supported my research, food policies and perennial coffee brewing. The group discussions and their critiques have been very helpful, for which I thank Dr. Michael Ermold, Ms. Kashma Rai, Ms. Anna Fox, Mr. David Delaine, Mr. Jared Coyle, Mr. William Norman, and Mr. Michael Warde. I am also thankful to Dr. Ondrej Hovorka, Dr. Maria Pia Rossi, Dr. Davide Mattia, and Dr. Ranjan Dash for many, many discussions, ideas, and knowledge sharing. I also thank the various lab-mates I have had in different offices during my stay. The friendly banter made working here enjoyable.

I thank my parents Jayant Shah and Bina Shah, my sister Payal and wife Ruchita for their constant support and encouragement.

Table of Contents

List of Tables

List of Figures

Abstract

Engineered Interfaces for Liquid Crystal Technology
Hemang J. Shah
Adam K. Fontecchio, Ph.D.

Liquid Crystals (LCs) are an exciting state of matter that exhibit unique electro-optic properties due to their chemical structure. They are widely used for manufacturing displays (LCDs), developing optical switches and for mimicking of biological interactions. An important factor that influences the image uniformity and switching characteristics in these applications is the surface alignment of the LC molecules. This thesis explains the control of LC molecules through surface morphology, surface polarization and doping the LC with carbon nanotubes (CNTs).

The influence of surface morphology was studied by patterning a polymer with grid features having dimensions of 500nm×500nm×100nm. LC alignment was observed through polarized light microscopy. Through image analysis of the microscopy images, we improved the resolution of alignment variations by three times. Our results are in agreement with predictions obtained through finite difference modeling of LC alignment on patterned substrates.

Our second approach involves the use of ferroelectric polymers to control LC alignment by dipolar interaction. Through control of the polymer processing, morphology, and composition, we have demonstrated a voltage- dependent visible wavelength progression, a phenomenon that can increase current display resolutions by 300%. These devices are applicable for LC display (LCD) technology as well as for use in optical communication as active wavelength filters. We have also demonstrated a proof-of-concept optical data storage device by writing charges on the ferroelectric polymers with the LC providing the optical readout. Finally, plasma processing was used to

modify the surface chemical functionality of the polymer to improve LC switching and alignment for display applications.

The structure of CNTs allows its use as a pipe for LC confinement and the electrical properties of CNTs influence LC switching. In this thesis, we have imaged LC confinement within open-ended CNTs using a scanning electron microscope. The effect of CNT conductivity on LCs was observed through electro-optic switching. Due to joule heating imparted by the CNTs, phase transition from the nematic phase to the isotropic phase was observed after application of electric field. This observation encourages the development of active materials that change phase in response to electric field.

Chapter 1. Scope of the Thesis

Since their discovery in 1891 [3], liquid crystals (LCs) have been widely used for a range of applications requiring switchable optical performance. Most of the applications use electric fields to achieve the optical switching of the LC molecules. Some common applications, which use liquid crystals are displays (LCDs), optical switches, photonic crystals, and thermometers. The performance of devices using liquid crystals (LCs) is heavily dependent on how the material is aligned. All of the typical parameters for device operation including switching voltage, picture clarity, response time, and light transmission or reflection efficiency are regulated by the arrangement of LC molecules on the surface. The desired arrangement refers to uniform LC alignment, which is achieved through numerous techniques, which are discussed in Chapter 3.

For this thesis, we shall focus on nematic LCs, a state in which most of the LC molecules are oriented along a single direction. The molecules may be permitted to deviate slightly from this direction, and a vector known as the director collectively describes them. When deposited on a surface, nematic LCs can prefer to orient along many directions forming a domain-like distribution. Locally, the LC molecules within a domain may be uniformly oriented giving an impression of uniformity in the alignment. However, when the different domains are considered, the average collective LC alignment across the device area is unclear. Such variations lead to structures known as defects, which not only hamper uniform image generation in displays but also are impossible to remove using typical electric fields.

The most common technique for imparting uniform LC alignment is rubbing of the surface usually a polymer (polyimide). Rubbing is performed through the rotation of a cotton or rayon cloth in contact with the alignment layer coated on the

substrate. This process leads to the development of grooves on the substrate, and the LC molecules align parallel to the rubbing direction. After the rubbing process, whether it is the change in surface morphology or the change in chemical structure that influences the LC alignment is a question that still remains unanswered today. To probe the influence of the surface morphology, this thesis reports on the alignment of LCs on patterned substrates. Chapter 6 describes the LC alignment on patterned PMMA substrates, which were formed using an unconventional instrument, the MTS NanoIndenter. A time variation study of LC alignment was studied on grid geometries using the polarized optical microscope (POM). To improve the resolution of finding alignment variations, an image analysis technique was applied to the POM images. Also, a basic 2D computational model was developed for study of LC interactions with patterned geometries.

Controlled alignment can also be achieved through modification of the chemical groups on the substrate surface. The chemical functionality of polyimide is varied depending on the type of alignment desired for the LCs. Different alignment configurations are required depending on LC applications especially for displays where a change from planar to a tilted alignment of LCs greatly improves the viewing angle. Different LCD architectures are required for meeting the design goals which include an improvement of viewing angle, contrast ratio, switching speed and voltage. An alternative approach of influencing the LC alignment through interactions with the surface polarization is described in Chapter 7. This is implemented by using ferroelectric polymers as the alignment layer. The charge in the polymer can be controlled using external fields in a process known as poling. Chapter 7 covers the performance of displays based on LCs aligned on rubbed polymers, and the development of optical data storage devices through locking the LC alignment on poled ferroelectric polymers. The response of devices to electric fields was studied using POM and optical spectrometry, and spectroscopy studies were performed on the polymer films for

identification of chemical functionality changes.

Biological interactions are another application where LCs are quite useful. LCs can mimic various biological cells including lipids. Investigation of their alignment within nanoscale cavities will serve two purposes; alignment configurations of these materials and the study of storage and transport of complex fluids through nanoscale carriers. Chapter 8 describes the imaging of LCs within carbon nanotubes (CNTs) using the environmental mode of the scanning electron microscope. The wetting of LCs is investigated at the macroscopic and at the microscopic scale. Chapter 8 also describes the wetting phenomenon through interfacial energy, a phase transition regulated through electric fields in LC - CNT composites, and the effects of CNTs on LC alignment for electro-optic applications.

This study sheds light on some topics, which are in their nascent stages of investigation. I hope you enjoy reading it as much as I have enjoyed working on it.

Chapter 2. Introduction to Liquid Crystals

Liquid Crystals (LCs) are a phase of matter, which exist in certain materials between the solid phase and the liquid phase. Since their discovery in 1891 by Reinitzer [3], they have been used for a variety of applications ranging from displays to imaging of biological cells [4–6]. Until the 1960s, they were just a topic of theoretical interest with no practical applications [7]. In spite of research accomplishments which include studying alignment of LCs on substrates [8], changing their alignment through magnetic fields [9], and knowledge about the optic axis in these materials [10], LCs did not have many practical applications. The Second World War contributed to an increased usage of cathode ray tubes (CRTs) for display of text and graphics. At the time, CRTs were perceived as the only reliable, long-term display solution but thankfully, not everyone was satisfied with its technology. This led to an extensive effort towards alternative materials and technology for display applications. It was during the Second World War that Indium-tin oxide (ITO), a transparent conductor was discovered for use as a heated windscreen material. ITO-glass proved to be a boon for LC display technology because until then, the electrodes used for LCDs were opaque and the field applied was perpendicular to the direction of light propagation [7]. Using ITO would allow the observation of LC molecules in response to applied field direction in the plane of light propagation. The biggest accomplishment for applied research on LCs was the demonstration of the twisted nematic LCD by Schadt and Helfrich [4]. Starting with displays for digital watches, LCDs have grown to cover many more applications, the most notable of which is the flat-screen television with display sizes greater than 100 inches (diagonal) being demonstrated by LC Philips and Sharp, respectively. LC technology has inspired many research directions, both physical and chemical, resulting in a $70 Billion industry for television products. In

this chapter, I will provide an introduction to the different categories in the wonderful material called liquid crystal.

Matter is known to exist in four principal states; solid, liquid, gaseous, and plasma. Each of these states has specific criteria for materials including symmetry, distribution of atoms, and degrees of freedom. For example, solids are known to have a higher density and degree of ordering when compared to liquids and gases. Conversely, liquids can flow due to the lack of definite ordering between the molecules. However, some materials exist that possess properties that overlap the discrete classification of the states of matter. Liquid Crystals (LC) are one such family of materials. As the name suggests, LC refers to crystals that are liquid in nature. One of the reference books on this material is aptly titled Liquid Crystals: Crystals That Flow [7]. LCs are found between the solid (crystalline) state and the liquid (isotropic) state. The liquid crystalline state is dependent on chemical composition, and LC materials are divided into two main categories: thermotropic and lyotropic. In thermotropic LCs, temperature variations are used to reach the liquid crystalline phase. These materials are generally pure LCs or a mixture of different LCs, which do not require the addition of solvents. The LC phase is totally dependent on the chemical composition of the individual components of the mixture. Most of the commercial electro-optic devices including displays (LCDs) for television and digital watches use thermotropic LCs. On the other hand, lyotropic LCs are a solute - solvent combination in which the LC phase is achieved by varying the solvent concentration. One of the common examples of a lyotropic LC is the residue found at the bottom of a soap tray. Lyotropics form micelle configurations, and are also commonly found in detergents. However, electro-optic applications for this family of LCs are not many to be found. For this thesis, we shall focus our attention to thermotropic LCs, and later we will narrow it down to one specific type of thermotropics.

2.1 Thermotropic Liquid Crystals

The LC state is a semi-crystalline state in certain materials, which is both liquid as well as crystalline [11]. Crystalline materials or solids are materials characterized by strong positional as well as orientational order. Positional or translational order is the degree of repetitiveness of molecular structure. Orientational order signifies the degree of orientation of molecules with respect to each other. In liquids, the molecular packing corresponds to weak ordering, which is why the molecules are free to move and traverse across in layers. The positional and orientational orders have low values for liquids. In gases, there is complete disorder in the molecules, which corresponds to negligible values for positional and orientational order. The liquid crystal phase is a mesophase, which occurs in the transition from solid to liquid (isotropic). As a result, positional order and orientational order have values between that of solid and liquids indicating some positional as well as orientational order. This is the reason why liquid crystals have a molecular structure, which can be classified based on the type of positional and orientational order.

For the liquid crystalline state or the mesomorphism, there are two conditions to be satisfied:

1. Anisotropy of the molecules. This means that the molecules should be rod or disc shaped.

2. There should be some degree of fluidity between the molecules.

Figure 2.1 illustrates the difference between the solid, liquid and the liquid-crystalline state.

The liquid crystal has multiple phases i.e. it is possible to transit from one liquid crystalline state to the other. We shall look at the various liquid crystalline phases later on. Thermotropic LCs exhibit the liquid crystalline phase by the variation of

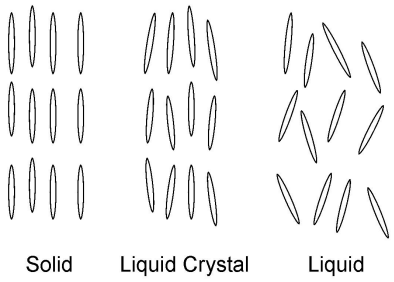

Figure 2.1: Phases of matter

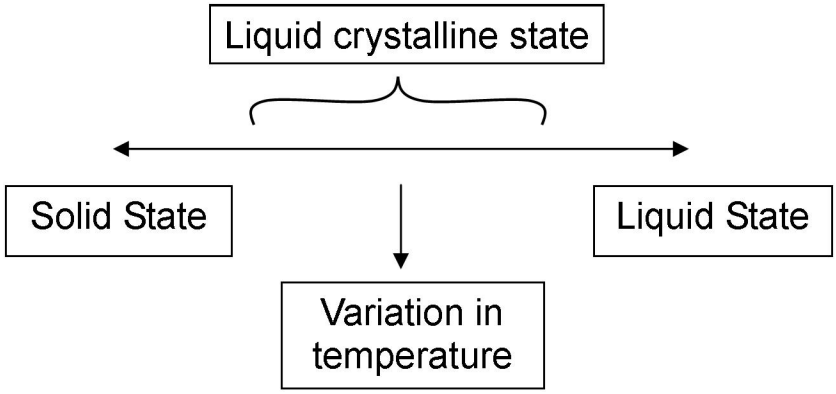

Figure 2.2: Phase transitions in liquid crystals

temperature. The molecules comprising thermotropic liquid crystals can be either calamitic (rod-shaped) or discotic (disc-shaped) [1]. As the temperature is varied from solid to liquid and vice-versa, the liquid crystalline state is reached. This is illustrated in Figure 2.2.

There are three main types of thermotropic liquid crystals:

1. Smectic Liquid Crystals

2. Nematic Liquid Crystals

3. Cholesteric Liquid Crystals

2.1.1 Smectic Liquid Crystals

Smectic liquid crystalline phase is the closest to the solid (crystalline) state. It consists of stratified layers with two-dimensional order between the layers. The representation of the smectic phase is shown in Figure 2.3. The molecules within each layer have a definite orientational as well as positional ordering between them. However, the inter-layer forces in smectic liquid crystals are weak in nature. This is the reason for the liquid crystal to be fluid in the smectic phase.

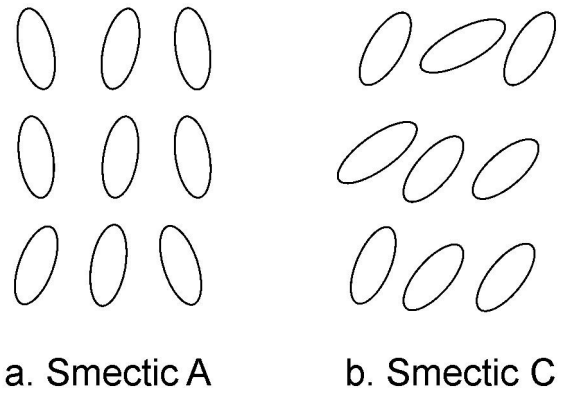

Figure 2.3: Smectic phase in liquid crystals

Smectic liquid crystals are a family of liquid crystals. There are various phases in this family: S_A, S_B, S_C, S_G, S_H, S_J, and S_K where S denotes the smectic phase and the suffix denotes the type. Some of these phases have three dimensional positional ordering but they have weak orientational ordering. Some phases, like the hexatic phases have three dimensional orientational ordering but weak positional ordering.

2.1.2 Nematic Liquid Crystals

Nematic liquid crystals are liquid crystals that are accompanied by orientational ordering but with a lack of long-range positional ordering. This implies that the molecules are oriented in a preferred direction. This arrangement of molecules is represented by a director $\hat{n}$ shown in Figure 2.4.

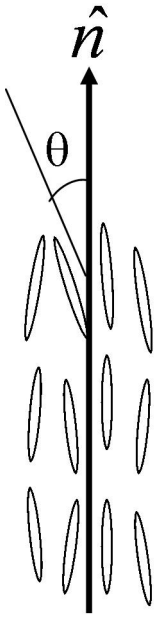

Figure 2.4: Nematic order in liquid crystals

The molecules orient in the direction given by the director varying by angle θ and their orientational order is defined as: [12]

$$S = \left\langle \frac{3\cos^2\theta - 1}{2} \right\rangle \tag{2.1}$$

$S = 0$ defines a state of no orientational order in the molecules i.e. an isotropic fluid, and $S = 1$ defines a state of complete orientational order i.e. a solid. For nematic liquid crystals, $S \sim 0.6 - 0.7$ and it varies with the temperature. This variation is shown in Figure 2.5.

The order parameter varies as per the temperature of the sample. T_c is the clearing point which signifies the transition from the liquid crystalline state to the liquid state. The transition shown is a first order transition implying a discontinuous transition. Certain nematics exhibit second order transition in which there is a continuous transition from the liquid crystalline to the liquid state.

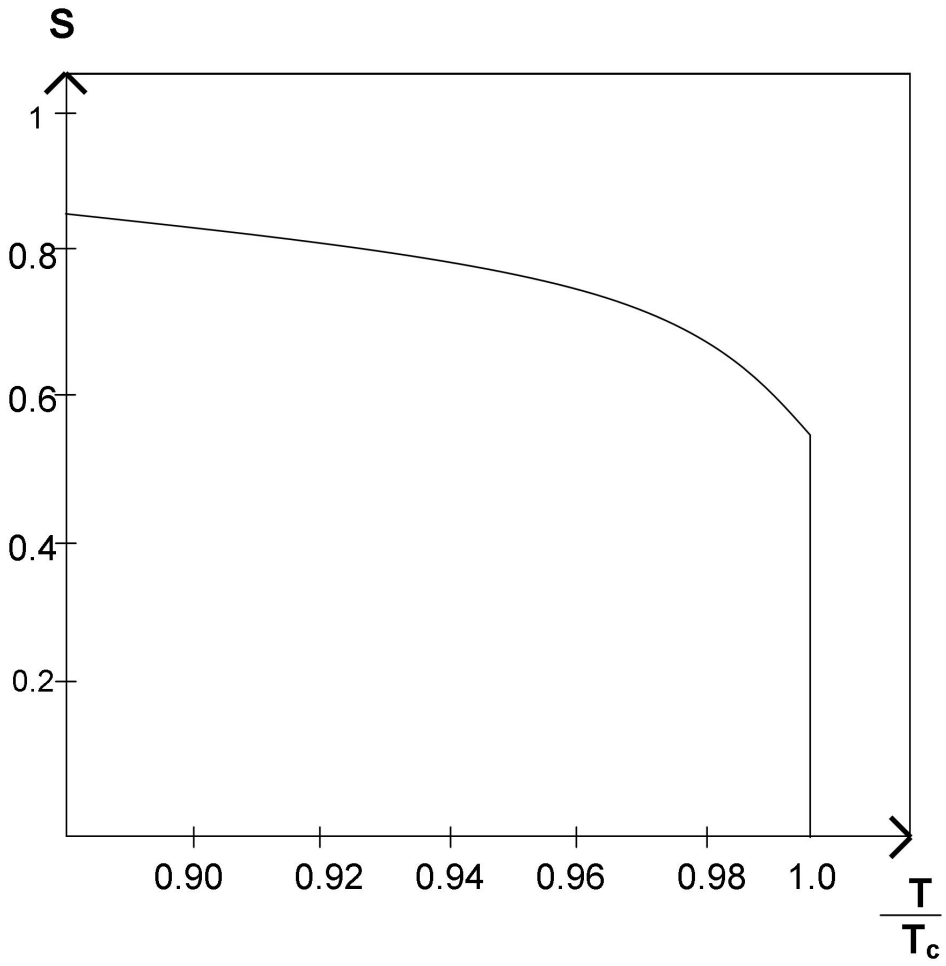

Figure 2.5: Relation between order parameter S and temperature

2.1.3 Cholesteric or Chiral Nematic Liquid Crystals

These liquid crystals are nematic liquid crystals with the difference being the presence of optically active molecules in the material [1]. Due to optically active molecules, the director receives a twist about the axis normal to the preferred molecular directions. The nematic consists of optically inactive molecules or racemic mixtures which give a helix of infinite pitch. In cholesterics, the pitch is of a finite value. Figure 2.6 illustrates the typical cholesteric structure. This spiral arrangement of the molecules is responsible for unique optical properties. The helical pitch of the cholesteric liquid crystals can be viewed as a grating. As a result, there is a selective reflection of circularly polarized light. Also cholesteric liquid crystals have rotatory power about a thousand times greater than that of an optically active substance.

The presence of optically active molecules is enough to make a normal nematic liquid crystal a cholesteric one. This is implemented by adding a small amount of chiral dyes to a normal nematic liquid crystal.

2.1.4 Discotic Liquid Crystals

These liquid crystals are, as the name suggests, disc shaped. These liquid crystals also demonstrate a variety of mesophases. They can be divided into two distinct categories: Columnar phases, and Nematic phases.

The columnar phase consists of discs stacked on top of one another aperiodically to form liquid-like columns with each column constituting a two-dimensional lattice. The nematic disoctic phase is similar to the nematic phase in calamitic (rod-like) LCs with the discotic molecules arranged in the nematic order. Illustrations of both phases are shown in Figure 2.7.

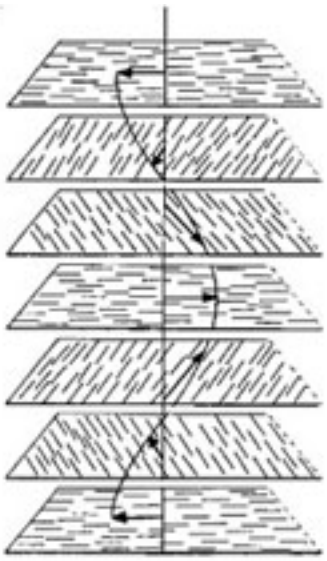

Figure 2.6: Illustration of the helical nature of molecules in chiral nematic liquid crystals [1]

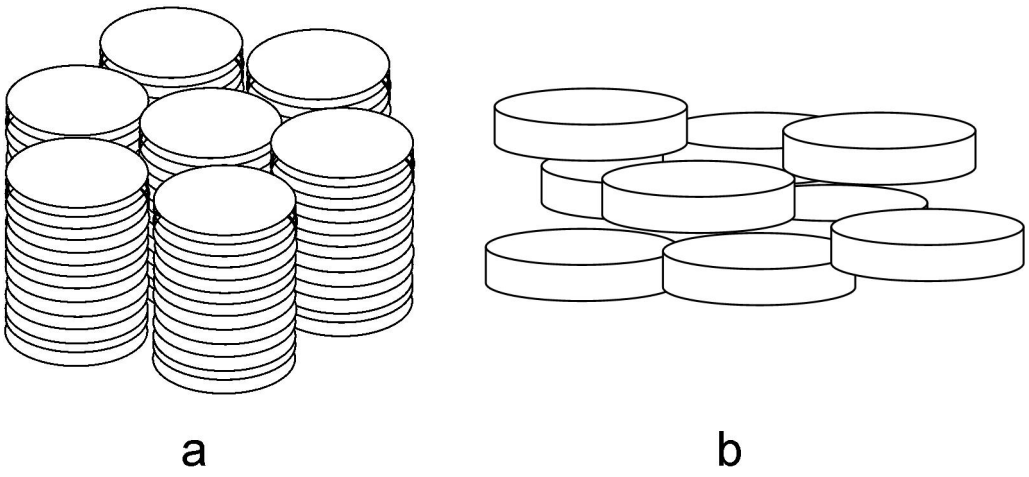

Figure 2.7: Discotic liquid crystals

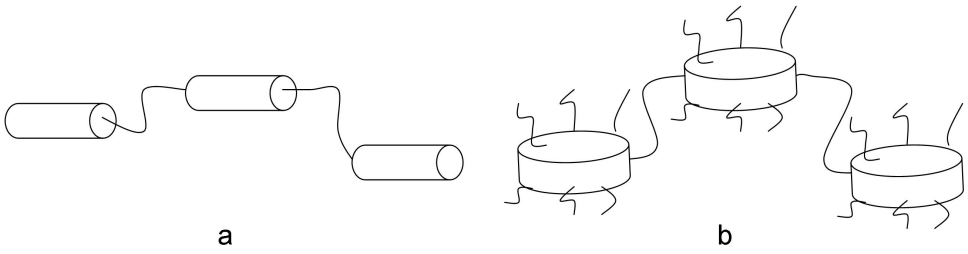

Figure 2.8: Main-chain polymer liquid crystals

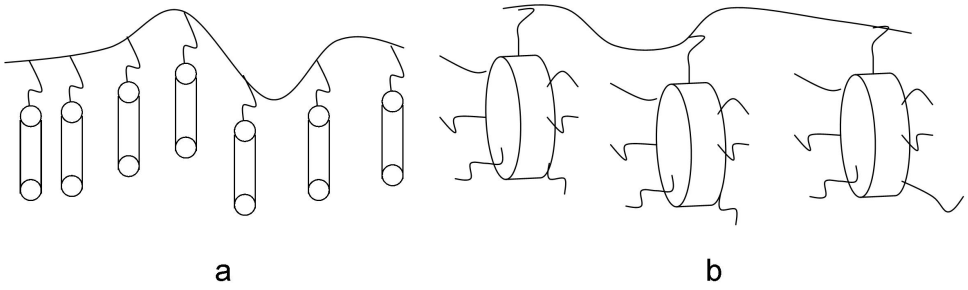

Figure 2.9: Side-chain polymer liquid crystals

2.1.5 Polymer Liquid Crystals

Certain polymers have structures that are responsible for the creation of liquid crystalline phases in them. The monomer units are arranged as rods or discs and are attached to the polymer backbone in the main chain or they are attached as side groups. This is as shown in Figure 2.8 and 2.9

Polymer liquid crystals are useful for liquid crystal stabilization. The presence of these chained liquid crystals in a confine liquid crystal structure enables the main liquid crystal molecules to align with the chains of the polymer liquid crystals. As a result, we have a stabilized liquid crystal enabling better response in the device which uses them.

From the scope of this thesis, only nematic LCs have been used for all the exper-

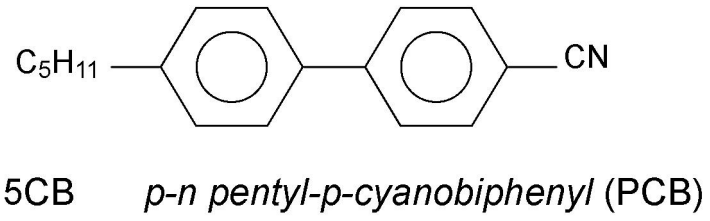

Figure 2.10: 5CB - Nematic liquid crystal

iments. The following subsections will explain the properties of nematics, which are used to develop new devices reported in this thesis.

2.2 Properties of Nematic LCs

2.2.1 Birefringence

The nematic LCs we have used for the material presented in this theses are chemicals based on cyano-compunds. These materials have two benzene rings in the middle with hydrocarbon end chains. Figure 2.10 shows the compound used in this study. Due to the chemical structure, the molecules forming the nematic phase exhibit two values of refractive index; one along the long axis called as the extraordinary refractive index, n_e, and the other value is found along the short axis, and is called as the ordinary refractive index, n_o. Of these, the ordinary ray directly follows the Snells law of refraction, whereas the extraordinary ray travels at a variable speed, which is dependent on the angle between the optic axis and direction of light propagation. The two refractive indices are represented as:

$$n_e = \frac{n_\perp n_{||}}{\sqrt{n_{||}^2 \cos^2\phi + n_\perp^2 \sin^2\phi}} \tag{2.2}$$

$$n_o = n_\perp \tag{2.3}$$

where n_e and n_o are known as the extraordinary and ordinary refractive indices. The resulting phase difference experience by light propagating through such a medium is expressed as:

$$\delta = \frac{2\pi}{\lambda}(n_e - n_o)d \tag{2.4}$$

2.2.2 Alignment of Liquid Crystals

The packing of nematic LCs is such that they are aligned parallel to each other. As a result, they are represented by a directional vector, $\hat{n}$. The orientation of a director can change continuously and in a systematic matter from point to point in the medium (except at singularities) [1]. Using the Oseen-Zocher-Frank equations, we can describe the free energy per unit volume of a deformed LC by:

$$\mathbf{F} = \mathbf{K}_{11}(\nabla \cdot \mathbf{n})^2 + \mathbf{K}_{22}(\mathbf{n} \cdot \nabla \times \mathbf{n})^2 + \mathbf{K}_{33}(\mathbf{n} \times \nabla \times \mathbf{n})^2 \tag{2.5}$$

where K_{11} is the Splay elastic constant, K_{22} is the twist elastic constant, and K_{33} is the bend elastic constant.

Additional factors that influence LC alignment are surface forces. Depending on the surface, there are two types of surface alignment for the liquid crystal:

1. Planar Alignment

2. Homeotropic Alignment

In planar alignment, the liquid crystals orient parallel to the surface planes. This is as shown in Figure 2.11. In homeotropic alignment, the liquid crystals orient in a direction perpendicular to the surface as shown in Figure 2.12.

The surface can be rubbed to get the desired alignment effects. It has been shown that spin-coated polyimide on a substrate, either glass or onto a glass substrate coated

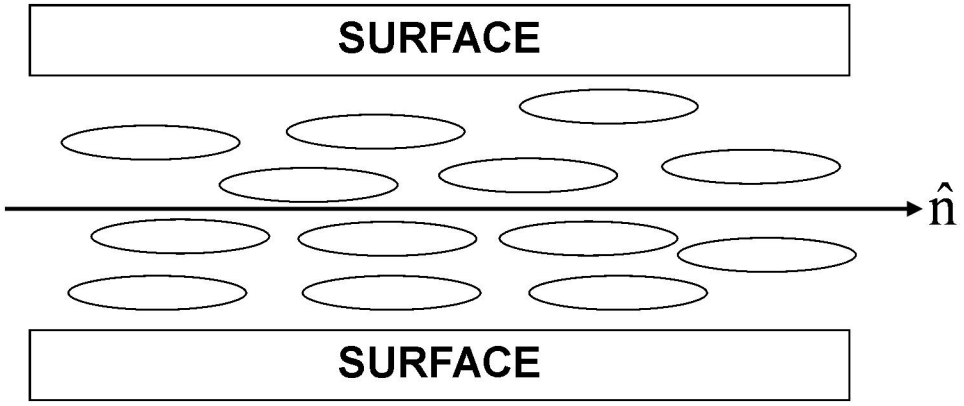

Figure 2.11: Planar alignment in nematic liquid crystals

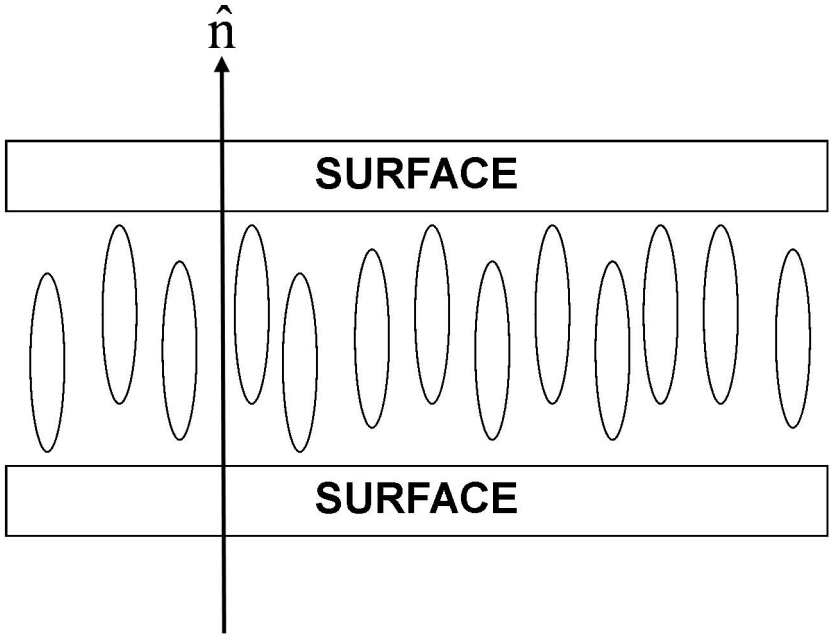

Figure 2.12: Homeotropic alignment in nematic liquid crystals

with Indium Tin Oxide (ITO), forms a template for alignment of the liquid crystal molecules. As a result, the director orients in the direction of the rubbing. The rubbing can be done by a large cotton cloth or by cat fur. Recently, researchers have shown that a substrate rubbed with the stylus of the Atomic Force Microscope (AFM) also serves the same purpose [13–15]. We will consider a more in depth review regarding the topic of surface alignment in the next chapter.

2.2.3 Effects of Electric and Magnetic Fields on Liquid Crystals

Liquid crystals have the unique property of being affected by the application of an electric field. The application of an electric field produces a dipole moment per unit volume i.e. the polarization given by $\vec{P}$. The polarization varies linearly as the electric field but the anisotropy of the liquid crystals forces it to have different values in different directions. $\vec{P}$ is related to $\vec{E}$ by the dielectric tensor $\vec{\chi}$

$$\vec{P} = \epsilon_0 \vec{\chi} \vec{E} \tag{2.6}$$

$$\begin{pmatrix} P_x \\ P_y \\ P_z \end{pmatrix} = \begin{pmatrix} \chi_{e\perp} & 0 & 0 \\ 0 & \chi_{e\perp} & 0 \\ 0 & 0 & \chi_{e||} \end{pmatrix} \begin{pmatrix} E_x \\ E_y \\ E_z \end{pmatrix} \tag{2.7}$$

where $\epsilon_0 = 8.854 \times 10^{-12} C/m^2$ is the permittivity of free space.

Equation 2.7 represents the director oriented along the z-axis. As it can be seen from the matrix equation shown, we have two different values for the electric susceptibility $\chi_{e||}$ and $\chi_{e\perp}$. These values are due to the anisotropy of the liquid crystal molecules.

Because of the polarization produced; there is a displacement of the molecules

given by:

$$\vec{D} = \epsilon_0 \vec{E} + \vec{P} \tag{2.8}$$

As a result, the molecules can be moved under the influence of electric field. Thus, on application of an electric field, the LC can be made to rotate in the direction parallel to the electric field. This is an important property which is exploited in applications like liquid crystal displays. Also, to obtain analyzable results of X-ray diffraction on liquid crystals, it is important to have the liquid crystal molecules aligned in a specific direction. Application of an electric field serves the purpose in this case.

Likewise, the magnetic field has an effect on the orientation of the liquid crystal molecules. In practical applications, magnetic field is rarely used because of the bulky set-up compared to that for generation of electric fields.

That we have described the principal LC properties used in this thesis, we will turn our attention to surface alignment of liquid crystals. The interface between the LC and the substrate provides one of the most important phenomenon affecting devices: surface alignment, which will be explained in the next chapter.

.

Chapter 3. Surface Interactions of Liquid Crystals

Surface alignment of liquid crystals (LCs) is one of the most important steps in the manufacturing of devices, especially LC displays (LCDs). Alignment of LCs on the substrate ensures uniform optical properties throughout the device thickness. The interaction between LC molecules is governed by long-range interactions. Hence, the alignment of these molecules at the surface monolayers can be easily transmitted to the bulk resulting in uniform alignment. Additional forces to impart alignment include dipole interactions with the surface, elastic forces due to surface morphology, and chemical interactions with the surface chemical groups. Of these, arguably, chemical interactions play the dominant role in enforcing surface alignment [16]. If alignment is absent, the device performance is poor due to lack of uniform control over the LC molecules. As an example, let us consider the architecture of a twisted nematic liquid crystal display (TN - LCD). This is an architecture very widely used in the display industry for manufacturing of computer screens, cellular phone screens, televisions, wrist-watches and calculators.

As shown in Figure 3.1, this architecture consists of two electrodes each coated with an alignment layer. The arrangement of the electrodes is such that on deposition, the LC molecules undergo a 90-degree twist through the thickness of the cell. The twist is influenced by the surface of the alignment layers, typically transparent polymers that are either rubbed using a cloth or photo-exposed. A bright state is observed between crossed polarizers with white light being transmitted from the source. Polarized light from the bottom layer enters the cell after which it is rotated by 90 degrees due to the LC molecules. Hence, a resultant output is observed after the top polarizer. On application of an electric field the LC molecules rotate to align parallel to the field direction. In this case, polarized light entering the cell does not experience

any rotation. Hence, the upper polarizer is able to block the light resulting in a dark state. A typical display has several million pixels with the same architecture with each pixel switched on and off with a set frame rate to generate the desired image. The key to the ideal functioning of the display described here is the 90-degree twist through the cell. If the twist has variations within the pixel or between different pixels, it will result in poor image generation. One of the main reasons for imperfect twist or switching is the alignment imparted by the polymer (or any other material). Other reasons include fringe fields from the driving circuitry, dust and impurities, and imperfect selection of materials (LCs as well as alignment layers).

The twisted nematic arrangement is one of the modes of operation for a display using LCs. Other modes include vertical alignment modes, multi-domain displays and in-plane switching modes. These modes rely on vertical anchoring of the LC molecules due to chemical interactions with the alignment layer. The reasons for such alternate architectures are improvements required in certain parameters such as the switching speed, viewing angle, image sticking, and contrast ratio. Typically, each mode requires one of many techniques used to impart LC alignment. In the next section, we will review some of the methods used for treating alignment materials.

Charles Maugin was the first to report LC alignment on clean glass surfaces in 1911 [8]. He also mentioned how the alignment varies when the top and bottom surfaces (between which the LC is placed) are moved. The alignment of LC on these surfaces cannot be guaranteed in one direction limiting its use for mass production. Also, after the removal of electric field, the LC should return to the initial position. If the LC alignment is not guaranteed always in one preferred direction, the initial state will not be retained after field removal. There are reports on preferential alignment being imparted by single crystal surfaces [10]. However, it is not feasible from a mass-production perspective to obtain a large supply of single crystal materials without defects. In that case, the materials need to be modified physically or chemically such

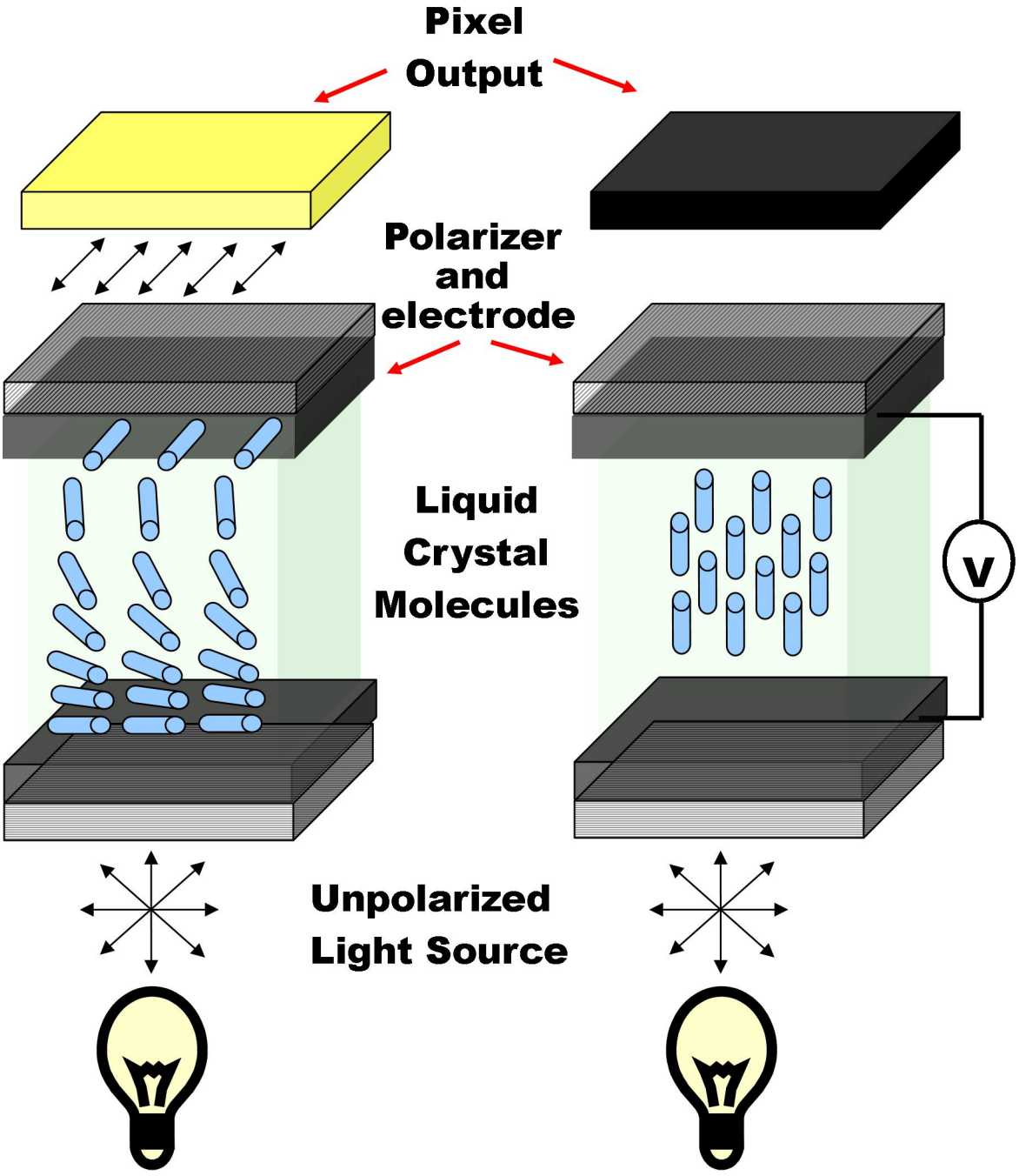

Figure 3.1: Schematic of a Twsited Nematic Liquid Crystal Display (TNLCD)

that on deposition the LC aligns preferentially along a particular direction. Before we talk about the methods used for treating materials, it is necessary to define certain terminologies used to describe alignment.

- **Surface Anchoring:** This is defined as the strength of the interaction between the LCs and the surface. As the name suggests, it is a quantity that describes the anchoring influence of the surface on the LC molecules. It has the units of energy (J/m^2).

- **Pre-tilt**: It is a quantity that describes the angle between the LC molecules and the surface normal.

- **Planar alignment:** When the LC molecules are aligned of the surface with a minimal pre-tilt angle, the alignment is referred as planar.

- **Homeotropic Alignment:** In this case, the LC molecules are aligned perpendicular (along the z axis) to the surface.

3.1 Techniques for Influencing LC Alignment

3.1.1 Rubbing

Rubbing is a process where a substrate surface is made to contact a cloth fiber roller, which is rotating at a high speed. When LC is deposited on the surface, it aligns parallel to the rubbing direction. Chatelain and Maugin first discovered this phenomenon, where they studied LC alignment on rubbed glass slides [17]. Depending on the type of the surface used, rubbing also leads to a definite pre-tilt of the LC [18, 19]. Control and uniformity of the pre-tilt angle contribute towards the improvement of switching response for LC devices.

The rubbing process is interesting from the surface alignment viewpoint. There are two different schools of thought on why and how the process works to align LCs.

Initial studies suggested that due to the contact between the cloth fibers and the surface, nanometer grooves are left behind. Groove morphology has been studied extensively using atomic force microscopy (AFM). On deposition, the LC molecules are aligned by flow (if they are in the nematic state) and by elastic interactions with the surface. For a rubbed surface, the LC interactions are stronger along the rubbing direction. Barmentlo et al. [20] have studied the LC interactions with the surface using Second Harmonic Generation studies of the interface between the polymer and the LC. In their reports, orientational asymmetry (difference between alignments along directions) was found to increase with the rubbing strength. Orientational asymmetry, which exists after rubbing, is the principal reason to align LCs and influence their pre-tilt.

Another factor that influences the alignment of LCs is the orientation of the polymer chains after rubbing. For low-pretilt alignment, main chain polymers are generally used as the alignment layer. Rubbing is responsible for aligning the main chains of the polymers, which in turn influences LC alignment [16, 21]. Also, depending if the polymer is odd-numbered or even-numbered (related to chain length), LC alignment and pre-tilt can be tailored for devices. In these polymers, the rubbing process causes a transformation in the conformation of the polymer chain, say from all-transoid to a trans-transoid conformation. Hence, polymer chain alignment due to rubbing is also a strong reason for influencing LC alignment. Changes in the polymer chain conformation are attributed to friction between the polymer and rubbing cloth. Contact with the high-speed fibers results in local increases of temperatures on the polymer surface, which exceeds the glass transition temperatures. In such a case, thermal annealing occurs at the surface monolayer for the alignment layer changing the chemical functionality/chain conformation for the polymer film.

Despite the two different schools of thought for the process, rubbing still continues to be the adopted method for providing LC alignment in commercial devices. As the

glass handling sizes increase from Generation 8 (7 ft x 8 ft), alternative methods to rubbing are being investigated to minimize the dust particles left behind, and frequent cloth changing and calibration.

3.1.2 Photoalignment

Photoalignment relies on the production of anisotropy in the molecules of the alignment layer after exposure to polarized light. This effect, also called as the Weigert effect, occurs when the transition moment of the dipole is matched with the electric vector direction of the polarized light. In photoalignment, the molecules can absorb the maximum photon energy leading to structural changes, also known as photochemical reactions. Both the residual molecules not affected by the light and by the photochemically produced structural changes influence the LC alignment [16, 22, 23]. Typically, UV wavelengths are used for the process. Photoalignment has mainly two categories, which are conformational changes and chemical changes.

- **Conformational changes:** This phenomenon also called photoisomerization relies on conformational changes produced in the alignment layer due to light absorption. Common changes include switching from cisoid to a transoid conformation in azobenzene dyes. The switching can be regulated by light wavelength and/or polarization changes. Such a change allows switching between planar (in-plane) and homeotropic (out-of-plane) alignment.

- **Photochemical changes:** These are related to changes in the chemical groups of the alignment material after exposure to light. One example of dimerization of the alignment material is when the double bonds of the molecules are broken to form a scissored configuration after light absorption. The LC alignment in this case is perpendicular to the direction of light polarization. Common materials used for photodimerization are Polyvinyl Cinnamates (PVCi), coumarin

dyes, and chalcones [16]. In photodecomposition, the light absorption causes an anisotropy in the length distribution of the materials including polyimide. The LC alignment is governed by the direction of anisotropy. Photoocrosslinking occurs when light absorption leads to production of radicals, which can crosslink to produce new chemical structure(s). These new structures developed in te material regulate the LC alignment. One example of crosslinking materials is benzophene. In addition to these above sub-classifications, hybrid modes also exist where the alignment materials undergo multiple changes including decomposition and crosslinking, which are used to align LCs.

The advantages of photoalignment techniques include easy control of the pre-tilt from 0 to 90 degrees without changing the alignment material, control over the anchoring energy and dust-free technique compared to rubbing. Major disadvantages include the cost for large-scale manufacturing and chemical stability of the materials.

3.1.3 Oblique Evaporation

This is a technique in which SiO is deposited obliquely on the surface using evaporation beams. Due to an effect called as the self-shadowing effect, a columnar structure of the material (SiO) is realized on the substrate. LC alignment is typically parallel to the columns. Through variations in the evaporation angle, the LC pre-tilt can be tailored from 0 to $\sim$50 degrees. Advantages of oblique evaporation are that its a non-contact technique and allows for high-pretilt LC alignment. The disadvantages are that this technique is not scalable for large-scale manufacturing, provides too much heat for arrays of TFT (transistor thin films), and could lead to non-uniform alignment [16].

3.1.4 Micro-Grooved Surfaces for LC Alignment

Microgrooved surfaces can provide alignment by influencing the elastic energy of the LCs. There are numerous techniques to provide the geometry of microgrooves on the surface. These include reactive ion etching of glass [24], holographic recording of patterns on surfaces, rubbing using the stylus of an atomic force microscope (AFM) [15,25], and imprinting [26]. Since the elastic interactions between the surface and the LC are strong, it is possible to use microgrooved surfaces for LC alignment. These are useful for the creation of multi-state displays [27]. The main drawbacks are that the techniques can be time-consuming and hence, not optimal for high-speed manufacturing.

3.1.5 Stretched Polymer Films

This technique refers to aligning LCs with the help of Van der Waals interactions with the stretched polymer chains [28]. Due to the alignment of the polymer chains along the stretching direction, the LC molecules can be aligned. First porous polymer films (polyolefins) are stretched mechanically. This process not only aligns the polymer chains but also reduces the film thickness and introduces birefringence in the film. Following that, the film is filled with the LC materials. To fabricate a device, the polymer LC composite film is sandwiched between two transparent electrodes to allow for switching studies. This method has the advantage that the alignment layer (stretched polymer) is prepared beforehand. It does not need to be spin-coated and annealed, which is the case with most polymer alignment layers, to make it suitable especially for plastic substrates for flexible displays. The disadvantages are that the LC alignment is not very uniform, the switching voltages required are a bit high for displays, and the adhesion of the polymer LC composite films to the electrodes must be ensured.

3.1.6 Transcription

This method refers to LC cell fabrication that exploits the memory effect of nematic LCs for alignment. A LC in its isotropic phase is filled into a cell comprised of a rubbed polymer surface and an unrubbed polymer surface. After the cell cools down to room temperature, the rubbed surface is taken out leaving behind the transcribed (previously unrubbed) surface and some LC. The next step requires formation of an LC cell with the two transcribed surfaces and the unremovable LC on their surface. The alignment from the transcription by the rubbed surface persists in these surface LC molecules due to memory effect in nematics, and this in turn aligns the new LC molecules introduced into the cell [29].

This is a non-rubbing approach which offers a reliable pre-tilt of 2 - 3 degrees, a requirement in order to prevent reverse tilt defects in TN - LCDs. However, the major disadvantages are material wastage of the polymer alignment layers and the LC. The approach also uses rubbing to transcribe surfaces but the lifetime or reusability of the rubbed surfaces is not clear.

3.1.7 Langmuir Blodgett Films

Langmuir Blodgett (LB) is a widely used technique for the formation of monolayers on substrates. There are different ways to form LB films. The material, which is to be transferred to the substrate, is usually stored over a liquid such as water. For example, if the desired material is hydrophobic in nature, it will form a monolayer film over a water body. This liquid is kept in a trough under suitable pressure. Following that, the substrate is either dipped or drawn or pressed over the liquid to facilitate the transfer of the desired material. The speed at which the substrate is introduced in the trough determines the number of monolayers to be formed. Depending on the chemical functionality of the film, the LC alignment can be induced [30]. This tech-

nique is suitable mainly for academic research due to the slow speed of the technique. Also, the operating conditions require frequent cleaning of the trough, and stringent operating conditions.

3.1.8 Flow Alignment

LC in its nematic phase can be aligned through its flow into the cell. This method generally works for any substrate. However, the absence of an alignment layer will lead to weak anchoring. Also, the flow cannot be reliably controlled leading to defects known as flow defects. [31, 32]

3.1.9 Alignment using Ion Beam Irradiation

In this method, the substrate is irradiated with an ion beam to induce an anisotropy or orientational order in the substrates to influence the LC alignment. This technique is suitable for polymers and inorganic substrates alike. Upon ion beam radiation, an orientational order is created in the substrates, due to breakdown of π bonds in imide rings, phenyl rings, and carbonyl groups for organic materials [33] and orienting the carbon groups including unsaturated carbon bonds in inorganic materials [34, 35]. This technique has been generally used to generate pre-tilt between 0 - 10 degrees and 80 - 90 degrees on substrates [34, 36]. Recently, Kim et al. have shown that through controlling carbon cluster orientation in SiC films after IB radiation, the pre-tilt can be varied between 67 to 90 degrees [34]. The factors, which determine the pre-tilt angle include the angle of incidence of the ion beam, irradiation times, and ion-beam energy. Two advantages of using the ion beam technique on inorganic substrates are the absence of image sticking for LCDs and the ability to overwrite previously written alignment directions on substrates. This technique works well for LCD applications. The only drawback is the equipment required to handle large-size

panels for display manufacturing. Another problem is related to the targets required to generate the ions. Over time, the bombarded target would degrade leading to particles being deposited over the glass.

3.1.10 Chemical Treatment of Surfaces

LC Alignment has been influenced for years using common chemicals including lecithin for promoting homeotropic alignment. In this case, the surface, typically glass or ITO-coated glass is treated with the desired chemical first following which the LC is filled. Interactions with the chemical groups on the substrate will promote the necessary (or desired) alignment [5, 12, 37].

We have now seen that there are many techniques to impart surface alignment. This manipulation of the interface between the LC and the substrate is a key process to the development of displays. Although, some of these techniques have been known for decades and the LCD performance meets most of the industry standards, there are still many unexplored areas.

3.2 Conclusion

As we move along to the next chapters of this thesis, we shall learn about LC alignment through patterned morphology and ferroelectric polymers. Lastly, we will study a topic of investigation since the new millennium; liquid crystals and carbon nanotubes and probe for interesting phenomenon by combining these two exciting materials. Table 3.1 summarizes the different methods we have discussed.

Table 3.1: Methods used to impart surface alignment of liquid crystals

Method	Advantages	Disadvantages
Rubbing	• Provides excellent alignment • Economical	• Leads to dust particles • Not suitable for larger substrates
Photoalignment	• Non-contact technique, which eliminates abrasion related particles • Can be easily extended for large substrate size	• Expensive • Stability of the photoaligned polymer
Oblique Evaporation	• Non-contact technique • Allows for high pre-tilt	• Not scalable for large substrates • Relative high temperature processing is not suitable for TFT-arrays
Micro-grooved surfaces	• Excellent technique for multi-mode displays	• Too time-consuming for large substrates
Stretched Polymer Films	• Alignment layer is made beforehand • Elimination of spin-coating, annealing and other processing steps	• Non-uniform LC alignment • High switching voltages and polymer films adhesion
Transcription	• Reliable pretilt of 2 - 3 degrees • Eliminates reverse tilt defects	• Material wastage of polymer and the LC • Lifetime of the rubbed surfaces
Langmuir Blodgett Films	• Excellent technique for nano-scale alignment	• Very slow technique • High degree of maintenance for stable operation
Flow Alignment	• Simple and economical	• Non-uniformity of LC alignment
Alignment using Ion Beam	• Absence of image sticking • Ability to overwrite previously written alignment	• Equipment unavailability for large substrates • Non-uniformity of LC alignment
Chemical Treatment of Surfaces	• Simplicity	• Stability and uniformity of alignment

Chapter 4. Literature Review

In Chapter 3, we discussed the working of a Twisted Nematic Liquid Crystal Display (TNLCD). This is one of the widely used architectures for LCDs used in commercial products such as wrist-watches and cellular phone screens. Proper functioning of the TNLCD mode is dependent on the twist imparted to the LC molecules by the alignment layer, which is typically a polymer material. The chosen LC material also needs to be light and flexible enough to undergo the twist. Other LCD architectures consider modes where the LC is aligned at an angle to the alignment layer for vertical alignment displays used for wide-viewing angle displays. The LC is also changed depending on the application in order to optimize parameters including contrast ratio, switching speed, and switching voltage for the devices. Depending on the application, different LCD architectures are required. In general, there are two approaches to influence the LC alignment within a single architecture:

- Alignment Layer: Either a new material could be investigated or some properties of the alignment layer could be used to influence LCs
- Liquid Crystal: This approach involves either synthesizing new materials or modifying current LCs through addition of particles such as dyes, nanorods, and nanotubes

In this thesis, we focus on modifying or controlling properties of the alignment layer and the addition of CNTs to influence LC alignment. Specifically, we have studied:

- The influence of surface morphology on LCs
- The influence of surface polarization on LC switching

- The addition of carbon nanotubes with different properties to understand its interactions with LCs.

4.1 Review of work on Liquid Crystals and Patterned Substrate

As we have already discussed, liquid crystal (LC) alignment depends strongly on surface anisotropy. Anisotropy can manifest itself in chemical composition or in physical features i.e. morphology. The current view of a majority of LC scientists and engineers represents that the surface morphology is the driving force behind LC alignment. As a result, much effort has been spent on obtaining different types of morphology at length scales ranging from nanometers to a few micrometers on substrates. The goals of such studies are to obtain a fundamental understanding of the influence of morphology on LC alignment, which can be applied for the development of devices including light valves [7, 25]. In recent times, due to the advent of optical communication, a large number of research programs are working towards development of electro-optic devices based on liquid crystals. These devices include photonic crystals [38], devices for optical data storage [39, 40], and lasers [41, 42]. In these devices, the LC is confined in a well-defined geometry recorded in a material, usually a polymer. The dimensions of the confinement areas are on the sub-micron scale, which is much larger than the length scales (a few nanometers) of pure chemical interactions. It is the morphology, which determines the quality of the alignment, the response of the device to electric fields, and the device efficiency. Also, in most of these devices, the cavities are interspersed in three dimensions. Microscopically, to this day, there are no effective techniques to visualize LC alignment without destroying the sample. Atomic force microscopy (AFM) and the scanning electron microscopy (SEM) are used to understand the morphology of the material that provides LC confinement. For example, one of the mentioned electro-optic devices requires dispersion of LC

within polymer cavities for applications including light reflection, diffraction, and beam steering. The configuration of the polymer cavities to meet the design goals is not random but of an ordered fashion to result in a Bragg grating. For such a design, holography at either visible or UV wavelengths [38, 43, 44] is performed to form the ordered spacing between polymer and LC such that a mismatch in the refractive index is produced, i.e. a Bragg grating. Ideally, for light reflection/diffraction purposes these devices should exhibit alternating layers of polymer and LC. Experimentally, it is very difficult to create such results. Typically, the LC layers are not uniform but rather they exist in patches of LC confined in polymer cavities. The geometry of these cavities is not perfectly spherical but they are ellipsoidal with the cavity surface having a dimpled structure [45]. The switching response of these devices is hugely dependent on the LC alignment within the cavities, which have a diameter within the range of 100nm - 1μm. One of the principal reasons for poor performance can be pointed to the influence of the dimpled geometry on the bulk LC. In that case, the resulting alignment depends on the surface forces, which are strong to the extent that an electric field of 5V/μm cannot overcome them.

Visualization of a LC in natural state (undestroyed/as designed) is ruled out because of microscopy limitations. Also, measurement cannot be performed *in situ* when the device is being formed due to the fast nature of the holography experiments and the lack of adequate probes. Developing structures through fabrication processes and then studying the effects of LC alignment can solve this problem. The exact dimpled geometry is extremely tough to realize experimentally mainly due to the random nature of the geometry and the unpredictable location of the polymer globs. In these cases, we have to start with simple structures such as lines and grid structures.

Recently, researchers have reported alignment in LCs by rubbing with the stylus of an AFM tip to form grooves [13, 15, 25, 27, 46]. In these experiments, an AFM was operated in the contact mode, and lines were inscribed on the surface of polyimide.

Rosenblatt et al. have also shown how the nematic to isotropic transition temperature is depressed [13]. Yokoyama et al. have shown bistable and tristable nematic liquid-crystal device using micropatterned surface alignment [27, 47]. These devices are still based on an arrangement of domains shaped in a parallelogram. The parallelogram is formed by rubbing lines parallel to each other at the nanometer scale.

However, LC alignment on patterned substrates has been studied only for surfaces that have patterns periodic in one dimension [13–15, 22, 25, 27, 48–51]. The patterns consist of parallel grooves or scratches. The LC thus faces confinement due to the sidewalls in the grooves. These studies are classified as LC alignment in 1D geometries. The biggest limitation of such geometries is that they cannot give the complete picture regarding the effects of confinement and competing surfaces on LC alignment.

4.1.1 Objectives of Work: LCs and Patterned Polymers

In our studies, we have considered 3D patterns that are written on a polymer surface. Specifically, we have considered grid structures which allow us to study LC alignment in grooves as well as confined wells. The alignment information is obtained through polarized microscopy experiments. To develop the patterns, we have used an indentation instrument, which is a novel approach of using a materials hardness testing tool for submicron lithography. The resolution of the optical microscope places a limitation on the length-scales at which the LC variations can be identified. In order to study the alignment better, we performed image analysis on the microscope images to improve our resolution by three times. Also, a 2D lattice model was developed to visualize LC directors on patterned substrates.

4.2 Review of work on Liquid Crystals and Ferroelectric Polymers

It can be safely said that every commercial LCD application (TVs, cell phones) requires a different AL and LC. One solution to the above problem is to develop a programmable layer to impart LC alignment. The programmable layer should possess a readily reconfigurable parameter. It can be surface charge, chain length in case of polymers, or orientation of the chains. In addition, it muse be compatible with LCD fabrication equipment in terms of developing large area films, optical clarity or reflectivity, and suitable dielectric permittivity. Some of the materials that have used such materials include the development of LCDs using azobenzene dyes [16]. An exposure of the material to UV light changes the orientation of the azo-dye, which controls and re-orients the LC molecules. The principal limitation is the relaxation of the dye to its initial state over time. Another option to develop such a material is to regulate the charge orientation using external fields. Ferroelectrics are materials that have a ready presence of dipoles that are oriented using electric fields to develop applications including random access memories (RAMs), diaphragms and piezoelectric sensors [52, 53]. Due to coupling with the polarization in the ferroelectric layer, LC alignment has been used to visualize the polarization domains [54]. Conventional ferroelectrics include ceramic-based materials, which have large dielectric constants. For LCD applications, they are not suitable due to multiple reasons viz:

- **Methods for growing their films:** Epitaxial growth is too time consuming. Most LCD manufacturers use spin coating or inkjet printing to coat the AL on large area substrates. With the current knowledge about these materials, it is hard to develop films of conventional ferroelectric using either spin-coating or inkjet printing.

- **High dielectric constant:** The AL layer is developed on top of the conductive and transparent electrode. If the AL has a high dielectric constant, most of the

applied voltage will be dropped across it leading to no or impartial LC switching. Conventional ferroelectrics are widely used for applications that require a high dielectric constant with these materials reaching values for ϵ greater than 200.

- **Transparency of the films:** Most of the LCDs require films, which are optically clear for maximum light transmission. Conventional ferroelectrics are opaque in nature whereas most LCDs function on light transmission.

Polymers are materials that are free from these limitations. Ferroelectric polymers have not been widely used to understand LC switching. Blinov et al. [55] have studied the influence of corona poled ferroelectric films on LC switching. In their study, the ferroelectric films were formed using the Langmuir-Blodgett technique. The coupling between the poled ferroelectric film and the LC led to a linear electro-optic response, a result quite different from the quadratic response typically observed. However, Langmuir-Blodgett technique cannot be implemented at the mass production scale. Geivandov and Palto [56] have reported LC switching on spin-coated ferroelectric polymer films of P(VDF-TrFE) in a 70/30 ratio. In their studies, they have reported an asymmetric switching response of LCs when they were switched at a low frequency of 0.01Hz. Through ferroelectric polymers, they were able to study the dielectric relaxation of the LC resulting in an equivalent circuit of their device configuration. However, the results shown so far have not resulted in any commercially-suited devices by using ferroelectric polymers as an alignment layer.

4.2.1 Objectives of Work: LCs and Ferroelectric Polymers

Most of the studies in current literature have covered only one type of polymer. In our studies, we have considered fourteen different polymers as the alignment layer. We have also applied a variety of processing techniques such as poling, plasma processing, rubbing, and doping of the polymer to study LC alignment. Most importantly, we

have demonstrated two commercial applications: an electro-optic device where the wavelength transmitted is controlled by applied field and an optical data storage device.

4.3 Review of work on Liquid Crystals and Carbon Nanotubes

Addition of dopants can also influence the properties of LCs. One such dopant gaining considerable attention in the field of LCs are carbon nanotubes (CNTs). The motivation for such experiments is mainly curiosity regarding the influence of CNTs on LC alignment and its behavior. One of the categories for these devices is displays where the addition of CNTs improves the LC behavior including faster rotational viscosity [26], reduces charge screening [57], and also reduces the residual dc build-up in nematics [58]. The reduction of residual dc has also been observed for addition of other nanoscale particles such as fullerenes [59] and ferroelectric nanoparticles [60–63]. The role of CNTs and other particles is not completely clear but these are great discoveries that will propel growth in this research direction. Another category of LC devices where CNTs and fullerenes have been introduced is gratings and holographic devices [64–67], enhancement of the first-order diffraction efficiency and two-beam coupling for homeotropically aligned LC cells [68], for homogenous alignment of LCs doped with C-60 [67, 69, 70], and also for dye-doped nematic LCs. Since these materials are in their nascent stages of implementation, other surprising results have also been observed such as a double-bump feature in diffraction efficiency of gratings and a voltage dependence of photorefractivity in a planar C60-doped LC [70, 71].

Another area of strong research is the probing of alignment effects of LCs on CNTs. Materials that have low-weight and shape anisotropy can be aligned when dispersed in nematics. This effect is purely due to the orientational order of the nematic LC provided the concentration of the dispersed material is low to prevent

aggregation and clustering. Lynch et al. first exploited this property when they deposited a suspension of CNTs and LCs on a porous membrane [72]. After the LC was filtered out, aligned CNTs exhibiting the nematic order were obtained. Other researchers have observed similar results and also reported on the switching of the CNTs within the LCs using electric and magnetic fields [73–75]. Since the CNTs can arrange to form liquid crystalline phases, a high concentration of their placement over a substrate forms films with orientational order, which are used to align LCs as it has been reported [76].

4.3.1 Objectives of Work: LCs and Carbon Nanotubes

The selection of the type of CNTs plays an important role in how the LCs are influenced. In our studies, we have used CNTs which are straight and open-ended on both sides. Also, the CNTs can be dispersed in organic solvents such as ethanol without aggregation. These properties are very different from the commercially available CNTs, which are not straight and tend to aggregate. Due to the open-ended CNTs, it is possible to study how the LC wets the inside of CNTs. Such a study is relevant to the understanding of LC alignment in devices, which confine them in cavities. One parameter, which has not been studied related to CNT dispersion in LCs is the electrical conductivity. The conductivity of the CNTs can be altered through annealing in a vacuum furnace. Dispersion of conductive CNTs has led to the observation of an electric-field controlled phase transition in the LC. This phenomenon has never been observed and is very interesting from a fundamental studies point-of-view as well as to develop novel materials that change phase in response to electric fields.

Chapter 5. Materials and Methods

5.1 Liquid Crystal

For all of our studies covered in this thesis, we have used the nematic liquid crystal (LC), 5CB. It is commercially available as K15 ($T_{NI}-34.5°C$), also known as 4-pentyl-4-cyanobiphenyl (5CB) and it was purchased from EM Industries (Hawthorne, NY). 5CB is a well-characterized LC, used widely for research purposes and is also one of the most economical LCs.

5.2 Patterned Substrates for Study of Liquid Crystal Alignment

Preparation of PMMA sheets. Clear Poly Methyl Metha Acrylate (PMMA) sheets were purchased from McMaster Carr, Inc (New Brunswick, NJ). The PMMA sheets of 1mm thickness were cut into blocks of 5mm x 5mm. This was followed by ultrasound cleaning of the PMMA blocks immersed in methanol. Subsequently, the PMMA blocks were characterized under the Atomic Force Microscope (AFM) to detect the presence of features or deformations. The surface roughness of PMMA used was 5nm and the patterns were formed in defect-free regions on the surface. The defect-free regions during indentation were identified by a video camera interfaced with our patterning instrument.

Methanol (99%) was purchased from Aldrich (Milwaukee, WI). Glass Microscope slides, pipettes and glass cover slips were purchased from Fisher (Los Angeles, CA).

5.2.1 Patterning Method

Numerous techniques can be applied for patterning a surface. Some of these methods are lithography, holography, and patterning using an AFM tip at a high force.

Photolithography is a two-stage process, typically. The first stage requires exposing a photosensitive material to light (usually UV wavelengths) and the second stage is concerned with the etching of either exposed or unexposed regions. The patterned geometry proposed in Figure 5.1 requires an instrument to place a mask with the pattern over the photosensitive material before exposure. The mask aligner available to us at Drexel University had a resolution limit of 1μm, too large a number for our desired dimensions. Holography is similar to the first case of lithography in the sense that it requires a photosensitive material, which is exposed to light. The need for a mask is absent because the desired pattern can be either generated from an object or by the interference of multiple beams of light. However, the transferred pattern is rarely smooth due to kinetics of the process, which leads to a dimpled geometry in the material. The option that we have used is to form the patterns using a metal tip at a force large enough to penetrate the surface and form the patterns. For such a task, there are two instruments that can be used; an AFM in the force mode or a NanoIndenter. Both of these instruments have a sharp tip, which is controlled in terms of force and velocity using automated machines to obtain surface morphology in the case of AFM whereas mechanical properties can be evaluated using the NanoIndenter. The reasons for preferring the NanoIndenter over the AFM include faster operation, ease of availability and most importantly, the length scales shown in Figure 5.1 are too large to pattern using an AFM.

5.2.2 Nano-Indentation to Develop Patterns

5.3 MTS NanoIndenter

The nano-indenter was used in the Standard Scratch mode with Cross Profiling using a Berkovich tip having a tip radius ∼100nm. The loads applied ranged from 1mN - 7mN for all the polymers used. Scratching on the material will lead to a pile-up

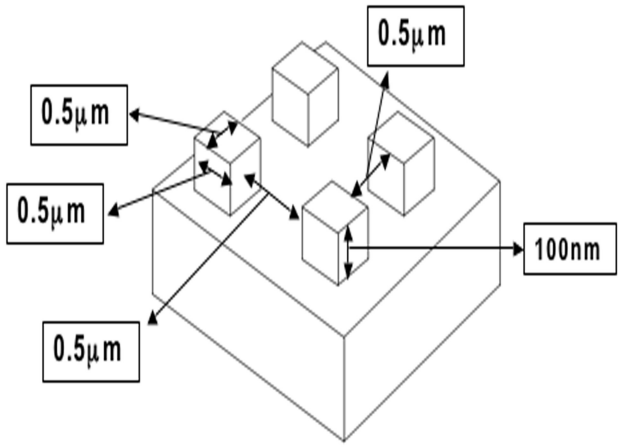

Figure 5.1: Schematic of the Patterned Substrate

surrounding the scratches. This pile-up has to be accounted for while deciding the spacing between the scratches.

One of the operating modes for the NanoIndenter is cross-profiling, which calculates the pile-up height and width due to the scratching process. For the indentations, a Berkovich tip with a tip-radius of ∼100nm was used. The instrument was operated at loads of 1mN at scratch velocities in the range of 25 - 35μm/sec. To obtain the 2D periodic patterns shown in Figure 5.1, we programmed a grid in the NanoIndenter. First, parallel grooves were scratched in the horizontal direction (0 degrees). After the horizontal grooves are formed, the nanoindenter tip is positioned to an area above the highest horizontal scratch, and vertically parallel (90 degrees) grooves are scratched. The spacing of the scratches must be taken into consideration for obtaining the desired dimensions. Empirically, the scratch width and the pile-up height at different loads were observed for determining the optimal load for minimizing spacing between two consecutive scratches. The patterned structure formed in our experiments is as shown in Figure 5.2. This geometry provides confinement regions to the LC in line structures (vertical and horizontal) for 1D restriction. The regions where the lines intersect forms well-shaped structures giving LC a 2D confinement and an area where

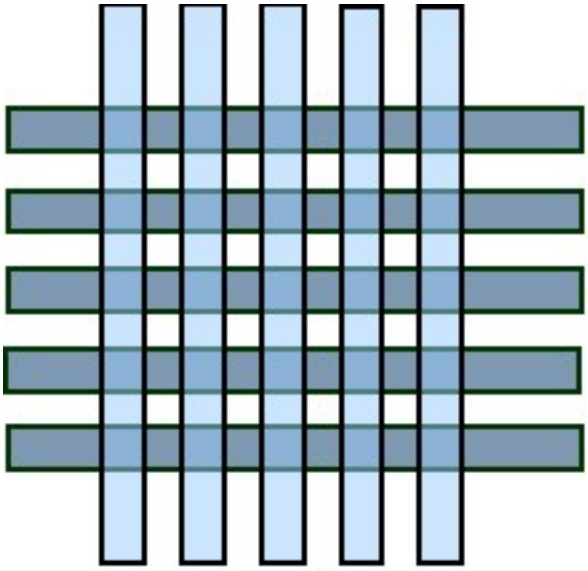

Figure 5.2: Grid scheme as programmed into the NanoIndenter

the forces between the horizontal and vertical lines compete.

5.3.1 Atomic Force Microscopy

We used the Nanoscope III A Atomic Force Microscope (AFM) manufactured by Digital Instruments for our measurements of surface morphology. The AFM was used in the tapping mode using SiN tips having tip constant 0.1N/m.

5.3.2 Alignment of Liquid Crystals

Once the samples were characterized, they were ultrasonically cleaned in a methanol bath for removal of impurities on the substrates. The patterns were located under the Polarized Optical Microscope (Olympus BX-51 Microscope). All our measurements with the POM are conducted in the transmissive mode. The 50x and 20x objectives were used in the polarized microscopy mode (cross-polarizers), and the 40x objective was used in the phase contrast mode. If the patterns were not easily identified in

the polarized microscopy mode, the phase contrast mode was used. A pipette was used to draw the LC in its isotropic phase from the container. Only a single drop was deposited on the substrate, and a glass cover slip was used to cover the sample. The alignment of 5CB on the patterned substrate was observed using the polarized microscopy mode. The configurations were then observed using the microscope. A video camera interfaced to a computer and suitable software (Spot Advanced) was used to obtain the images.

5.4 Liquid Crystals and Ferroelectric Polymers

5.4.1 Ferroelectric Polymer Materials

The following polymers were obtained in a powdered form from Solvay Solexis Inc.; PVDF homopolymers, PVDF copolymer with trifluoroethylene, P(VDF - TrFE), with TrFE in 25 mol%, 35 mol%, and 50 mol%; PVDF copolymer with hexafluoropropylene, P(VDF - HFP) with HFP in 12 mol% and 15 mol%; PVDF copolymer with chlorotrifluoroethylene, P(VDF - CTFE), with CTFE in 10 mol%, 15 mol%, and 20 mol%. Additionally, PVDF - nanoclay composite films were formed by adding Nanoclay 25A (Southern Clay Products, Inc.) in 1wt% to the polymer solution. The addition of the clay particles ensured that nanoclay and polymer combined to a 10% by weight concentration in the solvent (DMF). All of the above mentioned polymers are known to exhibit the ferroelectric phase [53, 77–80].

The polymer powders were mixed with organic solvents including methyl ethyl ketone (MEK), dimethyl formamide (DMF), dimethylsulfoxide (DMSO), ethanol, and 1-methyl-2-pyrrilidinone (NMP). The polymer - solvent mixes were stirred using a magnetic stir bar and heated at 80°C, simultaneously for four hours. Of these mixtures, some had formed optically clear solutions, some did not mix well, and some had formed gels. It was determined that DMF and NMP are the best solvents for

these powders. Also, it muse be noted that homopolymers tend to form gels after a few days when mixed with DMF.

The optically clear solutions were then baked inside an oven at 180°C. An overnight heating procedure was used after which the oven was turned off. The baking process ensured that the polymer was in its molten state following which it could crystallize at the room temperature. Well-crystallized films imply minimal defects in the polymer in addition to uniformity in the film thickness.

After baking, 5μm thick glass sandwich cells were prepared. Uniform cell thickness was maintained by using monodisperse polystyrene cylindrical glass spacers. A sandwich was formed using PVDF-coated ITO-glass and uncoated ITO-glass. The LC was filled using capillary action in its isotropic state at 40°C.

5.5 Liquid Crystals and Carbon Nanotubes

CNTs were synthesized with a non-catalytic CVD method using a commercial alumina membrane as a porous template (Whatman Anodisc®, nominal pore diameter: 200nm ± 10%; thickness: 60μm). Freestanding nanopipes were obtained after dissolution of the alumina template in a boiling 1M solution of sodium hydroxide. The diameter of the resulting nanopipes corresponds to the diameter of the original membrane, and length, after sonication, generally ranges from 5 to 10μm. After synthesis, the CNTs have a disordered wall structure [81]. In this thesis, these tubes are referred to as as-produced CNTs to differentiate them from annealed CNTs, discussed in the next section.

5.5.1 Annealed CNTs

The produced carbon nanotubes were dried overnight (100°C) after the neutralization of the NaOH solution and subsequently annealed in a vacuum furnace (Solar

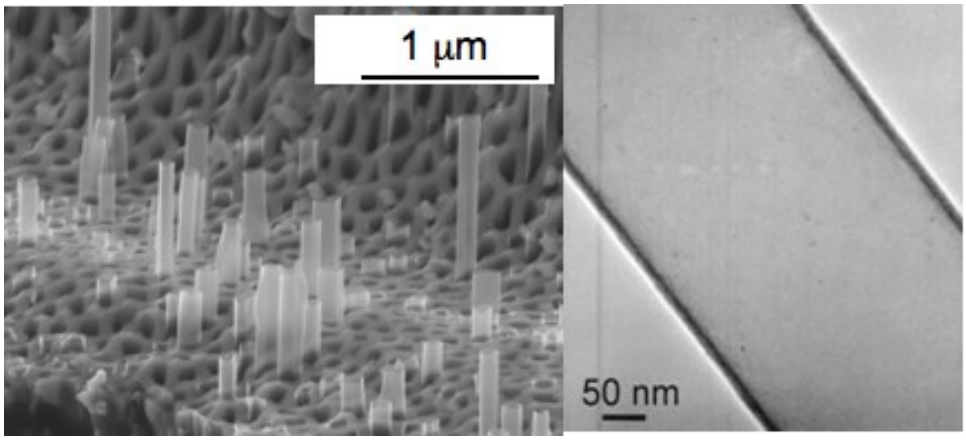

Figure 5.3: Microscopy of carbon nanotubes a). SEM microscope and b). TEM of a single tube indicating straight walls

Atmosphere, PA) with graphite heating elements under pressure of $\sim 10^{-6}$ Torr for 2 hours at 900, 1200, 1500, 1750, 1850 and 2000 °C [82]. The lowest temperature was chosen to be just below the threshold of 1000-1100 °C, at which bonds of functional end-groups break [83], leaving non-graphitic carbon devoid of functional groups. The upper limit was set at 2000 °C because at higher annealing temperatures incipient polygonization of CNTs occurs [82]. Conductivity measurements were performed on an individual carbon nanotube bridging the gap between two Au electrodes on a silicon wafer. Details of the process are reported elsewhere [81]. CNTs conductivity increased from about 1×10^4S/m for the as-produced tubes (670 °C) to 2×10^5S/m after annealing at 2000°C.

A 5μm sandwich-cell was manufactured by separating ITO-glass slides with glass cylindrical spacers. Prior to assembly, the ITO-glass was cleaned for presence of any dust particles using ethanol. It must be noted that no alignment layer was present in the sandwich cell. The LC - CNT suspension was sonicated prior to filling in the cell using capillary flow at 40°C, the isotropic phase for the LC. All the experiments mentioned in the paper were performed at room temperature.

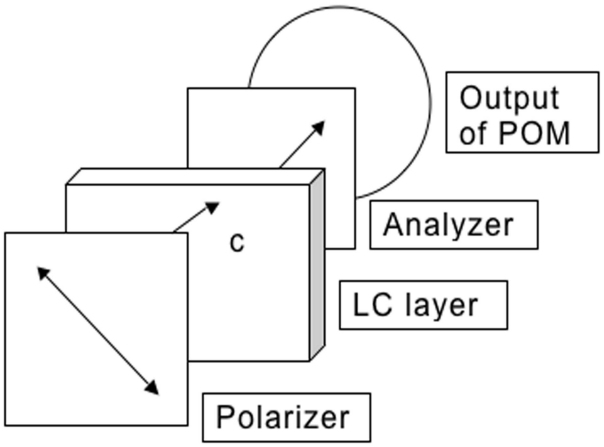

Figure 5.4: Arrangement in a polarized optical microscope

5.6 Experimental Techniques

5.6.1 Polarized Optical Microscope

Figure 5.4 shows the schematic of an optical microscope configured in the crossed-polarizer set-up to observe the alignment of the LC molecules. The intensity of light in the focal plane of the optical microscope is a function of the LC orientation on the surface and the phase retardation of the incident polarized beam. Using the theory described by Dierking [84], the phase retardation of light transmission through the birefringent LCs is given by:

$$\delta = \frac{2\pi}{\lambda}(n_e - n_o)d \tag{5.1}$$

where, the extra-ordinary refractive index is given by:

$$n_e = \frac{n_\perp n_{||}}{\sqrt{n_{||}^2 \cos^2\phi + n_\perp^2 \sin^2\phi}} \tag{5.2}$$

the ordinary refractive index is given by:

$$n_o = n_\perp (5.3)$$

where d is the thickness of the LC layer, λ is the vacuum wavelength, and ϕ is the angle between the optical axis of the LC and the projection of the incident wave vector of light.

For 5CB, $n_{||}$ is $\sim$1.73 and $n_\perp$ is $\sim$1.5 and considering uniform planar alignment, $n_e = n_{||}$ and $n_o = n_\perp$

The transmitted intensity of light coming out of the analyzer is given by:

$$I = I_0 \sin^2 2\phi \sin^2 \frac{\delta}{2} \tag{5.4}$$

where I_0 is the light intensity after the polarizer, and ϕ is the azimuthal angle i.e. the angle between the analyzer and the projection of the optic axis onto the sample plane. This is the intensity observed in the focal plane of the microscope. This is the intensity observed in the focal plane of the microscope. From equation 5.4, it can be seen that the transmitted intensity depends on the orientation of the LC molecules on the substrate. Thus, the intensity of the light can be used to evaluate the orientation of LC molecules on the surface.

5.6.2 Sandwich Cell Preparation

The set-up for manufacturing LC cells is quite simple. Typically, Indium Tin Oxide coated glass slides, ITO-glass, are required. ITO is a conductive coating, which allows for the application of electric fields to the LC. The slides are cut into desired dimensions using a glasscutter. Unless specified, for all of my experiments,1" x 1" slides are used. Following that, the slides are cleaned with organic solvents (ethanol or methanol) to remove dust and other surface impurities. The cleaned slides are placed into a spacer box with the ITO-side facing up. Within the spacer box there

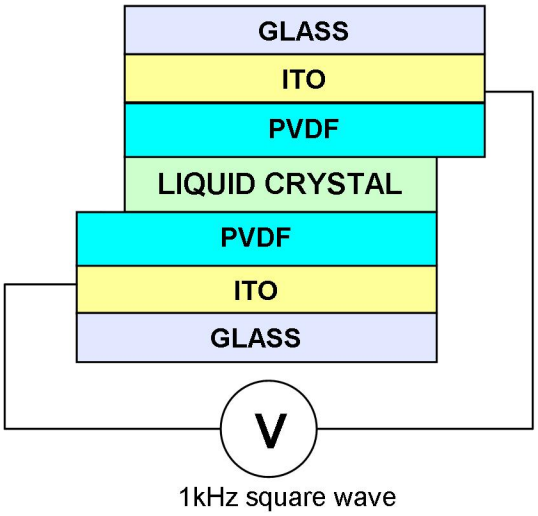

Figure 5.5: Schematic of a sandwich cell

are openings to add powders for particles measuring 5μm or 10μm in diameter. The particles are released using a pressure valve with the box closed to ensure uniform dispersion over the ITO. These slides are placed over ones without spacers to give a cell thickness determined by the spacer particle diameter. The two slides are glued using UV-curable glue, and the liquid crystal is filled in using capillary action. Figure 5.5 shows the schematic of a typical cell.

5.6.3 Rubbing Machine

Typically, commercial LCDs use a rubbing process for aligning LCs. Berreman [18] first experimented with rubbing of glass to align LCs. It was found that the LC molecules aligned in the direction of rubbing. Since then, a wide range of materials was investigated for imparting LC alignment. The material most commonly used in LCD manufacturing is polyimide. The polymer coated glass slides are rubbed using a fibrous cloth-based roller machine. The reasons for the LC alignment on rubbed polyimide include formation physical grooves formed on the surface of the polymer,

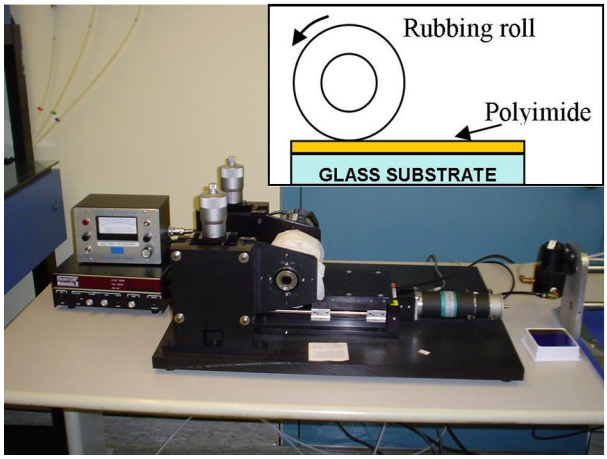

Figure 5.6: Rubbing machine

increased alignment of the polymer chains on the surface, and charge deposition due to fibers deposited on the surface. Figure 5.6 shows a rubbing machine and a schematic of its operating principle.

5.6.4 Spectrometry

In order to map the wavelength response as a function of the applied electric field, spectrometry measurements were performed using a crossed-polarizer configuration on the LC-PVDF cells. A halogen lamp source (Ocean Optics tungsten halogen lamp, λ = 300 - 800 nm) supplied white light, which was spatially filtered before incidence on the first polarizer. The light was fed through an optical fiber to the cell placed between crossed-polarizers, following which it was delivered to a 600μm core diameter fiber connected to a spectrometer (Ocean Optics USB2000 spectrometer, resolution = 0.36 nm).

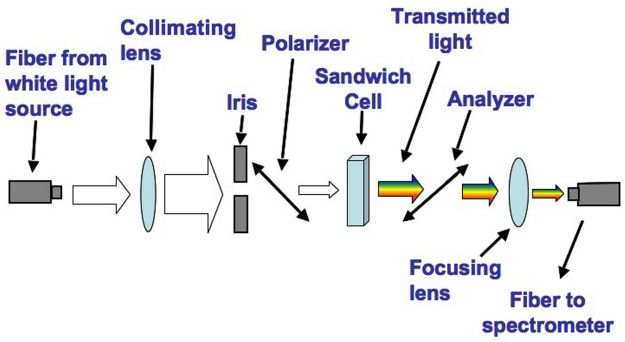

Figure 5.7: Spectrometry set-up

5.6.5 ESEM

The environmental mode is a special mode available in certain scanning electron microscopes (SEM), which allows the imaging of non-conductive substrates without the requirement of a metallic coating. A conventional SEM consists of an electron gun assembly, a target (sample) holder, and secondary electron detector places within a vacuum chamber. Using the electron gun, and appropriate bias and focusing conditions, electrons are emitted on the sample. If the sample is conductive, secondary emission results due to electron contact with the sample surface. The detection of the secondary emission electrons allows for the reproduction of the sample for the user. The typical resolution of a SEM is between 1 - 20 nm. The best imaging results are obtained if the sample is conductive in nature. Non-conductive samples have to be coated with a conductive layer, which is usually gold or platinum using a sputter-coater. The reason is that if these materials are imaged without a conductive layer, on the first scan of the electron beam, a negative charge is deposited on the material. This negative charge repels all further electron beams resulting in a strong collection of beams at the secondary emission detector. Consequently, the image appears saturated (white spots), and this phenomenon is referred as charging.

An environmental mode allows for imaging within an ESEM under low pressures (1

Figure 5.8: FEI XL30 Environmental SEM

- 50 Torr) and high humidity (about 100%). The humidity is achieved by having a flow of water vapor within the SEM chamber. The requirement of the environmental mode requires special apertures and a different electron detector referred to as the Gaseous Secondary Electron Detector (GSED). For a detailed review about the ESEM, please refer Reference [85]. The advantage of imaging under high humidity is that for non-conductive samples, the water vapor is able to neutralize the surface charge. This eliminates the process of charging because the electron beam faces minimal repulsion from the uncoated non-conductive sample. Also, on their way to the GSED, the secondary electrons are further scattered by the water vapor in the chamber. This results in a strong detection at the GSED enabling high quality imaging of non-conductive materials including fluids. For best imaging, one has to experiment with the pressure, humidity levels, and electron beam strength for the optimal conditions. Needless to say, the best conditions for one material do not guarantee the same quality of images with other materials.

Figure 5.9: Renishaw RM1000 Raman Spectrometer

5.6.6 Raman Spectroscopy

Raman spectroscopy is a technique where information about materials can be garnered depending on the frequency and the amount of light it scatters. In a Raman Spectroscope, monochromatic light is made incident on the sample. When light interacts with matter, it is reflected, scattered or absorbed. The scattered light could have the same frequency (Rayleigh scattering) or have a shift in the frequency (Raman scattering). The Raman spectroscope measures the shift in the wavelength and this data allows us to characterize the chemical bonds responsible for the shift in energy (wavelength). For our studies, we have used the Renishaw RM1000 Raman Spectrometer.

5.6.7 Fourier Transform Infra Red (FT-IR) Spectroscopy

Fourier Transform works on the principle of measuring infrared absorption by a material to obtain information regarding its chemical structure. It consists of a broadband infra-red light source, which is followed by a Michelson Interferometer. The inter-

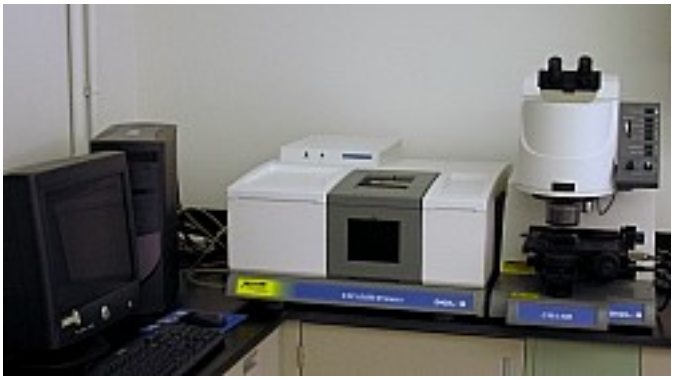

Figure 5.10: Excalibur FTS-3000 FTIR

ferometer consists of a fixed and a movable mirror to realize light interference. The position of the movable mirror is varied to produce a sinusoidal interferogram at different infra-red light wavelengths. The transmission of different wavenumbers by the sample is recorded by at the detector with the final output corresponding to the Fourier Transform of the recorded intensities. This procedure helps in obtaining an interferogram which plots Intensity versus wavenumber (or frequency) [86, 87]. The Excalibur FTS-3000 FTIR was used for the studies in this thesis.

Chapter 6. Liquid Crystal Alignment on Patterned Substrates

One way to influence liquid crystal (LC) alignment is through surface morphology. Morphology plays an important role especially in devices that confine LCs in cavities. These devices are typically polymer dispersed LCs, which arrange the polymer-LC mixture into a grating structure to develop electro-optic devices that include displays, photonic crystals, and lenses [38, 43, 44, 88]. The understanding of LC alignment is limited by current instrumentation. One approach to understand the morphological influence is through patterned surfaces with dimensions similar to those in experimental devices. In order to obtain a reasonable understanding it is necessary to pattern 3D structures. As we have discussed in Chapter 4, most of the patterned substrates used for understanding LC alignment have 2D structures, which are mainly lines. The LC alignment can be only understood along one dimension in these cases using characterization techniques including microscopy and spectroscopy. A 3D structure, as shown in Figure 6.1 provides a close approximation to practical geometries. Additionally, using the technique we have selected for patterning, LC alignment can be studies in lines as well as in well structures providing 1D and 2D analysis.

There are two principal studies, which are similar to what we are proposing. One is by Nuzzo et al., where they have performed FT-IR spectroscopy on LC placed between two parallel inter-digitated electrodes [89]. The height of the LC sample was as low as 40nm and they reported on higher anchoring energy leading to better LC alignment. This excellent study, however, did not answer the questions related to competition provided by morphology in terms of confinement because they provided only 1D confinement. Recently, Clark et al. have developed 2D structures using imprint lithography to generate a grid structure, which has the dimensions 50μm x 50μm x 360 nm [90]. They have discovered a bistable effect observed in the LC

due to the confining geometry of the imprinted substrate. However, 50μm is too large a distance to accurately pinpoint the effect of surface morphology on LCs. The correlation length of LCs is a 100nm at the most, and at distances larger than that, any alignment observed is due to long-range interactions within the LC molecules. The surface, of course, sets the tone for initial alignment. In our studies, performed four years earlier in 2002 [91], we have patterned 2D periodic surfaces to study LC alignment as shown in Figure 6.3a. The LC confinement will result in alignment configurations as shown in Figure 6.3 b and 6.3c, which can be studied in wells of different dimensions. The confinement wells for LCs are formed by the intersection of grooves. The confinement from the front and back walls in 2D periodic surfaces will result in different alignment schemes whereas within the grooves the LCs orients as per the groove direction.

The contents of this chapter are as follows: first, we will briefly review the experimental details related to the formation of the patterns; second, we shall describe the LC alignment on these patterns using polarized optical microscopy; third, to improve the resolution of the microscopy images, we have developed image analysis algorithms in MATLAB; finally, a simple Monte-Carlo algorithm was developed to simulate LC alignment on patterned substrates. This will be described in the last section of the chapter followed by conclusions.

The proposed pattern has a region of confinement between the square blocks and a region of competition in the intersection region shown in Figure 6.1. LC alignment is studied by deposition of the molecules on this surface and observation of the change in alignment as a function of time. Thus, the LC will be imaged real-time without any sample destruction.

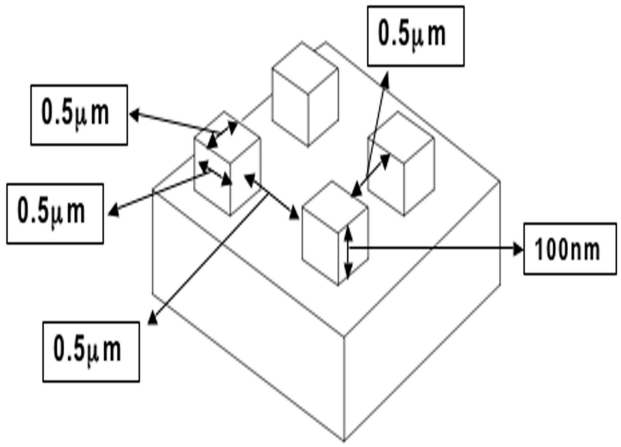

Figure 6.1: Schematic of the Patterned Substrate

6.1 Procedure for Formation of Patterns

6.1.1 Materials

The liquid crystal K15 (T_NI 34.5 °C), also known as 5CB, was purchased from EM Industries (Hawthorne, NY). Methanol (99%) was purchased from Aldrich (Milwaukee, WI). Clear Poly Methyl Metha Acrylate (PMMA) sheets were purchased from McMaster Carr, Inc (New Brunswick, NJ). Glass Microscope slides, pipettes and glass cover slips were purchased from Fisher (Los Angeles, CA).

Preparation of PMMA sheets. PMMA sheet of 1mm thickness was cut into blocks of 5mm x 5mm. This was followed by ultrasound cleaning of the PMMA blocks immersed in methanol. Subsequently, the PMMA blocks were characterized under the Atomic Force Microscope (AFM) to detect the presence of features or deformations. The surface roughness of PMMA used was 5nm and the patterns were formed in defect-free regions on the surface. The defect-free regions during indentation were identified by a video camera interfaced with our patterning instrument.

6.1.2 Patterning Method

The method we have used to form the patterns is to use a metal tip at a force large enough to penetrate the surface and form the patterns. This task was performed using a NanoIndenter. The MTS NanoIndenter was used in the scratch mode with cross-profiling to pattern the PMMA substrate. The instrument was operated at loads of 1mN at scratch velocities in the range of 25 - 35μm/sec. A grid structure was inscribed on the surface to obtain the desired structure.

6.2 Characterization of Patterned PMMA

The surface morphology of the PMMA substrates was characterized using an AFM. The PMMA blocks had a surface roughness of $\sim$5nm. The velocity and the load used during the nanoindentation play a significant role in the dimensions of the patterns obtained. In our experiments, we observed the effects of varying the load in the range of 0.01mN - 5 mN. At low loads the instrument does not give stable patterns and high loads lead to groove overlaps. A tip load of 1mN gave us the optimum results and our experiments are performed at this load. The scratch velocity determines the amount of time for which time the NanoIndenter tip will penetrate the surface for the desired length at the desired load. Low velocities ensure that the tip has sufficient time to penetrate the surface causing a deep scratch. However, scratching at low velocities also signifies an increased scratch width and hence, pile overlap. Experimentally, we have found that velocities in the range 25 - 40μm/sec are best suited for the patterns desired. Lower velocities of about 5 - 15μm/sec, as expected, resulted in deeper, wider features. Higher velocities of the order of 90 - 100μm/sec were not enough to cause scratches on the PMMA. The elasticity of the substrate did not allow for the scratches to be significantly visible under the AFM. Also at higher velocities, the scratches lose their uniformity because of the drift along with low loads will cause the

tip to vibrate as it scratches. The morphological results of varying scratch velocities on PMMA are illustrated in Figure 6.2a, where Figures 6.2b and 6.2c illustrate the variations in groove width and depth as a function of the scratch velocity.

6.3 Liquid Crystal Alignment

The energy associated with LC molecules is given by the Franks equation of free energy

$$\mathbf{F} = \mathbf{K}_{11}(\nabla \cdot \mathbf{n})^2 + \mathbf{K}_{22}(\mathbf{n} \cdot \nabla \times \mathbf{n})^2 + \mathbf{K}_{33}(\mathbf{n} \times \nabla \times \mathbf{n})^2 \tag{6.1}$$

where K_{11} is the Splay elastic constant, K_{22} is the twist elastic constant, and K_{33} is the bend elastic constant.

Equation 6.1 does not consider external forces acting on the LCs. For our experiments, the LCs experience surface forces from the PMMA layer. Due to the morphology of the substrate, the anchoring energy will play a dominant role in the orientation of the LCs. This additional surface energy term is denoted by F_{surf} and should be included in the above equation.

6.3.1 Time Response of LC Alignment

The LC orientation is dependent on the groove morphology and orients along the groove direction. For a patterned surface as in our case, the LCs from the vertical grooves interact with the LCs in the horizontal grooves. Thus, the intersection regions are expected to contain larger number of defects as shown in Figure 6.3c. This is in contrast to complete alignment in the verticgal/horizontal grooves. Due to the interaction described above, the LC takes a finite time before settling into a final state. Figure 6.4 illustrates the time variation of the LC on patterned areas. The region of interest is the area where the horizontal and the vertical scratches intersect.

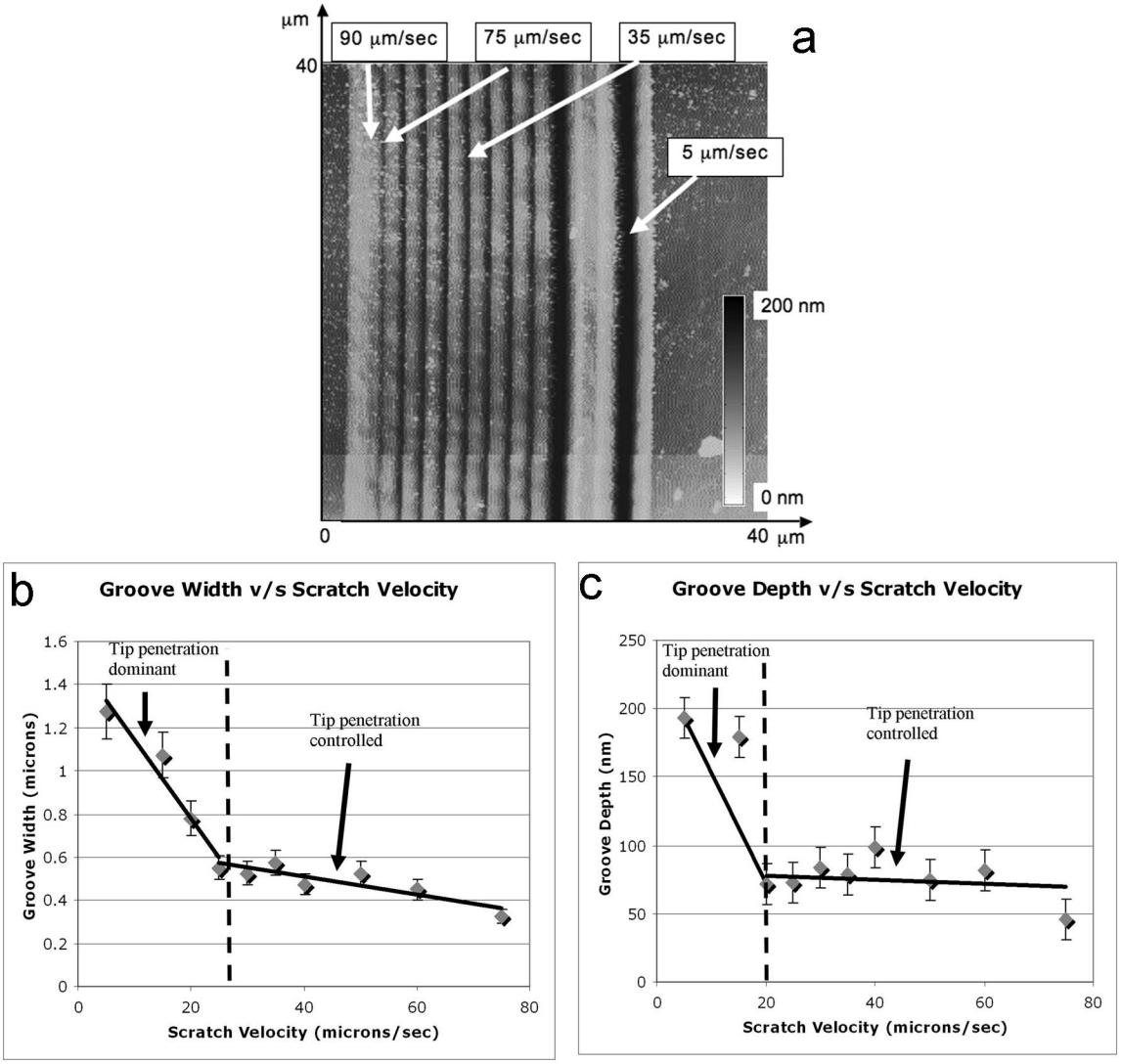

Figure 6.2: Effect of scratch velocity on groove dimensions; a) AFM image of scratches at different velocities. All scratches performed at 1mN, b) Variation of groove width as a function of scratch velocity. The error variation is 10%, c) Variation of groove depth as a function of scratch velocity. The error variation is 5%

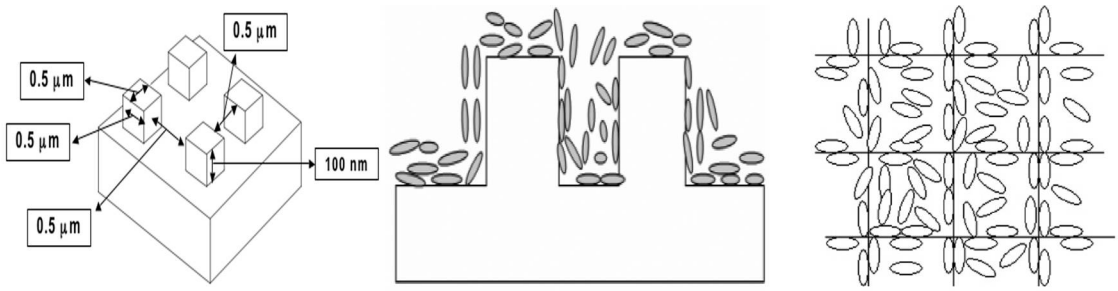

Figure 6.3: Hypotheses of LC alignment on patterned substrates; a). Schematic of the patterned structure, b). Side-view hypothesis of the LC deposition on the structure, c). Top view hypothesis of the LC deposition on the structure

These are the grid structures shown in the schematic in Figure 6.4. In this region, the LC can be viewed to undergo defects due to orthogonal orientation angles. Hence, these regions are distinct from the rest of the patterned area. The rest of the surface represents the randomly aligned state of the LC. This can be seen in the Figures 6.4c, 6.4d and 6.4e in the areas other than where the grid is patterned. Figure 6.4f shows the variations in the intensity of images as a function of time. The intensities are calculated for the four grid structures shown in Figures 6.4c, 6.4d, and 6.4e. The variation in the intensities signifies the interaction of LCs with the surface.

6.3.2 Alignment in Different Patterns

As another set of experiments, grooves were patterned at different angles and LC alignment was observed in each groove. In the grid schematic shown in Figure 6.5a, there are grooves at 45 degrees to horizontal, horizontal and vertical grooves and grooves at 60 degrees to the horizontal. The 60-degree grooves were made to intersect the grid region. LC material was deposited on this patterned substrate and we compared the alignment in each . 6.5b and 6.5c show the patterned substrate before and after LC deposition respectively. The alignment of the LCs on the surface will determine the angle of rotation of the polarized light. Only the component of the ro-

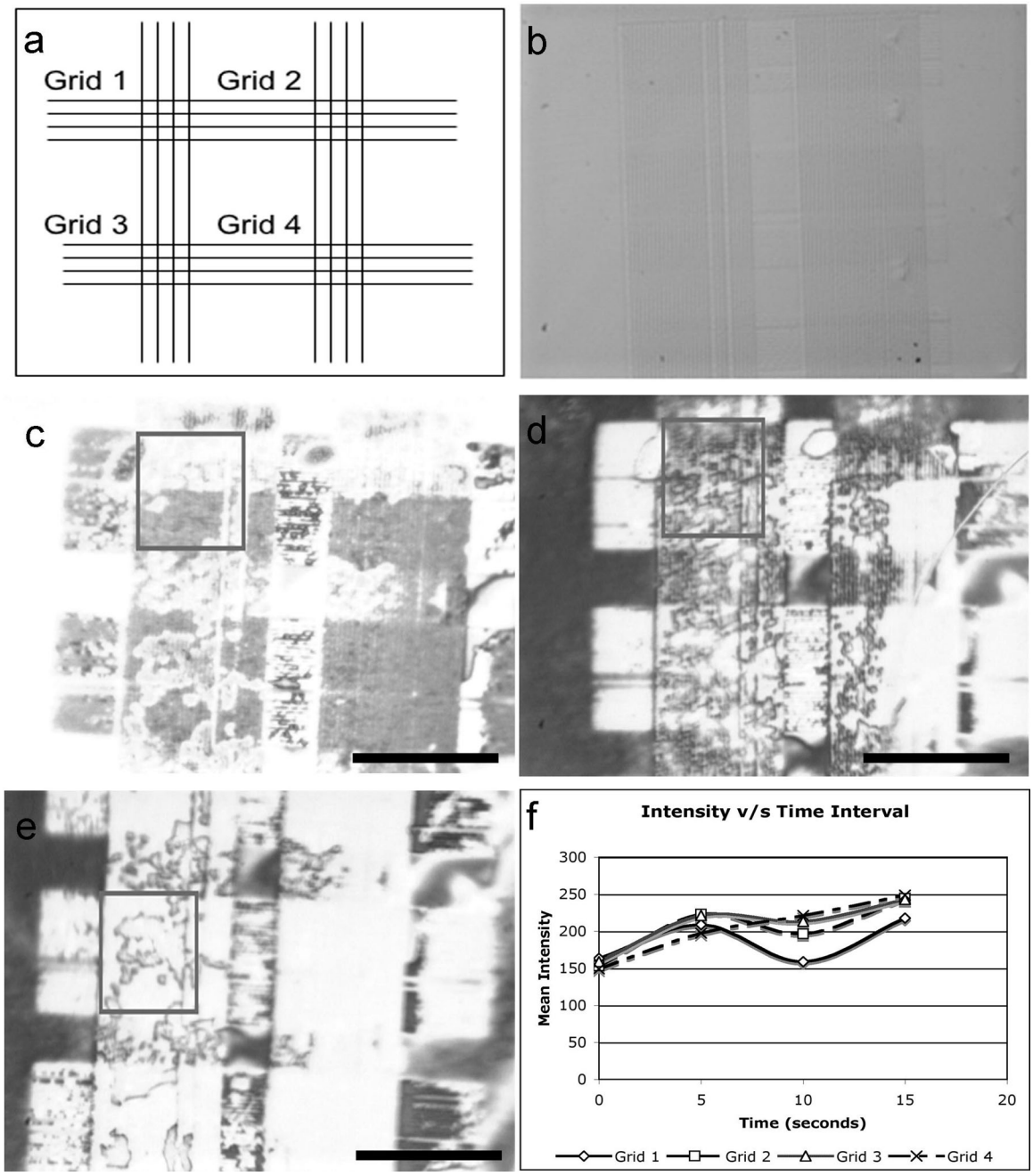

Figure 6.4: POM images of the LC alignment within the nano-patterned PMMA surface. The square box in the images can be used track changes for images in a-d Scale bar represents 50μm; a) Schematic of the patterned grid, b) Without LC Deposition, c) LC alignment 5 seconds after deposition, d) LC alignment after stabilization (time = 10 seconds), e) Final state of LC (time = 15 seconds), and f) Time variation of the light intensity

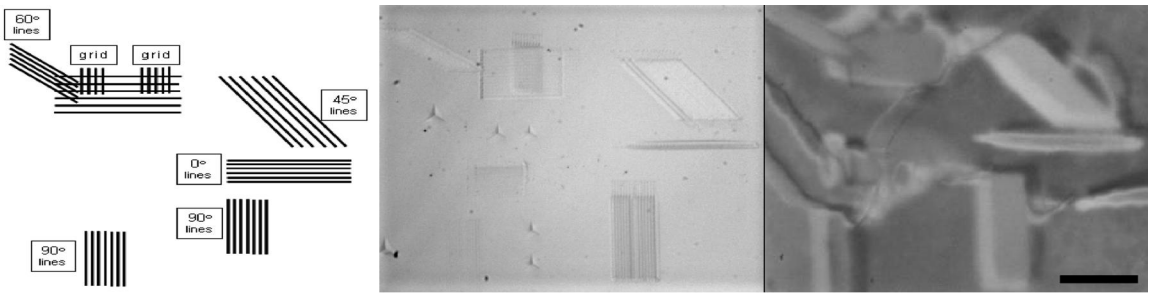

Figure 6.5: LC alignment within patterned PMMA. a) Desired Patterns, b) Image of the patterned substrate without LC, c) Patterned substrate after LC deposition

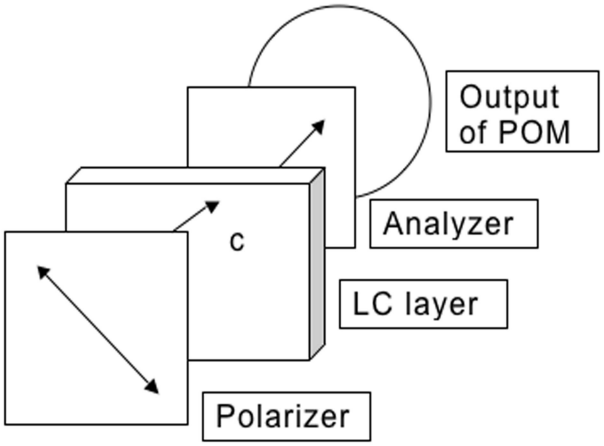

Figure 6.6: Schematic of a polarized optical microscope

tated light that is parallel to the analyzer emerges. Any changes in light intensity thus signify a change in orientation of the LC molecules within the pattern. The alignment of the molecules would therefore determine the intensity of the light observed. Figure 6.6 shows the schematic of a Polarized Optical Microscope. The intensity of light in the focal plane of the optical microscope is a function of the LC orientation on the surface and the phase retardation of the incident polarized beam. Using the theory described by Dierking [84], the phase retardation of the polarized light on the LC is

given by:

$$\delta = \frac{2\pi}{\lambda}(n_e - n_o)d \tag{6.2}$$

where d is the thickness of the LC layer, λ is the vacuum wavelength, and ϕ is the angle between the optical axis of the LC and the projection of the incident wave vector of light. The extra-ordinary refractive index is given by:

$$n_e = \frac{n_\perp n_{||}}{\sqrt{n_{||}^2 \cos^2\phi + n_\perp^2 \sin^2\phi}} \tag{6.3}$$

and the ordinary refractive index is given by:

$$n_o = n_\perp \tag{6.4}$$

For 5CB, $n_{||}$ is $\sim$1.73 and $n_\perp$ is $\sim$1.5 and considering uniform planar alignment, $n_e = n_{||}$ and $n_o = n_\perp$. The transmitted intensity of light coming out of the analyzer is given by:

$$I = I_0 \sin^2 2\phi \sin^2 \frac{\delta}{2} \tag{6.5}$$

where I_0 is the light intensity after the polarizer, and ϕ is the azimuthal angle i.e. the angle between the analyzer and the projection of the optic axis onto the sample plane. This is the intensity observed in the focal plane of the microscope. From equation 6.5, it can be seen that the transmitted intensity depends on the orientation of the LC on the substrate. Thus, the intensity of the light can be used to evaluate the orientation of LCs on the surface.

6.4 Image Analysis

For characterization of the POM images with respect to the alignment observed in patterns, we have developed an Image Analysis algorithm in MATLAB®, a software product by MathWorks, Inc., (Natick, MA). The POM images do not provide enough information to identify the variations in LC alignment along the length of individual grooves. The alignment variation is studied by mapping each pixel of the POM image to a color scale. The scale can be calibrated to match the intensity of a pixel to the alignment nature. The program to map the pixel intensities to color-map is implemented using MATLABs image processing functions. First, morphological operations are performed on the POM image. This process involves dividing the image into different objects of a fixed radius that can be worked upon by the image-processing module. For the mapping, the objects chosen were disks and had a radius of one pixel. Other object shapes were also tested but their results were far inferior as compared to using disks. The grayscale intensities of each pixel are mapped to a colorbar. In this case, the image data is scaled to the full range of the color-map provided in MATLAB. Every pixel is thus mapped to a color as per its intensity. The color mapping is not sufficient by itself to reveal the alignment variations. Following the color-mapping, hue-shift operation is performed to identify gradients on the color-mapped image. The gradients correspond to the alignment variations within a pattern. This is implemented by varying the hue of every pixel by a fixed amount and the resulting image is again color mapped.

The alignment variation of the LCs in the patterned regions is studied by means of POM images. Due to practical considerations including vibrations during indentation, and the positioning and repositioning of the indenter tip, the patterns show feature variations of the order of few nanometers. As a result, the alignment will vary across the length of a single groove. The imperfect surface of each groove will also lead the

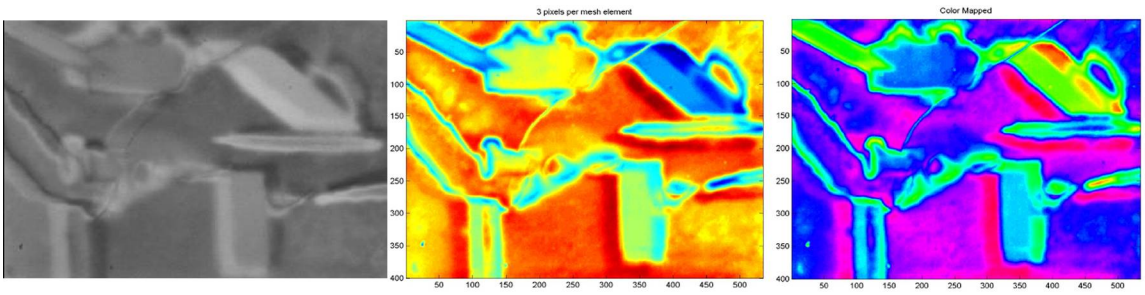

Figure 6.7: Image Analysis Results; a) POM of LC on patterned PMMA, b) Color mapped pixilated intensities of image a, c) Gradient analysis of image b

alignment at the surface to be different than the alignment in the bulk of the groove.

The alignment changes between the patterns are identified by color mapping of the POM image. The input image for the algorithm is Figure 6.7a and the result is shown in Figure 6.7b. The different colors associated with different grooves indicate alignment changes. A closer look inside any pattern on the image will indicate minor color changes. This is due to morphological variations in each pattern due to reasons including tip vibrations during indentation, and surface roughness of the substrate. The hue-shift operation applied to this image will identify the gradients in Figure 6.7b. The results of the hue-shift operation are shown in Figure 6.7c. Thus, comparing Figures 6.7b and 6.7c, we can identify alignment variations more systematically as opposed to merely observing the POM images.

6.5 Liquid Crystal Modeling

The field of modeling and simulation of LCs employs a very active scientific community and their interest has helped to develop several techniques to understand LC simulations. The reasons for conducting modeling and simulation studies for LCs include the ability to observation gradients in materials, the interplay between different parameters over time, temperature or any other physical quantity, and establishment

of relationships between molecular characteristics and bulk properties [92]. In terms of observing the nematic alignment on patterned substrates, not all information can be obtained through experimental observation. Modeling the LC alignment on these substrates could be used to understand the alignment of the material near the surface, to observe the defects in liquid crystal and to predict the final state of the material after its deposition. Considering these objectives, a finite-difference code has been developed to model the alignment of nematic liquid crystals (LCs) on patterned substrates. LC directors are modeled for simulation and representation purposes on rectangular, triangular, and sawtoothed shapes for the substrate.

Theoretical work on interactions of LC with surfaces is reviewed in many excellent monographs [92, 93]. Various *ab initio* and thermodynamic approaches, such as molecular dynamics, Monte-Carlo methods, or finite element methods can be found in Reference [94]. Molecular simulation studies for nematics have focused on various topics that include calculation of stability in order parameter [95], intermolecular structure [93], and calculation of parameters such as rotational viscosity [96] and flexoelectric coefficients [97]. Molecular simulations either solve for force equations between different molecules or atoms (Molecular dynamics) or they solve for energy minimization for a minor move in one of particles parameters such as orientation (Monte Carlo) [92]. However, these simulations cannot be used at larger length scales simply because the computation power and time required are too large to achieve convergence. For our purposes, coarse-grained models which describe interactions of LC with surfaces on mesoscopic scales are sufficient. In this approach all interactions are included in a proper energy functional and stable states of the entire system are then found via energy minimization [94, 98].

6.5.1 Model to Visualize LC Alignment on Patterned Substrates

We will assume that the interaction of liquid crystal molecules with the substrate can be described by the Franks model (Equation 6.1). In this model, the stable liquid crystal states correspond to minima of equation 6.1 discussed before:

$$\mathbf{F} = \mathbf{K}_{11}(\nabla \cdot \mathbf{n})^2 + \mathbf{K}_{22}(\mathbf{n} \cdot \nabla \times \mathbf{n})^2 + \mathbf{K}_{33}(\mathbf{n} \times \nabla \times \mathbf{n})^2 \tag{6.6}$$

where n is the directional vector describing orientation of a cluster of LC molecules, and is also known as a director, $\mathbf{K}_{11}$ is the Splay elastic constant, $\mathbf{K}_{22}$ is the twist elastic constant, and $\mathbf{K}_{33}$ is the bend elastic constant.

We have also minimized a special case of the Frank's equation, which is represented as:

$$E = -\sum 2\cos(\theta_i - \theta_j) \tag{6.7}$$

Equation 6.1 and 6.7 are discretized in two dimensions yielding model where LC directors are distributed on two dimensional rectangular lattice with interactions between only the nearest neighbor interactions. The surface geometry is incorporated by holding the first layer of the director molecules fixed in their orientation through strong planar anchoring with the substrate.

6.5.2 Energy Minimization: Metropolis Algorithm

Energy minima of the discrete system developed in the previous section are obtained using standard simulated annealing process [99] based on the Metropolis algorithm [100]. The simulated annealing algorithm is based on the Metropolis algorithm for random walks. For our simulations, we pick a director at random and record its energy given by equation 6.6. The director is then given a random shift in the

orientation angle. The reduction in energy is readily accepted whereas an increase in energy is accepted with a probability P where

$$\mathbf{P} = exp\frac{-\Delta E}{T} \tag{6.8}$$

where ΔE is the change in energy before and after the shift and T is the temperature of the system. The idea behind accepting energy increases is an effort to reach global minima. The probability of reaching local minima increases if the energy rises were not taken into consideration. The above described process is repeated for all the directors for many cycles. To implement the annealing part, we start at an initial temperature which is typically a temperature outside the isotropic range of the LC chosen. The temperature is reduced by a percentage every N iterations. The number N is large enough to accumulate enough statistics for a particular configuration. The temperature is reduced to a value below the nematic range of the liquid crystals. Throughout the procedure, the least energy configuration is recorded and at the end of the simulation, we obtain the alignment configuration most favorable to the LC molecules.

6.5.3 Details of our Simulations

We used an array of 120x120 directors with each director representing about 10 LC molecules. Each LC director is assumed to have only a rotational degree of freedom. The system elements (directors) are given orientation angles randomly and they are annealed to equilibrium by using the simulated annealing algorithm. The directors are iterated on a geometrical surface. The surfaces that we have considered are of three geometrical shapes: 1. Rectangular shaped surface 2. Triangular shaped surface and 3. Sawtoothed surface. The schematic of the surface structures is shown in the

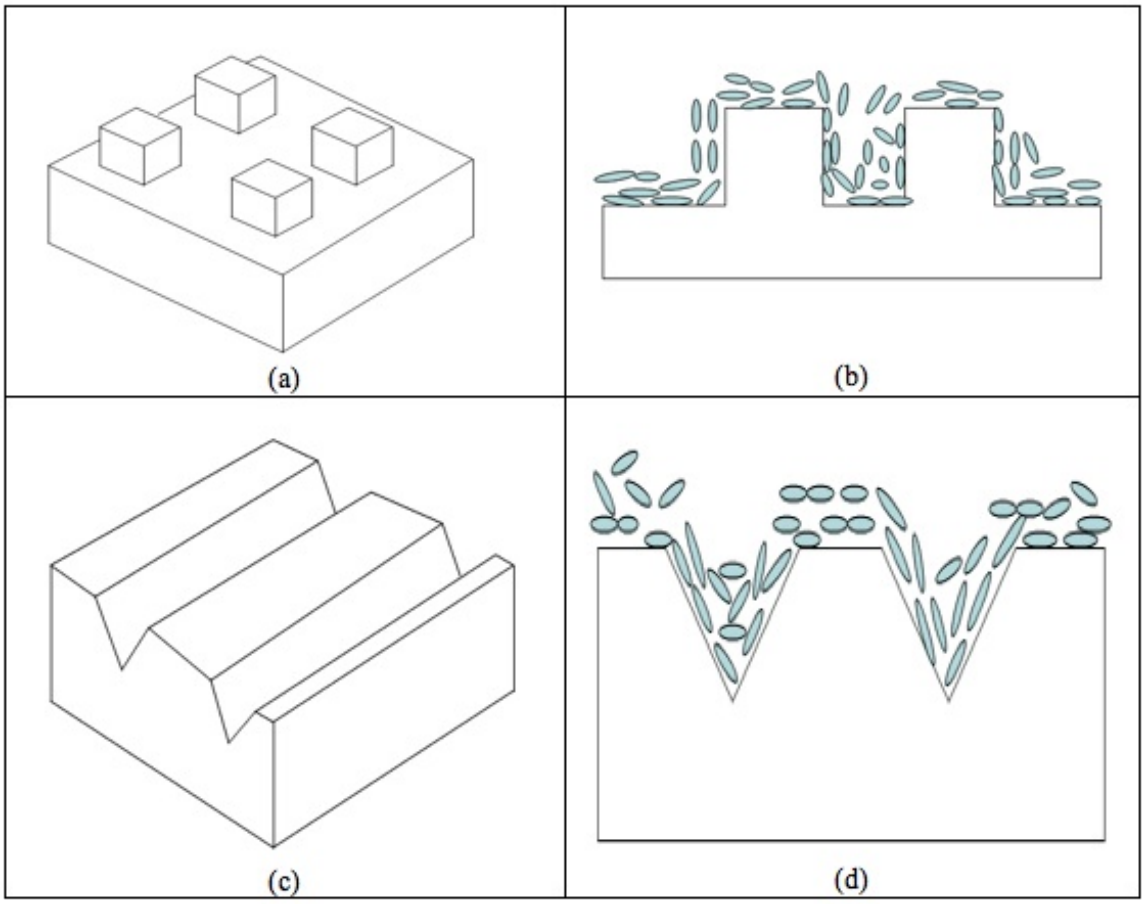

Figure 6.8: Schematic of the patterned substrates and LC alignment visualizations

Figure 6.8.

Figure 6.9 also shows a snapshot of the simulation. The length scales of the structures are about 250nm considering each director represents 10 LC molecules and each LC molecule is about 5nm long. This length scale is appropriate for finite difference schemes and the molecular interactions between the LCs would not be required to represent the interactions between the directors. The director orientation is described by two angles and is denoted as:

$$\hat{n} = (\sin\theta\cos\phi, \sin\theta\sin\phi, \cos\theta) \tag{6.9}$$

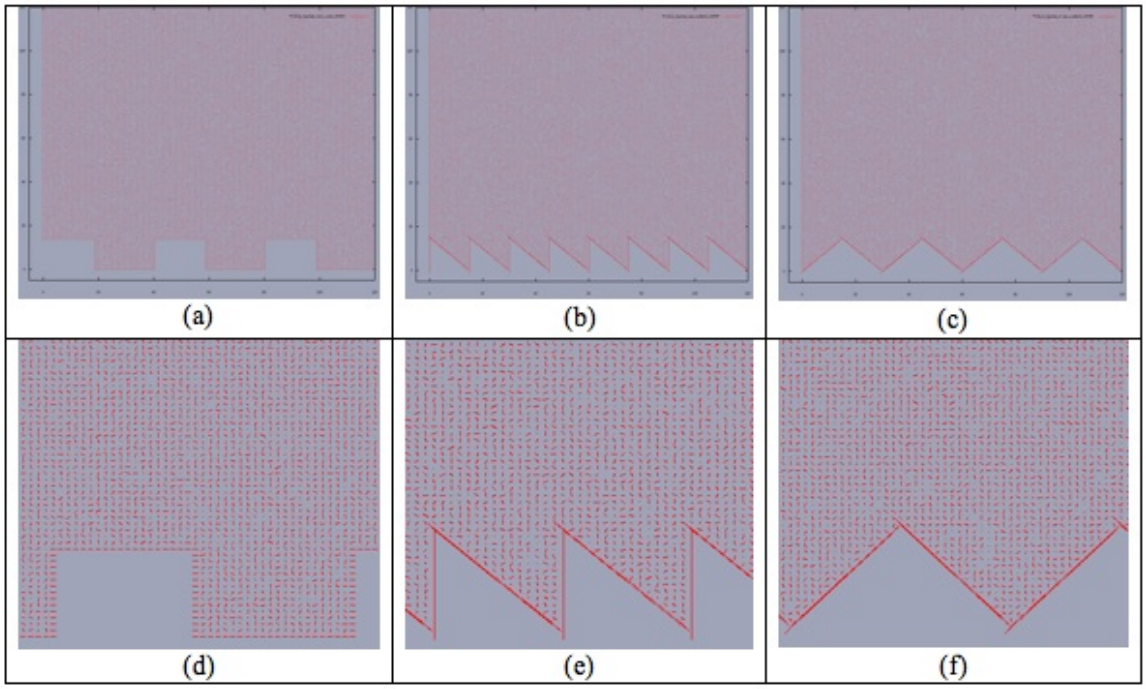

Figure 6.9: Snapshots of the actual system implemented a-c and zoomed versions of the same in d-f

For the simulations, different boundary conditions can be applied to the geometries considered. The side walls could be assumed to be infinite in nature in which the boundaries would be periodic or an alignment nature (homeotropic or planar) could be specified. At the surface, we can observe the alignment of LCs considering a planar or homeotropic alignment specified. The alignment could also be observed considering a pre-tilt. The aim is to model the various alignment schemes employed to get different pre-tilt anchoring conditions. The results can be obtained for different types of LCs provided information regarding the elastic constants are available.

The current study is limited to considering the rotational displacement of the LC directors. As a result, the electrostatic forces between the directors are assumed to be equal on all directors. Hence, the only force that influences the LC alignment is due to elastic forces, which are taken into consideration by the Franks equation.

6.5.4 Results and Discussion

We conducted tests for alignment on patterned substrates in different conditions. Alignment on each of the three patterns was observed under mainly two side-wall conditions: periodic and finite boundaries. Periodic boundaries represent an infinite wall case and the LCs are free to move along the sidewall as compared to the finite wall case where they are anchored either planar of homeotropic. The LC on the substrate was aligned parallel to the surface with some variation in its orientation. This variation is due to the interaction forces from the neighbors which are one step away from the surface. The points where the edges of the walls meet force the LCs to be aligned in a direction that is equivalent to the resultant direction of the two edges. The LCs in those surrounding regions are in a state between the orientation of the closer edge and the neighbor. The alignment changes as the distance and in the bulk, it is free to take upon any direction. However, the LC in bulk remains relatively

Table 6.1: Elastic constants for the two liquid crystals considered in our simulations

Liquid Crystal	**K11(pN)**	**K22(pN)**	**K33(pN)**
BL038	13.7	0	27.7
ZLI5400	10	5.4	19.9

aligned to the surface, this can be thought of as the long range anchoring forces of the substrate morphology. The same theories can be explained to the alignment at the top and the side walls.

The alignment was observed for two liquid crystals: ZLI5400 and BL038. Table 6.1 shows the two LCs considered with their elastic constants. ZLI5400 has a higher degree of freedom due to the presence of the twist elastic constant and can have more variation in the alignment at the surface. This additional degree of freedom could lead to a different defect configuration at equilibrium. Also, the splay and bend elastic constants of BL038 and ZLI5400 are different in magnitude. How that would affect the alignment of LCs remains to be studied. The results of the various simulations we have performed are illustrated in Figures 6.10 - 6.15

For each of the substrate shapes, results for ZLI5400 and BL038 are shown. In Figures 6.10 and 6.11, the alignment for ZLI5400 and BL038 is shown on a saw-toothed substrate. It can be seen that the alignment at the surface edge, highlighted in the Figures 6.10 - 6.15, the alignment is different in both the cases. This is the case for any region in Figures 6.10 - 6.15. The variations can be attributed to the difference in the elastic constants of the liquid crystals used. The magnitudes of the elastic constants give degrees of freedom the LC allowing it to settle in a preferred configuration. Also, at the surface, perfect alignment of the immediate LC layer is not observed. This can be attributed to the elastic constants which influence the interactions between the LC molecules. The LC-surface interaction dominates the immediate layer and the resultant is a configuration that has a pre-tilt.

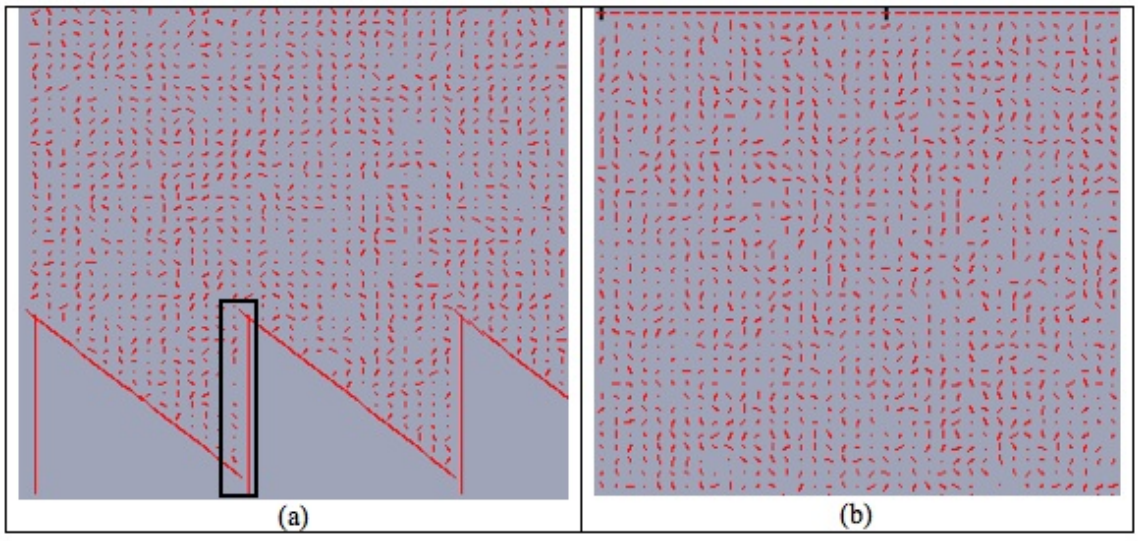

Figure 6.10: Alignment of ZLI on saw toothed substrate. The sidewalls are periodic.

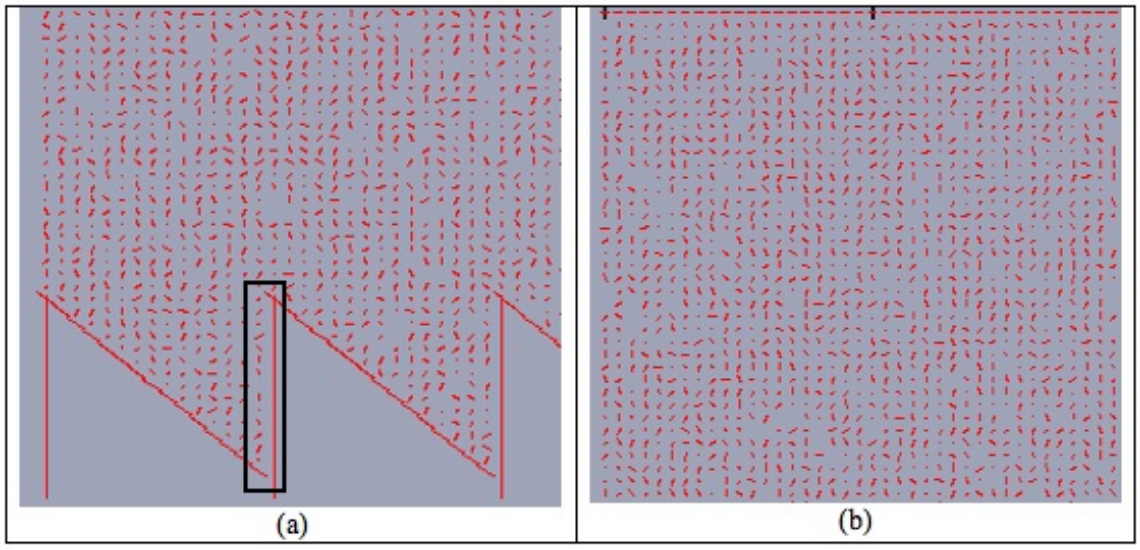

Figure 6.11: Alignment of BL038 on saw toothed substrate. The sidewalls are periodic.

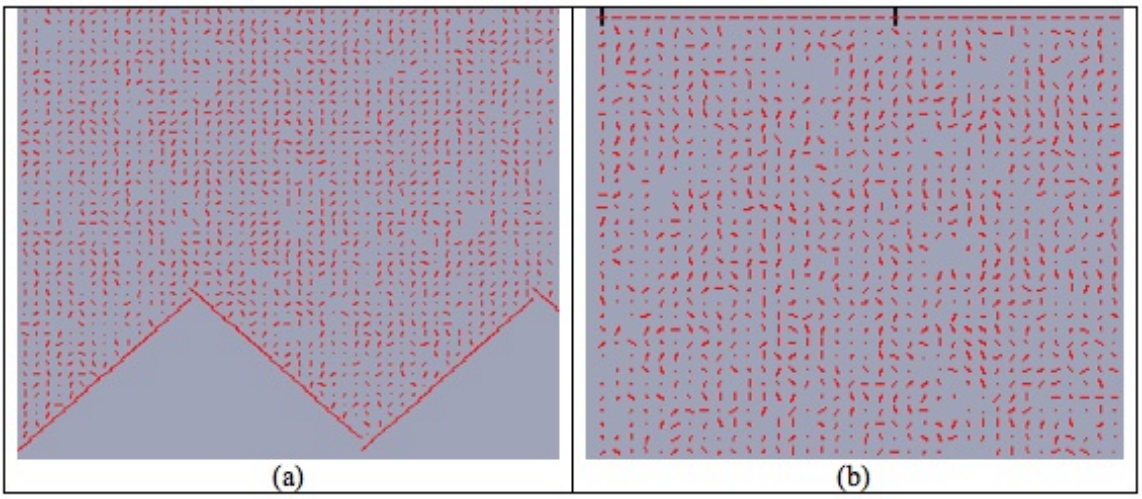

Figure 6.12: Alignment of ZLI on triangular substrate. The sidewalls are periodic.

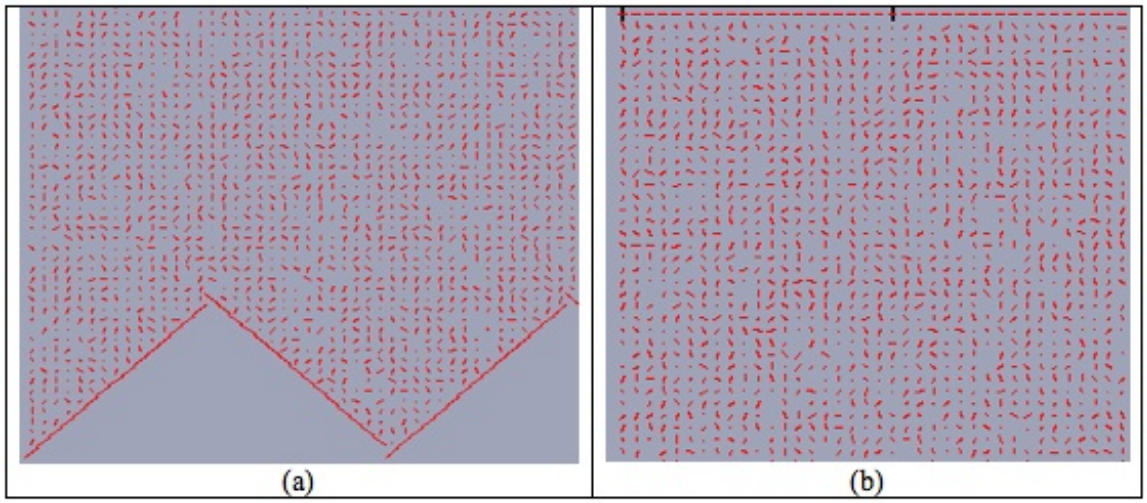

Figure 6.13: Alignment of BL038 on triangular substrate. The sidewalls are periodic.

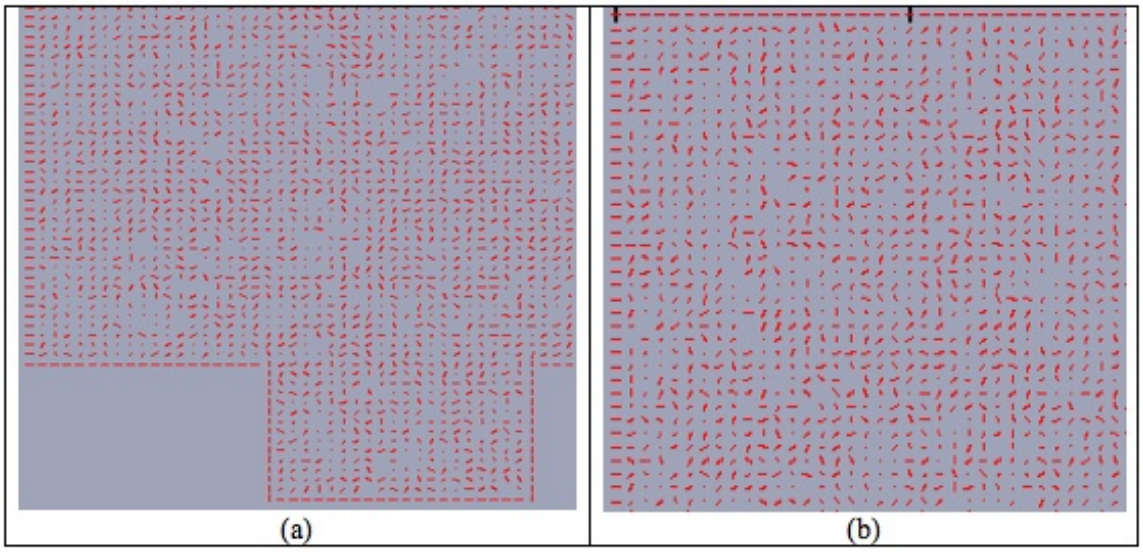

Figure 6.14: Alignment of ZLI on a rectangular substrate. Planar anchoring is specified at the sidewall

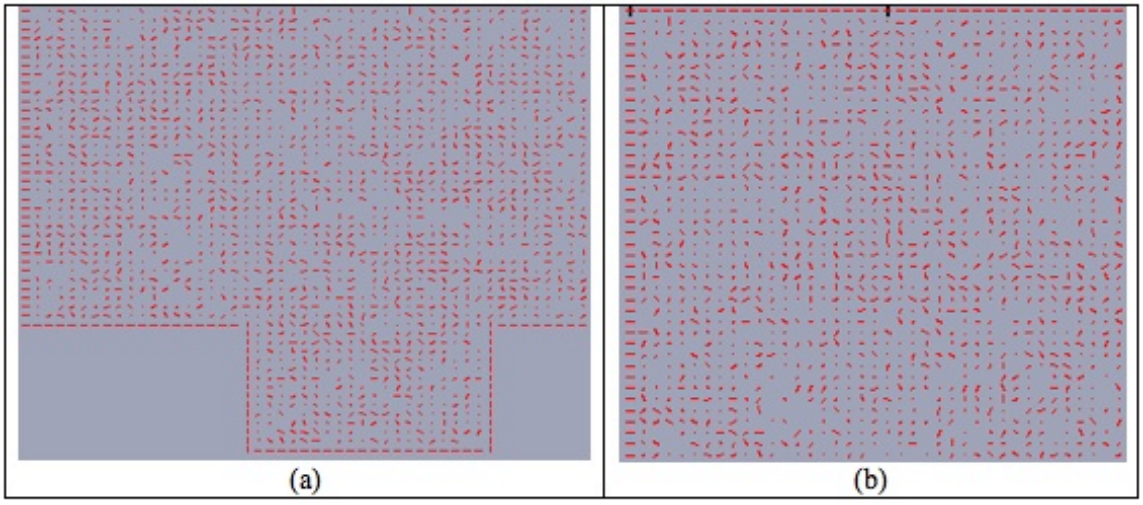

Figure 6.15: Alignment of BL038 on a rectangular substrate. Planar anchoring is specified at the sidewalls

Also, it can be observed from Figures 6.10 - 6.15 that the LC orientation at the surface edges indicates the presence of defects. These would be useful for imaging systems including biological cells that have varying surface morphology using LCs. The defects would indicate the surface variations that may not be identified clearly by a regular microscope.

6.6 Conclusions

In this chapter, we have seen how LC alignment varies with the patterns inscribed on polymers. The surface exerts alignment forces on the LC molecules forcing them to align as per the morphology. The alignment was studied using polarized light microscopy on patterned PMMA. Patterning was performed by using the MTS NanoIndenter, a hardness testing instrument, programmed to scratch patterns including lines and grid structures. To better identify variations in LC alignment, image analysis was performed on the microscopy images. After image analysis, the resolution of identifying changes in intensity was improved by a factor of three. Also, a finite difference model was developed to understand LC alignment on patterned substrates. Results were obtained for alignment on different shapes. The results obtained are for only rotational degree of freedom. Our future work will consider translational freedom also. In addition to that, the system considered is a 2D system, albeit with rotation in 3D. For modeling alignment in devices accurately, it is necessary to consider a complete 3D system.

Chapter 7. Ferroelectric Polymers for Liquid Crystal Alignment

Liquid Crystal Displays (LCDs) have different operating modes, which vary in mainly two different ways: the LC alignment through the cell and how the electric field is applied to switch the LC. Though these are only two options there are many possible ways to align the LC molecules including in-plane alignment, twisted-nematic alignment, vertical alignment and patterned vertical alignment. The electric field is applied either in-plane or vertically (though the thickness of the cell). However, different displays can require patterned electrodes for the application of the switching voltage. Considering the different options, LCDs can be designed and developed in a large variety of operating modes, which are customized for different applications including mobile phone, televisions, and computer screens. Each of these modes specifies the kind of LC required (nematic or smectic), presence of any dopants including dyes, dielectric anisotropy, and LC temperature range. The alignment layer (AL) also changes depending on the mode required. Some of the different modes to induce LC alignment include rubbed polymers, AL with ridges, photo-exposed AL and AL with different chemical functionalities. The two materials, AL and LCs, usually do not give the flexibility of keeping one constant and varying the other. For example, a Twisted Nematic LCD (TN - LCD) prefers a LC with a positive anisotropy and an AL, which provides a low pretilt angle to the LC. On the other hand, a vertical alignment LCD (VA - LCD) requires a LC with negative anisotropy and an AL that provides a high pretilt angle to the LC. If the AL for these modes is polyimide, it has to differ in its chemical functionality to ensure proper alignment of the LCs. Thus, it can be safely said that every commercial LCD application (TVs, cell phones) requires a different AL and LC.

A solution to the above problem is to develop a programmable layer to impart LC

alignment. In this Chapter, we will discuss how surface polarization in ferroelectric polymer is used to develop displays and optical data storage devices. Ferroelectric polymers are advantageous from a mass-production perspective because they can be spin-coated using common organic solvents, they generally have a low dielectric constant (ranging from 8 - 15) [80] and their films are optically clear. Their major limitation is the uniformity in dipole orientation, which is not as controllable and strong as found in conventional ferroelectrics. However, the dipoles have a greater degree of freedom offering the capability of developing ferroelectrics with dipoles oriented at different angles for electronic applications.

One of the largest families of ferroelectric polymers are polymers based on polyvinylidene fluoride (PVDF). PVDF has a chemical structure $CH_2 - CF_2$, which is between the highly flexible polyethylene $CH_2 - CH_2$ and polytetrafluoroethylene $CF_2 - CF_2$. In PVDF, the polarity difference between the CH and the CF bonds leads to the presence of dipoles. Additionally, the CH_2 bonds serve to dilute the CF_2 - CF_2 interactions imparting additional flexibility in the polymer chains. For this reason, PVDF can attain multiple stable chain configurations, which can be programmbed to obtain the ferroelectric phase. The most common phases of PVDF are the α phase, where the polymer chains exhibit the $tgtg^+$ configuration and the β phase, where the polymer chains exhibit the $tttt$ configuration.

7.1 Applications of PVDF

Fluorinated polymers are materials best suited for transport and containment of fluids due to their low surface energy. One clear example of use of these materials in a domestic use is Teflon®, a fluoropolymer widely used for the manufacture of non-stick cook ware. Compared to other perfluorinated polymers, which include polytetrafluoroethlylene (PTFE), ethylenetetrafluoroethylene (ETFE), PFA (a polymer of

tetrafluoroethylene and perfluorovinylether), and FEP (a polymer of tetrafluoroethylene and hexafluoropropylene). Compared to these polymers, PVDF has qualities of low melting temperature, lower density, better mechanical properties, higher coefficient of thermal expansion, and lower volume resistivity [80]. As a result, PVDF is widely used for building pipes to transport chemicals especially in the semiconductor industry, for jacketing of cables, membranes for biological cells and lithium batteries, and for petroleum applications (barrier layers and pipes). All of these applications require a material that will be non-toxic, free from contaminants (over time), and non-degradable. It is interesting to note that the ability of these materials to be used for electronic devices largely remains non-utilized. These applications include RAMs, NVRAMs, pyroelectric devices, and piezoelectric devices [52, 101, 102].

For display manufacturing, PVDF and its polymers are very attractive, mainly due to the following reasons:

- **Ferroelectricity:** The charge distribution can be manipulated to realize various display architectures. Also, it allows for the development of optical data storage devices. These applications and their working will be discussed in greater detail in the following sections.

- **Low melting point:** PVDF and its polymers have a melting range of 134 - 180°C. These temperatures are suitable for ITO-coated glass and flexible polymer sheets. One of the new directions for display technology is to develop flexible displays. These devices will replace ITO-coated glass by ITO - PET sheets or a suitable polymer. A melting point for the alignment layer that is very high is detrimental to the ITO - PET substrate.

- **Free from contaminants:** Nothing hurts a working LC display (LCD) more than contaminants. If the alignment layer introduces defects over time, the LCD response will degrade through observation of dead pixels and/or slow switching

response.

- **Uniform alignment:** If uniformity is absent in LC alignment, then the material used is not an alignment layer. Virtually any material can be studied for LC alignment and the literature is abundant with such discoveries. However, alignment should persist at large scale dimensions to be considered as a decent candidate for opposing the existing materials. PVDF and its copolymers, P(VDF - TrFE) in a 65/35 ratio in particular, have exhibited uniform LC alignment at length scales of over 1mm.

- **Optically clear films:** Every alignment layer should be as transparent as possible. This is to prevent any color losses or color variations through pixels in LCDs. PVDF and its copolymers form optically clear films when mixed with appropriate organic solvents.

All the above-mentioned results make PVDF and its polymers suited for the study of LC alignment, to develop displays and other electro-optic devices. In the following sections, we shall take a look at the different phases in ferroelectric polymers, the processing techniques that can be used to obtain the desired phase, and experimental details.

7.2 Phases of PVDF

In its solid state, PVDF has shown the existence of four different phases or polymorphs. These are classified as α, β, γ, and δ for Form II, Form I, Form III, and Form IV respectively. The numerical classification is to list the phases in the order of their discovery [53]. The most common of these phases is the α phase, which is formed by cooling the polymer film from the melt. The crystal structure of the α phase for PVDF is shown in Figure 7.1.

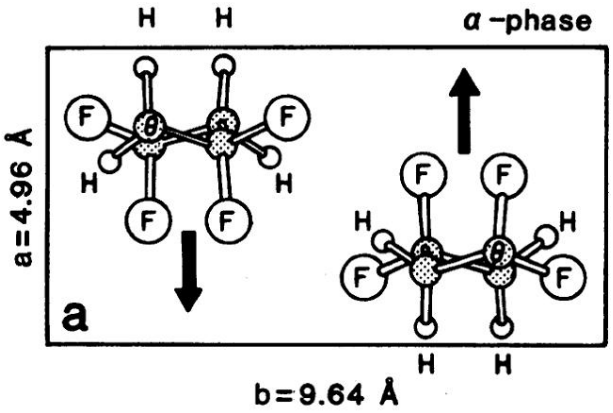

Figure 7.1: α Phase of PVDF. From [2]

The α phase has a $tgtg^+$ polymer chain conformation. In terms of dipole interactions, the chain conformation for the α phase results in a cancellation of the charges. Hence, this phase is considered as the non-ferroelectric phase. The lattice dimensions of the α phase are: a 4.96Å, b = 9.64Å, and c = 4.96Å.

The β phase of PVDF is the most polar of all the phases where the polymer has an all-trans *tttt* conformation. The structure for the β phase is shown in Figure 7.2. Due to the chain conformation, the dipoles are all uniformly oriented in the same direction. This phase is a thermodynamically stable phase, and the dipole orientation can be manipulated using several techniques. Hence, the β phase of PVDF is also known as the ferroelectric phase, which has unit cell dimensions of a = 8.58Å, b = 4.91Å, and c = 2.55Å. Only the β phase in PVDF allows for a controllable manipulation of the dipoles. Within the α phase, the dipoles are randomly oriented and hence limiting the control over the charge orientation for any application.

Application of electric fields to the α phase could result in a polar phase, which is classified as the δ phase. The δ phase is known to exist if the electric field used for poling has a value of 100V/μm. If the field applied approaches 500V/μm, the δ phase is converted to the β phase of PVDF [53]. Since the δ phase is the polar analog

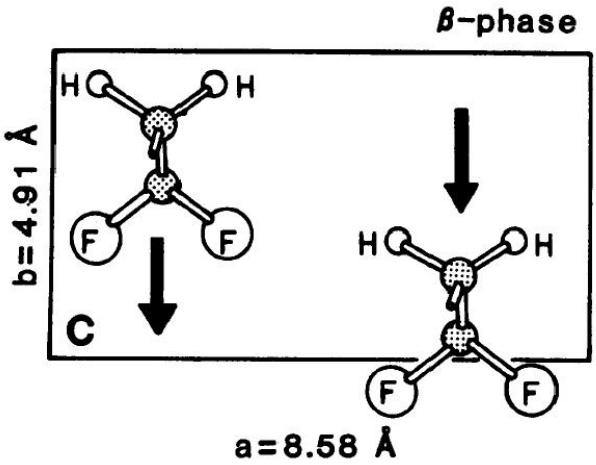

Figure 7.2: β Phase of PVDF. From [2]

Table 7.1: Phases of PVDF

Phase	**Properties**
α Phase	Non-ferroelectric
β Phase	Ferroelectric Phase
γ Phase	Small Polarization
δ Phase	Polarized version of α Phase

of the α phase, its lattice dimensions are the same as that of the α phase. Figure 7.3 shows the structure of this phase.

The γ phase of PVDF has the $tttg^+tttg^-$ chain conformation, which has a small polarity associated with it. The only methods of obtaining it are through crystallizing the polymer at a high temperature or by solution casting it from dimethylacetamide (DMA) or dimethylformamide (DMF). Its unit cell has the spacing of a = 4.96Å, b = 9.58Å, and c = 9.23Å. At the time of this writing, no practical application demands the γ phase in PVDF, and hence it is not widely investigated.

We have summarized the properties of these phases in Table 7.1.

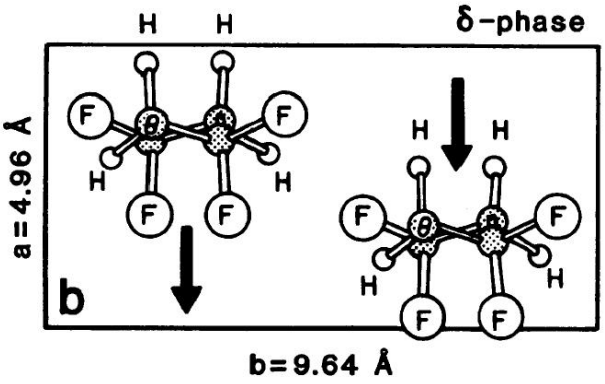

Figure 7.3: δ Phase of PVDF. From [2]

7.3 Importance of the β phase

Of all the phases of PVDF, the β phase remains the most important for the development of next generation electronics. The ferroelectricity of this phase manifests in an ideal remnant polarization of 130mC/m^2. Considering that 50% of the polymer is crystalline, the measured value of remnant polarization is 60mC/m^2. Ferroelectricity also implies that the polarization direction can be reversed using an electric field in the opposite directions. This property is useful for data storage, where the polarization direction can be used to record the data bits. Additionally, the β phase also exhibits large piezoelectric and pyroelectric constants, which are useful for the development of devices such as sensors and transducers. For display engineering, the β phase allows for the possibility of coupling the polymer dipoles to LC molecules. Their interaction can be used to create LCDs with defined pre-tilt, which is stable over a large time periods. Such a display will have stable alignment, uniform picture quality, and faster switching response. A stronger coupling between the dipoles of the polymer and LC could be used to develop optical data storage devices.

The β phase in PVDF is very important from a research perspective mainly due to the opportunity of charge manipulation in a polymer. However, in PVDF films, the

α phase is the most commonly formed phase. In order to obtain the β phase, one or more processing techniques have to be implemented. Typically, the polymer films are annealed to improve the crystallinity and also to minimize defects. Annealing refers to cooling the PVDF films from melt to either room temperature at a predefined rate. This process by itself is not sufficient to cause α phase transition to the β phase. In addition to improving the film qualities, it does lead to the γ phase. For the β phase, annealing is typically followed by either drawing under tension, stretching of the films, high-pressure treatment, and electric poling to obtain the β phase.

These methods are described in the following pages. At the end of each description, I have provided reasoning whether it can be suitable for the experiments performed in this thesis.

- **Stretching:** This is one of the most widely used techniques, which requires the PVDF film to be stretched under a constant load at room temperature. The film must be formed by a slow annealing (10 - 20°C/min) procedure from the melt. After annealing, it is possible that the film is not in the α phase but rather in the γ phase. The stretching procedure is also sufficient to result in the β phase. Though the technique is simple to implement, it is not optimal for obtaining a β phase film with uniform dipole orientation. Also, our devices require alignment layers that have a thickness ranging from 100 - 500nm. The thickness limits reliable techniques to strip the films for stretching after they are spin-coated. Assuming that a method allows for stripping these films, stretching them could easily lead to mechanical defects such as tears and result in large values of surface roughness. Mounting the films to fabricate LCDs would also be a tremendous challenge. Hence, our films were not stretched to obtain the β phase.

- **Rolling:** As the name suggests, a freestanding film is rolled under a specified

force and speed to obtain the β phase. Like stretching, rolling also generates the unoriented β phase in PVDF. Also, for our work, the disadvantages associated with stretching also apply to rolling and it was not used for this study.

- **Solvent-based techniques:** One of the methods is called solution casting, which requires the polymer powder to be dissolved in solvents such as polar hexamethylphosphorictriamide (HMPTA) or dimethylacetamide (DMA). The solution is then cast or precipitated to form a thick film, which is found to exhibit the β phase. Another approach is to crystallize the film from a 0.02% boiling cyclohexanone solution. All of these approaches work well for thick films, which do not need to be optically clear. Generally, the films formed through solution casting are opaque in nature making them unsuitable for fabrication of LCDs. Also, in the case of casting the film from a boiling cyclohexanone solution would render this technique out of contention for developing flexible displays.

- **Quenching:** Rapid quenching of polymer films into a liquid nitrogen reservoir has also been shown to result in the ferroelectric phase. This is one of the approaches that could work for displays with possibly posing as a problem for flexible displays due to fracture of the polymer films such as Indium tin oxide (ITO) coated on Polyethylene terephthalate (ITO-PET) films. One drawback this technique poses for manufacturing is the expense and storage tanks for the liquid nitrogen treatment. Another modification for the conventional quenching technique is to perform it while keeping the polymer film under high pressure.

- **Electric poling:** This method calls for the application of high electric fields to the polymer film. Electric fields of value greater than 100V/μm are able to rotate the dipoles in the polymer such that they align parallel to the field direction [103]. Upon field removal, the dipoles stay in the aligned position resulting

in the ferroelectric β phase of PVDF. This is a very common technique and easy to implement for any application requiring a uniform β phase. Electric poling can be performed at room temperature as well as at elevated temperatures. For the latter case, annealing and electric poling are performed simultaneously in order to rotate the dipoles from the melt state itself. This method is suitable for mass production, is not invasive to the samples and consumes low power as the process requires low currents (μA) for operation. Hence, it has been investigated in a modified form of corona poling for our studies.

- **Material composition:** One of the easiest methods to introduce ferroelectricity is to change the material composition of the polymers. Addition of chemicals in forms of copolymers and doping PVDF with materials including nanoclay is known to influence the phases of this material. Since the polymer chain is quite flexible (the trans and gauche bonds are statistically equal), the new particles can force certain chain conformations. One such example is the addition of trifluorethylene (TrFE), a common copolymer for PVDF. The TrFE atoms prevent the $tgtg^+$ conformation of PVDF while forcing the $tttt$ conformation. Numerous other copolymers are being investigated. Apart from improving the ferroelectricity, other reasons include the improvement of piezoelectric coefficient, changing the phase transition temperatures, and improving the dielectric properties of PVDF.

7.4 Morphology

An optical microscope was used to study the polymer morphology. Specifically, two modes of the microscope were used; polarized microscopy mode and the phase contrast mode. Polarized light microscopy refers to a mode where the sample is imaged under crossed polarizers of a microscope. This mode allows for imaging of birefrin-

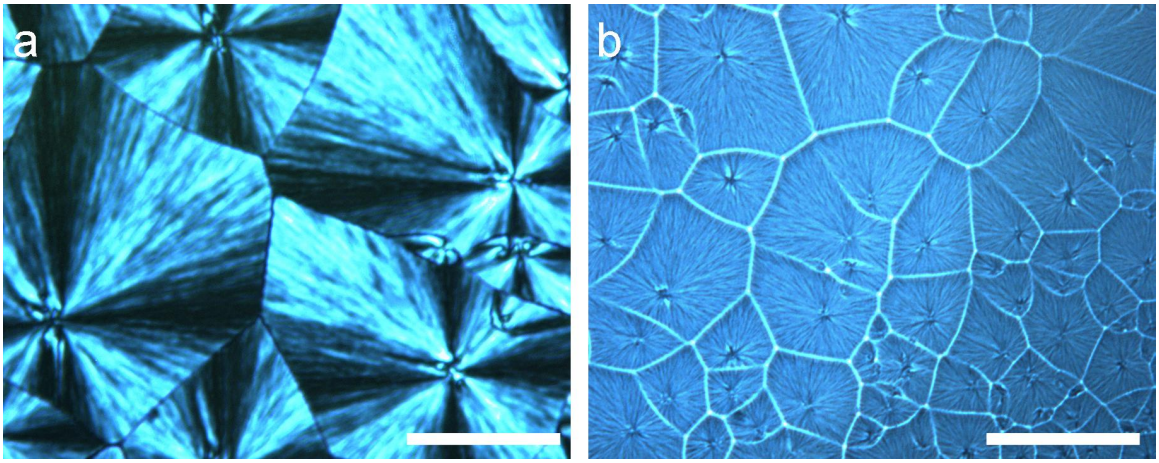

Figure 7.4: Spherulites of PVDF. The scale bar represents 50μm.

gent materials. The phase-contrast imaging mode allows for better identification of variations in the refractive index across the sample area.

The homopolymer films generally demonstrate a morphology, which is characterized as spherulites as shown in Figure 7.4.

Spherulites refer to a radial, lamellar growth of the polymers when crystallizing from the melt. In PVDF films, the spherulites represent the crystalline portion of the polymer chains [53]. The chain growth is initiated from certain nucleation sites from which the radial growth proceeds. PVDF molecules are oriented perpendicular to the the surface of the lamellae. A spherulite will grow its boundaries till it impinges on those from a neighboring spherulite. Figure 7.4b indicates the core of each spherulite, from where it nucleated. It also highlights the boundaries of each spherulite.

If the polymer-solvent mixture is not ideal, films which exhibit poor wetting are observed as shown in Figure 7.5.

The copolymer films of P(VDF - HFP) also exhibit the spherulite morphology. However, the diameter of the spherulites is much smaller when compared to those of the homopolymers. The copolymer films of P(VDF - CTFE) exhibit a morphology

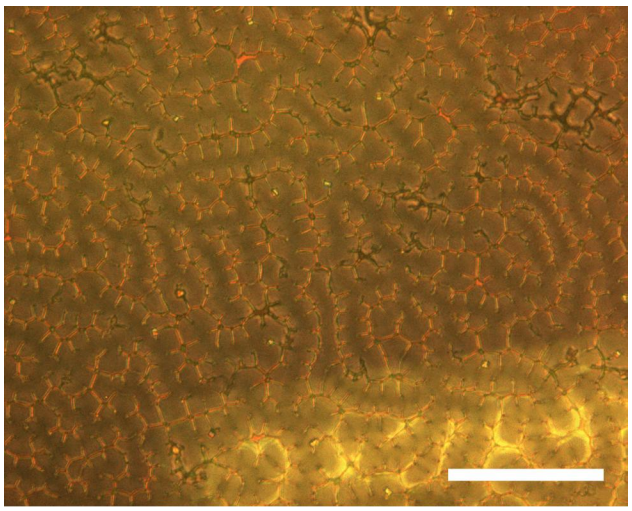

Figure 7.5: Poor wetting in PVDF Homopolymer Film. The scale bar represents 50μm.

which seems as if the spherulite growth had initiated but the large number of nucleation sites prevented any further growth. This is as shown in Figure 7.6. Finally, the copolymer films of P(VDF - TrFE) have exhibited a featureless morphology as shown in Figure 7.7. The morphology of the film can be related to the phase of the polymer film. Generally, the α phase of the polymer is associated with the presence of spherulites [53]. P(VDF - TrFE) films in a 65/35 ratio have always shown a large ratio of β phase components [53, 104].

For films were also prepared with the addition of nanoclay platelets, the morphology of the homopolymer films changed completely. These films never exhibited spherulites, and their morphology exhibited a distribution of particles as will be discussed later in the chapter. The only difference in these films was the presence of nanoclay platelets, which are known to aggregate within the polymer and induce a specific ordering (intercalated) of the PVDF chains [79, 105–107]. As a result, the PVDF chains arrange such that a stronger ferroelectric phase is obtained.

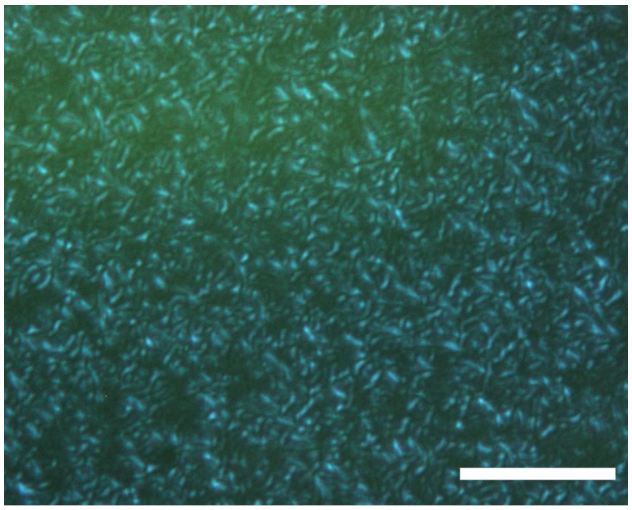

Figure 7.6: Morphology of P(VDF-CTFE) films. The scale bar represents 50μm.

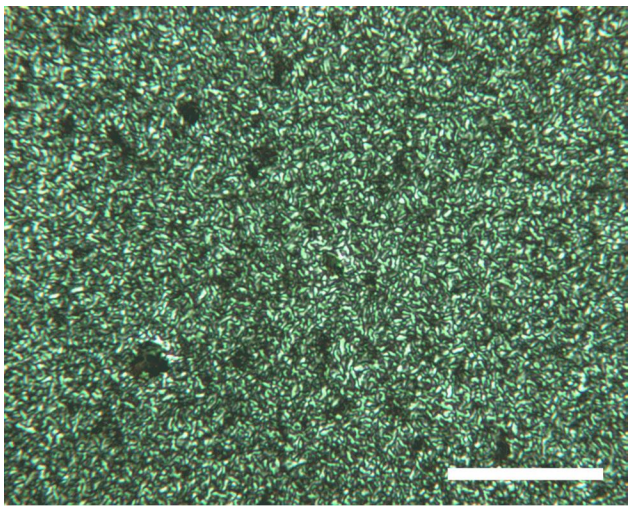

Figure 7.7: Morphology of P(VDF-TrFE) 65/35 film. The scale bar represents 50μm.

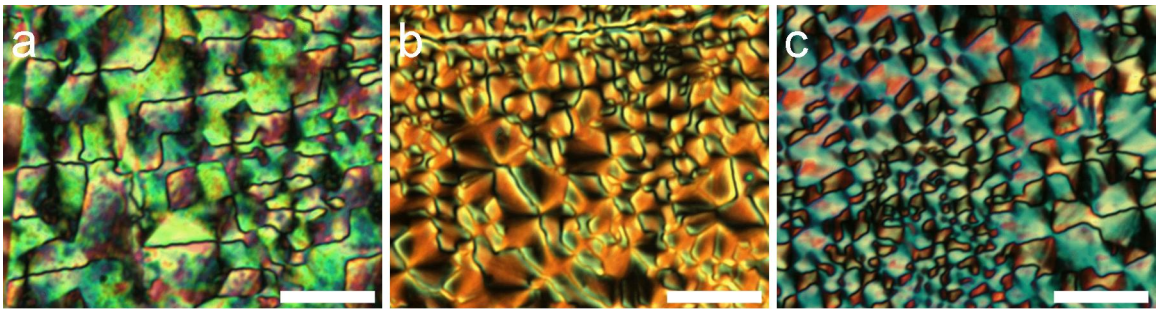

Figure 7.8: LC wetting on P(VDF-HFP) films. The scale bar represents 50μm.

7.5 Liquid Crystal Alignment and Switching

Surface wetting experiments performed by depositing LC on the PVDF films demonstrated complete wetting (wetting angle ∼0 degrees) signifying planar alignment of the LC. A CCD camera in conjunction with a computer was used to capture the images. The LC alignment will show variations that map the charge domains in the ferroelectric polymer. This technique called the domain visualization technique has been used to study the domains in ferroelectric crystalline materials including triglycinesulfate and lead-zirconate titanate [54].

Figure 7.8 shows the LC wetting on PVDF homopolymer films as observed through the crossed polarizers of a microscope. The transmitted intensity observed through crossed polarizers depends on the orientation and the elevation of the LCs on the substrate [84]. Each color in Figure 7.8 corresponds to the orientational and pretilt angles of the LCs on the substrate. Thus the LC alignment provides an optical visualization of the microstructure-like arrangement of dipoles on the surface of the film. In some areas, the LC wetting indicates domain boundaries in PVDF as shown in Figure 7.9 To observe the change in the LC alignment as a function of applied voltage, an electric field was applied through the thickness of the cell. An Agilent function generator supplied a square wave signal to the LC cell operating at a frequency of 1

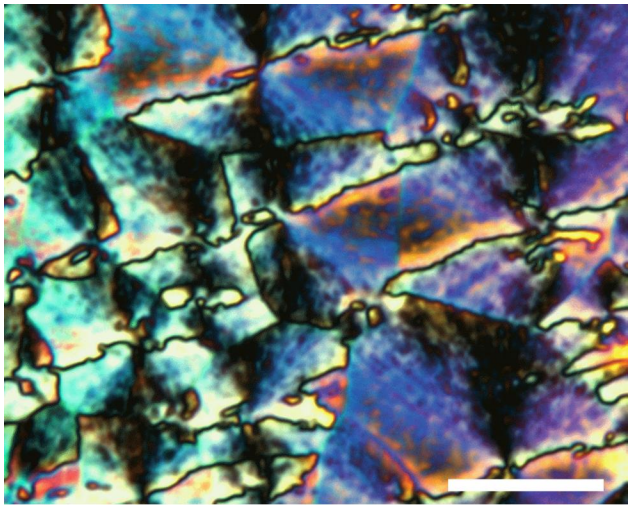

Figure 7.9: Domain boundary in PVDF as indicated by LC alignment

kHz. Figure 7.10 shows the wavelength progression in the cell as observed through crossed polarizers.

Due to the dielectric anisotropy of the LC, the external electric field exerts torques on the LC molecules changing their orientational angles, causing them to rotate in the direction of the applied field. As the molecules rotate to align themselves parallel to the applied field, the polarized light from the microscope experiences different birefringence magnitudes. The physical interaction between the PVDF films and the LC can be approximated for the surface LC layers using dipole-induced dipole interaction and can be represented as: [108]

$$w(r) = -\frac{\vec{u_1}\vec{u_2}}{4\pi\epsilon_0 r^3}[2\cos\theta_1\cos\theta_2 - \sin\theta_1\sin\theta_2\cos\phi] \tag{7.1}$$

where $\vec{u_1}$ and $\vec{u_2}$ are the respective dipole moments, θ_1 and θ_2 are the elevation angles of the dipoles, and ϕ is the azimuthal angle ofthe induced dipole. Figure 7.11 illustrates the dipole-induced dipole interaction. The PVDF dipoles are permanent

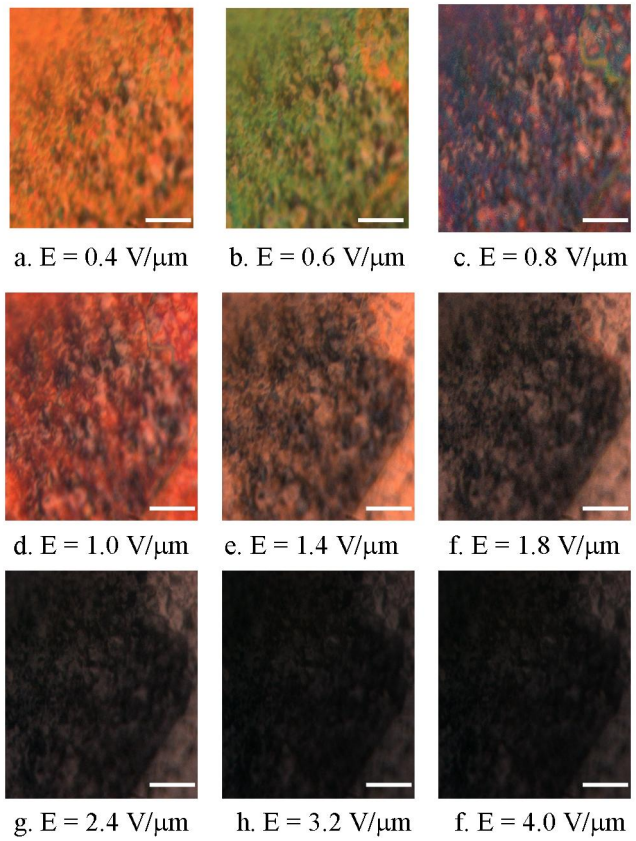

Figure 7.10: Visible wavelength progression due to liquid crystal switching on PVDF films. Scale bar represents 50μm

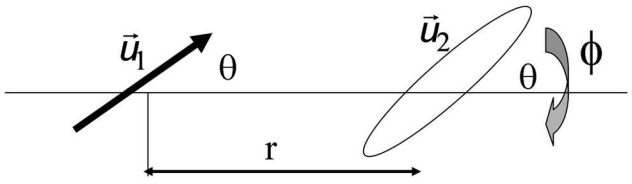

Figure 7.11: Dipole - induced dipole interactions

dipoles whereas the LC, being a non-polar material, leads to a freely rotating induced dipole. Since the polymer polarization is fixed, the LC will rotate in azimuthal and elevation directions until reaching an equilibrium state where the interaction energy is minimized. The surface LC alignment however propagates into the bulk via long-range interactions between the LC molecules. It must be mentioned that the polarization by itself would not be able to influence the LC alignment, especially on a smooth film. The polymer morphology would lead to fringe fields that would be able to interact with the first few monolayers of LC on the surface. Thus, an applied electric field will face competition with the surface anchoring of the LC. As a result, a variation in the transmitted intensities and colors is observed through crossed polarizers as shown in Figure 7.10. The wavelength progression has been observed for LC switching on all films used including copolymers of PVDF. It must be also noted that most of the voltage drop is across the LC layer, and there is no ferroelectric switching in the polymer layer. The maximum voltage applied across the 5μm cell was 20V_{pp} at 1kHz. Using the R-C equivalent circuit for the sandwich cell schematic, the voltage drop across the polymer layer is given by: [54]

$$|V_{PFE}| = V_0 \Big/ 1 + \left[\frac{\epsilon_{PFE} t_{LC}}{\epsilon_{LC} t_{PFE}}\right] \tag{7.2}$$

where $|V_{PFE}|$ is the voltage dropped across the ferroelectric polymer layer, V_0 is the applied voltage, ϵ_{PFE} and ϵ_{LC} are the dielectric permittivities of the polymer and LC layer, respectively, and t_{PFE} and t_{LC} are the respective layer thicknesses. Considering the effective value of dielectric permittivity for the LC layer, we get:

$$\epsilon_{LC} = \frac{2\epsilon_{\perp} + \epsilon_{||}}{3} \tag{7.3}$$

Using value of 6 for $\epsilon_{\perp}$ and 26.1 for $\epsilon_{||}$, we get the value of ϵ_{LC} as 12.67 [109]. The

range of ϵ_{PFE} varies from 9 to 12 at room temperature for the different PVDF samples [80]. Using equation (2), we get $|V_{PFE}|$ to range from 0.81 V to 1.35 V implying that almost 90% of the applied voltage is dropped across the LC layer. The electric field across the polymer layer ranges from 4.1V/μm to 6.75V/μm. These magnitudes are much lower than the 100V/μm minimum required to switch the dipoles in the polymers [78, 103] which indicates that the external electric field influences only the LC molecules.

In order to map the wavelength response as a function of the applied electric field, spectrometry measurements were performed using a crossed-polarizer configuration on the LC-PVDF cells. A halogen lamp source (Ocean Optics tungsten halogen lamp, λ = 300 - 800 nm) supplied white light, which was spatially filtered before incidence on the first polarizer. The light was fed through an optical fiber to the cell placed between crossed-polarizers, following which it was delivered to a 600μm core diameter fiber connected to a spectrometer (Ocean Optics USB2000 spectrometer, resolution = 0.36 nm, wavelength range 300 - 800nm).

Figure 7.12 shows the transmission of 650 nm (red), 532 nm (green), and 450 nm (blue) wavelengths transmitted through two LC cells with PVDF and P(VDF-HFP) films, respectively, as the alignment layer. The variations in the visible wavelengths transmitted through the cell as a function of applied electric field can be clearly observed. Figure 7.12c compares the intensity progression in the two cells as a function of electric field. The intensity was calculated using the following formula used for image reproduction in displays:

$$\mathbf{I} = 0.3\mathbf{R} + 0.59\mathbf{G} + 0.11\mathbf{B} \tag{7.4}$$

where $\mathbf{I}$ is the intensity, and $\mathbf{R}, \mathbf{G}$ and $\mathbf{B}$ represent red, green, and blue wavelengths. The intensity progression can be described as starting from an initial value (P1) until

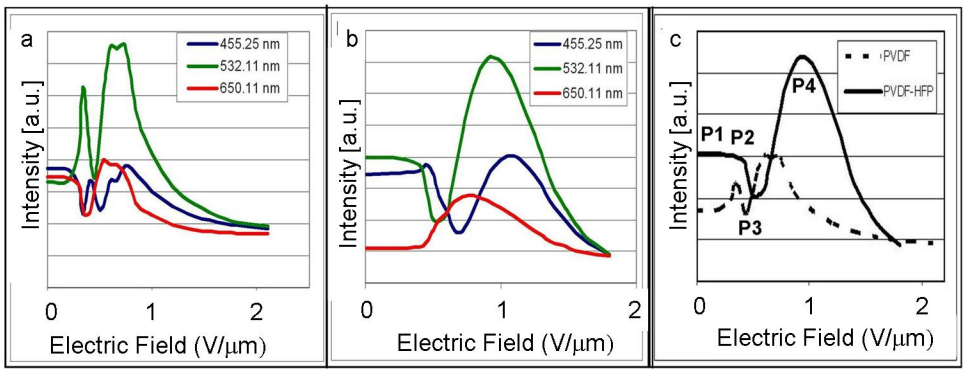

Figure 7.12: Spectrometry response of Red (650.11 nm), Green (532.11 nm) and blue (455.25 nm) as a function of electric field. a) PVDF homopolymer is the alignment layer, b) P(VDF - HFP) is the alignment layer, and c) Intensity v/s electric fields for LC on PVDF, and on P(VDF HFP).

it reaches a certain state (P2), followed by a decrease to local minima (P3), after which it rises to the maximum intensity (P4) before dropping to the cell OFF state. This progression is true for LC switching on any of the PVDF films as the alignment layer, and the cell switches OFF at a magnitude of $\sim$2V/μm. MATALB analysis was also performed on the spectrometry data to better understand the switching phenomena. The intensity of light transmitted through a LC material placed between crossed polarizers is described as:

$$I = I_0 \sin^2 \phi \sin^2 \delta \tag{7.5}$$

$$\delta = 2\pi(\Delta n)d/\lambda \tag{7.6}$$

where I_0 is the measured intensity of light transmitting through the crossed polarizers, ϕ is the azimuthal angle of the LCs, δ represents the phase delay experienced by light, which depends on d the cell gap, λ is the wavelength of light, and Δn is the

birefringence of the LC.

The switching response shown in Figure 7.12 can be divided into three regions. In the first region, the applied voltage is very weak such that a constant intensity of light is measured by the spectrometer. In the second region, the applied field faces competition from the polymer surface to affect the LC molecules. As a result, the LC molecules do not follow the field direction but instead, they also experience an azimuthal shift in their motion. In this region $\phi \propto V$ and $\Delta n \propto 1/V$ where V is the applied voltage. The third region is where the applied field completely overcomes the surface forces and the LC molecules follow it linearly. In this case, the ϕ variations are eliminated and only Δn variations contribute to the reduction in light intensity. The transition is shown in Figure 7.13. Variations observed between the switching trends of LC on the different films are due to the different surface charge magnitudes of the polymer in the different PVDF formulations. The maximum rise time and fall time observed are ∼3.5msecs and ∼1.5msecs respectively. For dynamic displays, switching times less than 10msec are ideal indicating the suitability of PVDF for display manufacturing purposes. The switching response of PVDF-HFP films is shown in Figure 7.12b. By comparing Figures 7.12a and 7.12b, it can be observed that the LC alignment is not completely uniform and the switching follows the quadratic response for intensity switching in LCs. $\mathbf{I} \propto \mathbf{E}^2$ where $\mathbf{E}$ is the magnitude of the applied electric field and $\mathbf{I}$ is the intensity of light measured through crossed polarizers.

Also, the electric field required to switch off the displays is higher by 1V/μm compared to commercial LCDs. The techniques that can be used to overcome these disadvantages include changing the material composition, physical modification of the polymer film using rubbing, and poling the polymer film to enhance the β phase. Rubbed PVDF films has shown excellent alignment uniformity and a more controllable wavelength progression [110]. In the next section, we present the results of changing the polymer film composition through the addition of nanoclay.

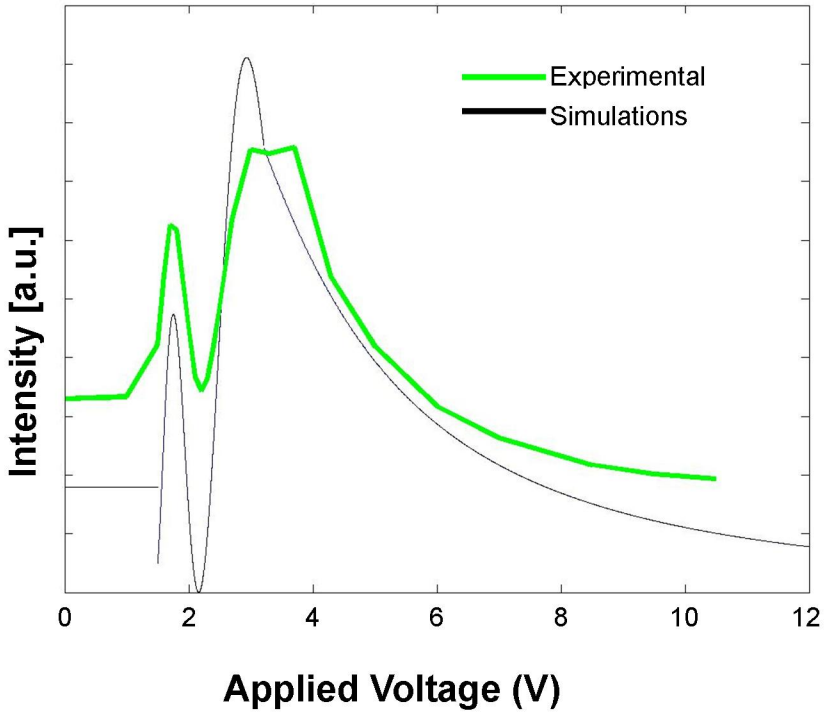

Figure 7.13: Tracking the wavelength response in PVDF-LC cells. I is the region when the applied voltage is too small to affect the LC, II is the region where the external voltage faces competition from the ferroelectric polymer resulting in ϕ variations of the LC, and III is the region where the external voltage completely influences the LC.

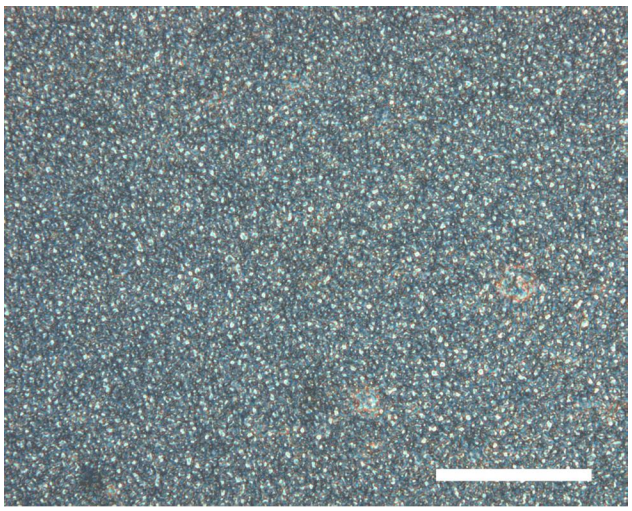

Figure 7.14: Morphology of PVDF - Nanoclay film. The scale bar represents 50μm.

Optically clear films of polymer - nanoclay composites were obtained through the spin-coating and annealing processes. Under crossed polarizers, the morphology of the polymer films appears as shown in Figure 7.14. In terms of morphology, the films are quite uniform. The reason for this uniformity is attributed to the disruption of the chain folding process by the nanoclay platelets. Other studies explained the change in polymer chain ordering resulting in the β phase [79, 105–107].

As a result, the LC alignment on these films shows more uniformity compared to the films without nanoclay. The alignment of LCs on P(VDF - CTFE) films is shown in Figure 7.16. LC alignment on such films will map the uniformity of the charge distribution, and the resulting LC textures should exhibit minimal defects. Figure 7.16 shows the LC alignment on a P(VDF - CTFE) film which was doped with nanoclay (25A). The LC alignment is much more uniform than previously observed (Figure 7.8). If the LC alignment is uniform, a reduction in the switching electric field is expected. Figure 7.15 compares the switching of LC on a P(VDF - CTFE) film with one which was doped with nanoclays. The wavelength progression observed in these devices is more controlled as opposed to that observed in the spin-coated films.

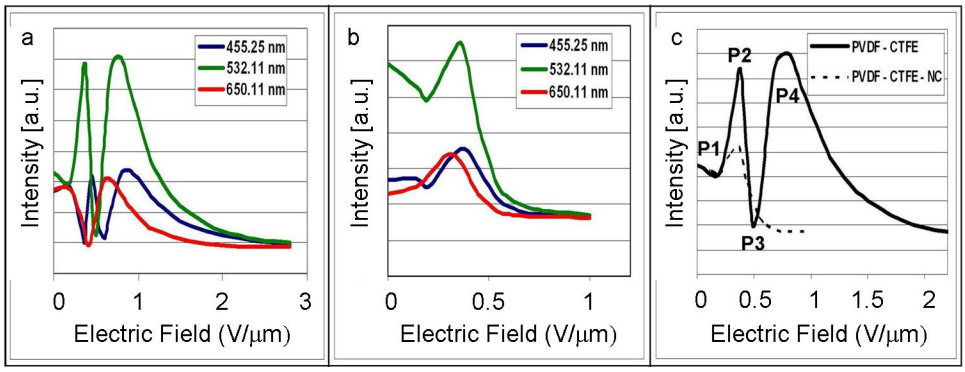

Figure 7.15: Spectrometry response of Red (650.11 nm), Green (532.11 nm) and blue (455.25 nm) as a function of electric field. a) P(VDF-CTFE) is the alignment layer, b) P(VDF-CTFE) Nanoclay composite film is the alignment layer, and c) Intensity v/s electric fields for LC on P(VDF-CTFE) and on P(VDF-CTFE) Nanoclay composite film.

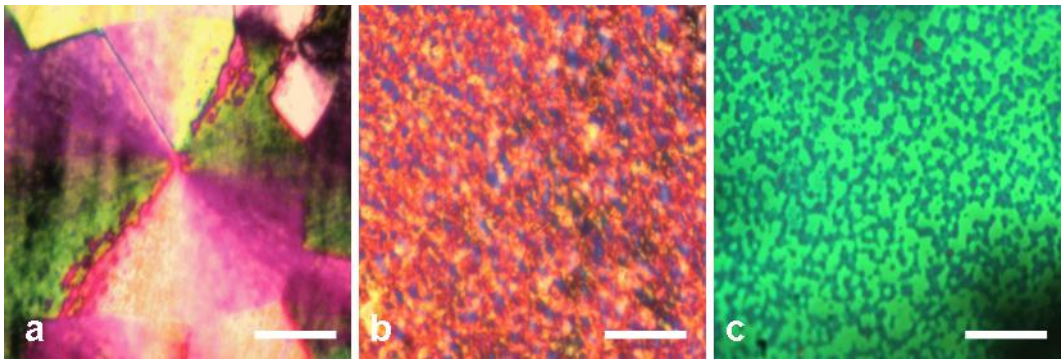

Figure 7.16: Polarized Optical Images of LC alignment on a) PVDF film b) PVDF - Nanoclay film, and c). P(VDF-CTFE) - Nanoclay film. The scale bar on all images represents 50μm. The blue spots in b) and c) are the clay aggregates.

Ferroelecricity implies an ordering of the dipoles causing a build-up of an internal electric field. In these cases, an applied external electric field has to overcome the internal field before it can affect the LC molecules. As a result, it leads to a linear electro-optic response, which is similar to what we observe in Figure 7.15 [55]. Also, the switch OFF voltage in these devices is ∼3V or an electric field of 0.6V/μm. This is an improvement of approximately 300% over 2V/μm required in the previous devices. Thus, changing the alignment layer material composition can have significant effects on the response of the device. Laptops have an internal dc source of 1.2V for operating transistors and other elements in the computer processors. Commercial displays are also manufactured using a 2μm thickness for the LC layer. Thus, the switching field of 0.6V/μm is compatible with the internal source in laptops. Most notably, the operation of the LCDs manufactured is with 5CB, a generic and inexpensive LC. Commercial LCD products use custom-made LCs that are not only expensive but also available in small quantities due to the difficult synthesis process. Thus, PVDF - nanoclay composites are suitable for replacing alignment layers and color filters in LCDs for a variety of applications.

7.6 Rubbed Ferroelectric Polymer Films

So far, we have discussed the electro-optic performance of the LC on polymer films, which did not undergo any post-baking processes. In this section we present the effects of rubbing P(VDF-TrFE) films in a 65/35 molar ratio. After baking, the P(VDF-TrFE) films were rubbed using a cloth-based rubbing machine. The polymer film exhibits uniform morphology with no discernible features after rubbing, as shown in Figure 7.17 [110]. The sandwich cell had the rubbed films present on both ITO-glass slides. The resulting variation in the transmitted intensities and colors due to LC switching is observed through crossed polarizers as shown in Figure 7.18. The

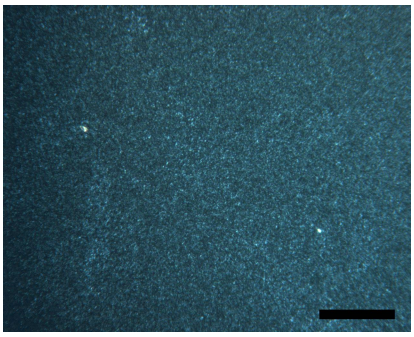

Figure 7.17: Morphology of a rubbed P(VDF - TrFE) 65/35 film

wavelength of light is uniform across a larger sample area and also encompasses the visible spectrum, which is an ideal property for displays. The entire visible wavelength progression occurs at a magnitude below 1V/μm. At higher magnitudes, the transmitted light reduces in intensity, indicating increased alignment of the LC molecules in the direction of the applied field (z-axis). Multiple switching cycles reproduced the identical wavelength progression through the cell. This phenomenon is ideal for the manufacture of displays where the required visible wavelength can be generated by applying the corresponding voltage. Consequently, the display resolution will increase by 300% when compared to the conventional method of using three pixels to generate one color.

The variations in the colors transmitted through the cell as a function of applied electric field can be clearly observed. The cell switches OFF at a magnitude of $\sim$2V/μm. Variations observed between the switching trends of LCs on different films are due to the different surface charge magnitudes of the polymer in the different PVDF formulations.

From Figure 7.19, it is evident that the electro-optic response is more linear compared to the ones observed in Figures 7.12 and 7.15, highlighting the suitability of these polymer films for developing displays and color filters.

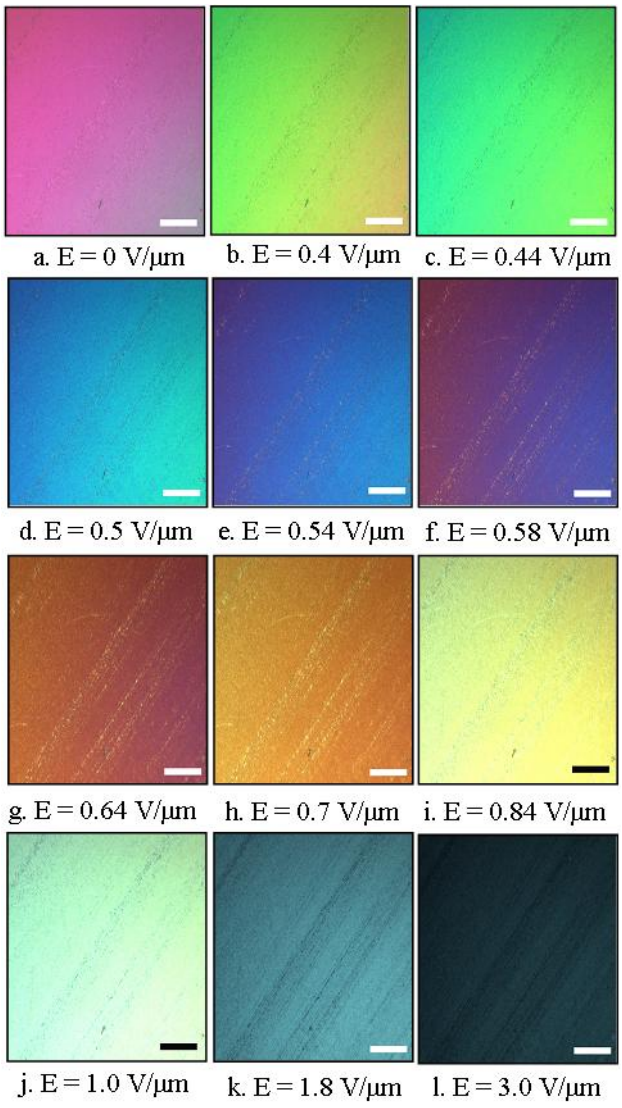

Figure 7.18: Visible wavelength progression due to liquid crystal switching on rubbed P(VDF TrFE) films. Scale bar represents 200μm

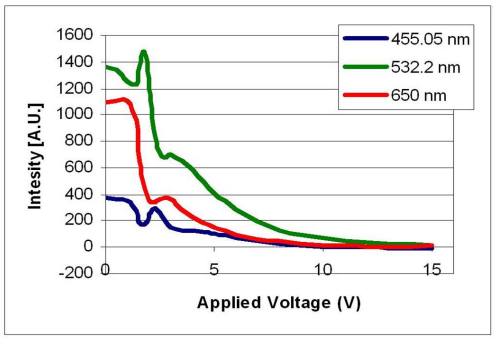

Figure 7.19: Transmission of 650 nm (red), 532 nm (green), and 450 nm (blue) wavelengths transmitted through the sandwich cell as observed with a spectrometer

7.7 Corona Poling

In this section, we describe the development of optical data storage elements using ferroelectric polymers and LCs. This application requires a medium that translates data into charge for writing purposes and an optical readout that varies as per the charge (data) magnitude. The ferroelectric polymer - LC system can meet the above requirements provided that uniform charge can be stored in the polymer. A schematic of the proposed device is shown in Figure 7.20. In this device, the polymer functions as the data (charge) storage layer. If the polymer had a uniform dipole orientation as shown in the left part of the figure, a deposition of LC alignment would lead to a vertically aligned state. The reason for such LC alignment is due to dipole-dipole interactions. In such a configuration, transmission of white light will result in the measurement of a definite color and intensity at the detector. If the dipole orientation is now switched such that it lies in-plane, the LC alignment will be planar. This is shown in the right side of the image. Such a configuration will lead to the measurement of a different color and intensity at the detector under transmission of the same white light. The two polymer orientations represent the orientations for data bits (1 and 0) while the LC alignment allows for optical readout of the stored

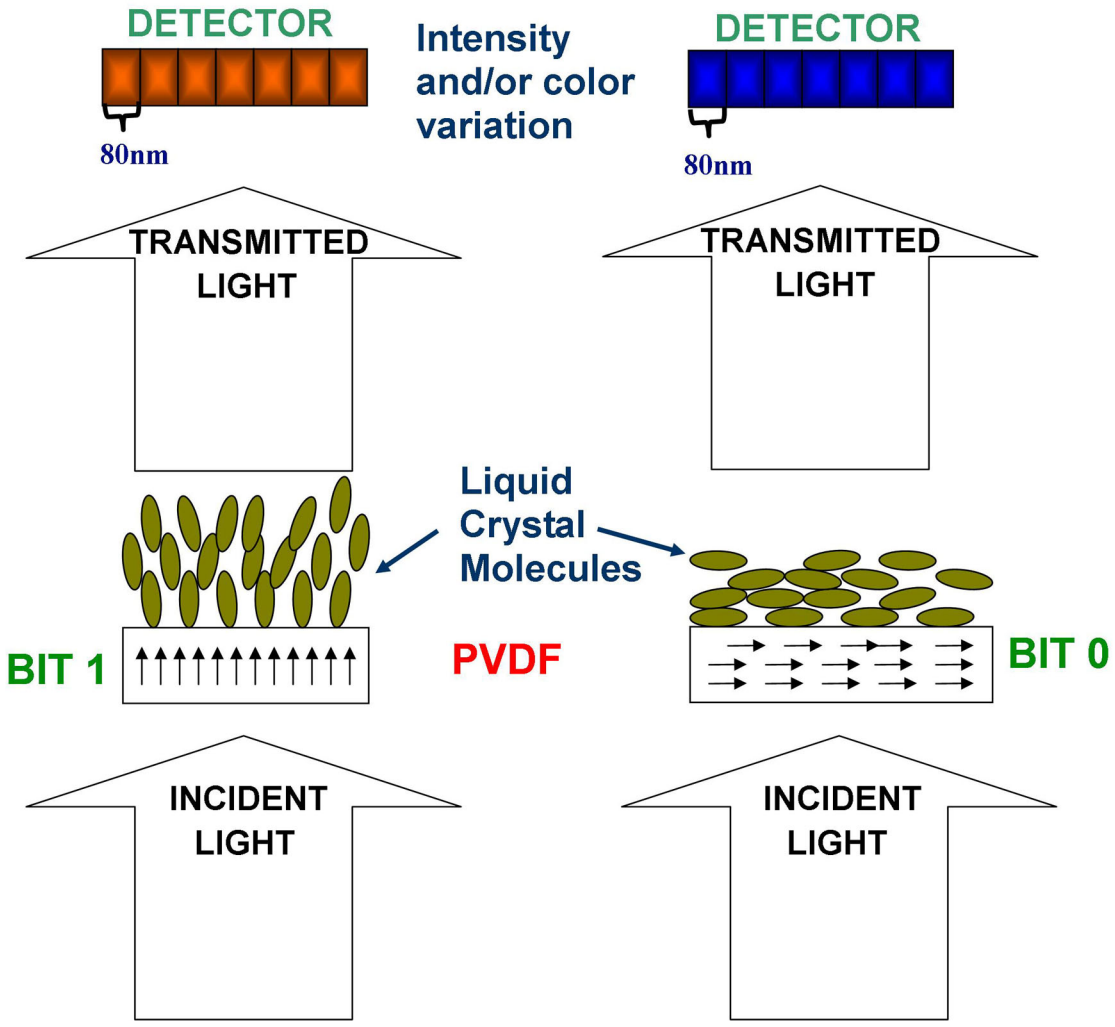

Figure 7.20: Schematic of the Optical data storage device. The ferroelectric polymer layer allows for data (charge) writing and the LC alignment provides the optical readout.

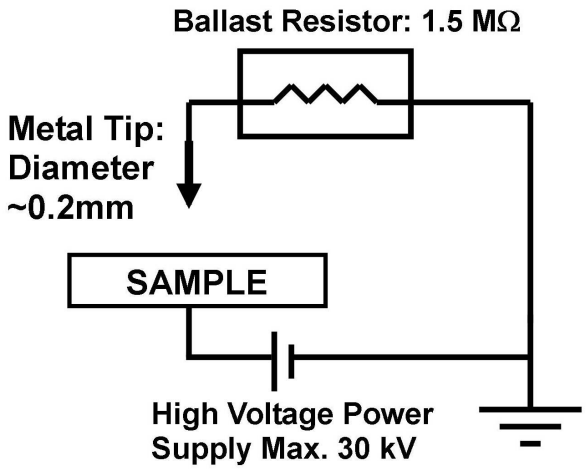

Figure 7.21: Schematic for the corona discharge. The metal tip is stationary while the sample is controlled by an X Y translation stage to facilitate horizontal scanning

data. Using a nematic LC for the optical readout places a limitation on the up and down states of dipole orientation because for the nematic state, the up and down states are the same. However, PVDF and its copolymers allow for rotation of the polymer dipoles in increments of 60 degrees [53]. The in-between orientations could be used to construct at least two optical states for data representation.

Uniform charge storage will require techniques including corona poling or electrical poling using an AFM to locally write charges oriented in a specific direction. We have selected corona poling due to the ease of operation, simplicity of set-up, and proven results of phase transition in the polymeric material used [55, 78, 111, 112]. The coupling to the LC layer will be through dipole induced dipole interactions. For our experiments, we have used a negative corona poling technique for writing charges. The experimental set-up is shown in Figure 7.21. The set-up uses a metallic pin measuring approx 0.2 mm in diameter as the corona discharge tip. The sample is the PVDF thin film coated on a conductive plane (Indium Tin Oxide, which has resistivity of 200Ω/sq). A negative voltage of magnitude 4 - 4.5kV is applied between

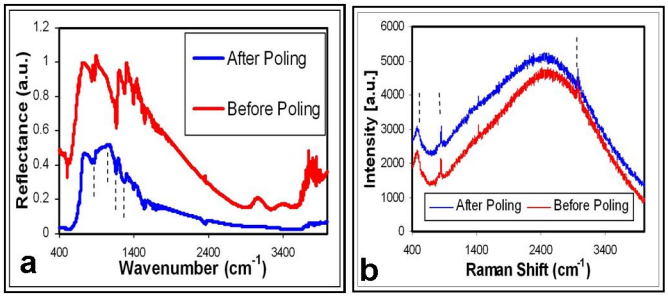

Figure 7.22: Phase Change due to Corona Poling. The images compare the spectra before and after corona poling. The piped lines show the β phase components. a) FTIR spectra of a P(VDF-TRFE) film, and b) Raman Spectra of a P(VDF-HFP) film.

the pin and the grounded sample to result in a glow discharge (approximate current: 5μA). Higher voltages resulted in arcing, which led to the degradation of the polymer film. The gap between the pin and the sample is $\sim$2mm. In order to obtain charge patterns on the films, the samples were mounted on an X-Y translation stage, which facilitated scanning of the glow discharge.

FTIR and Raman Spectroscopy experiments were performed to verify the phase changes in the polymer films. Figure 7.22 shows the respective spectra corresponding to P(VDF - HFP) films and P(VDF - TrFE) films. In the films, which primarily exhibited the α phase, a phase transition to the β phase was observed due to corona poling. For the films, which exhibited β phase components before poling, there was an increase in their intensity after corona poling. After the corona exposure, the PVDF films exhibited absorption bands at $510cm^{-1}$ (CF_2 bending), $840cm^{-1}$ (CH_2 rocking), $1279cm^{-1}$ (CF out-of-plane deformation), and $2975cm^{-1}$ (CH_2 symmetric stretching) [113, 114]. Thus, corona poling enhances the β phase components in the polymer films. The effect of enhanced β phase is the result of an induced voltage in the polymer region [55]. Thus, corona poling enhances the β phase components in the polymer films. The effect of enhanced β phase is the result of an induced voltage

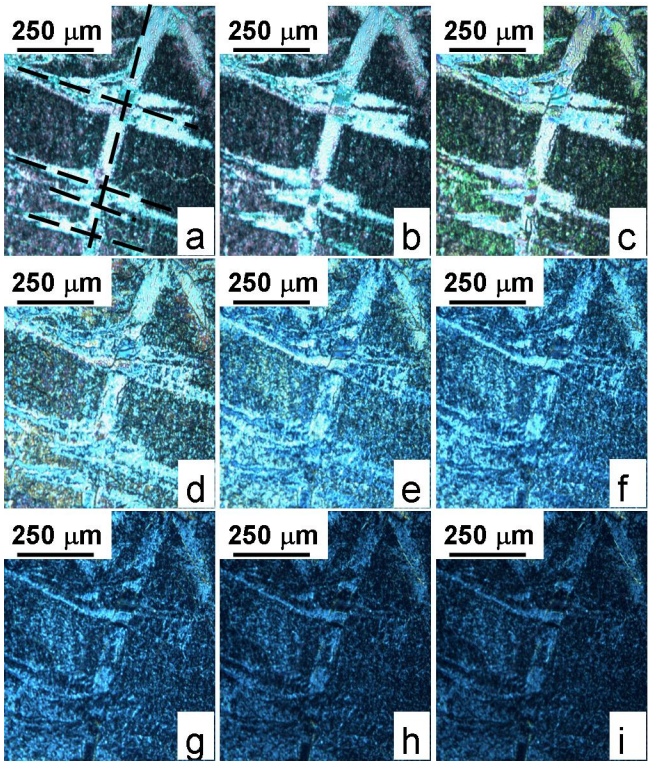

Figure 7.23: Switching transition of LCs on a charge patterned line. a: 0V/μm, b: 1V/μm, c: 1.2V/μm, d: 1.6V/μm, e: 2V/μm, f: 2.4V/μm, g: 3V/μm, h: 3.6V/μm, i: 4 V/μm

in the polymer region [55]. The oriented dipoles should regulate the LC alignment after its deposition.

Using the translation stage, a grid-like pattern was inscribed on a PVDF film by having multiple horizontal corona lines intersect a long vertical line. Figure 7.23 shows the switching of LCs on this charge-patterned region as observed through crossed polarizers. Compared to with Figure 7.10 and 7.18, no similar wavelength progression was observed on the corona exposed regions. Even on increasing the applied electric field to 1V/μm, the LC alignment did not vary from the initial state, which corresponds to no electric field. This is due to the internal field assembled in the polymer layer, which the external field has to overcome in order to influence the LC layer.

On further increasing the applied electric field, the transmission of light through the cell decreases with the applied field. However, even at 4V/μm, the cell does not switch completely off. The LC state in the corona patterns is still visible, albeit faint in comparison to the initial state at 0V/μm. The results obtained here differ from one previous report mainly due to the thickness scale of the polymer films [55]. The polymer layers are spin-coated in our experiments whereas Langmuir-Blodgett films were used in the previous study.

Ferroelectric polymers are characterized by a distribution of dipoles within their layers. In the polymer films obtained directly after the spin-coating process, ferroelectricity exists albeit randomly. Consequently, the LC experiences a lesser magnitude of dipole-dipole interactions with the polymer. Also, due to ferroelectric domains, the LC alignment tends to vary through the length of the polymer films.

Corona poling causes an increased alignment of the dipoles in PVDF films resulting in enhanced ferroelectricity in the film in addition to the development of an internal electric field in the polymer layers. Consequently, when LC is deposited on poled ferroelectric films there is an increased interaction with the polymer dipoles. This phenomenon results in an alignment state that is much more uniform as compared to the one on unpoled films. Also, on application of electric fields to the configuration, the internal field developed in the poled polymer layers needs to be overcome before it affects the LC molecules. Considering the film thickness, 100nm to be much less than the thickness of the LC layer, 5μm, we can estimate the electric field to have the magnitude as: [54]

$$E_d = \frac{P_s}{\epsilon_0} \cdot \frac{\mathbf{w}}{d} \tag{7.7}$$

where E_d represents the internal electric field, P_s represents the internal polarization of the polymer, ϵ_0 is the free space permittivity, w is the polymer thickness, and d

represents the thickness of the LC layer.

For PVDF, $\frac{P_s}{\epsilon_0}$ can have a value of $0.1C/m^2$ at 20°C.[19] Considering $\frac{w}{d} = 20 \times 10^{-3}$ for our case, we get a value of 220V/μm for the internal electric field. This is a large number, which can pin the LC alignment even in the presence of an external field. As a result, in Figure 7.23, even on increasing the applied electric field to 1V/μm, the LC alignment did not vary from the initial state, which corresponds to no electric field. This is due to the internal field assembled in the polymer layer, which the external field has to overcome in order to influence the LC layer. On further increasing the applied electric field, the transmission of light through the cell decreases with the applied field. However, even at 4V/μm, the cell does not switch completely off. The LC state in the corona patterns is still visible, albeit faint in comparison to the initial state at 0V/μm.

The corona poling process works for charge patterning as well as for modification of a uniform surface. Figure 7.24 shows the switching response of LC on a select area of a PVDF film. The corona was scanned over the shown area only following which LC was deposited. Figure 7.25 shows the LC switching response over another area on the same polymer film with the exception being that this area was not exposed to corona discharge. Upon this region, we see the familiar color switching response of the LC indicating that the corona poling procedure is apt for local modification of the polymer films. With advent in mechanisms for the production of microdischarges in corona, it will be interesting to probe the maximum resolution for optical data storage devices using PVDF and nematic LC.

7.8 Surface Modification of Ferroelectric Polymers

In this section, we will consider the effects of modifying the surface of ferroelectric polymers using an RF plasma. For our experiments, an enclosed system, STS DRIE,

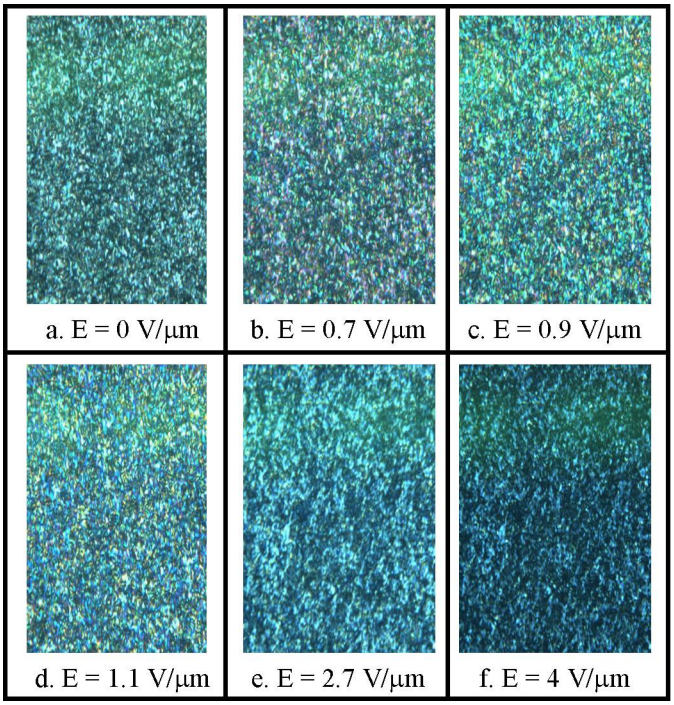

Figure 7.24: LC switching on a film exposed to uniform corona discharge

was used for the plasma generation. The instrument allows the generation of plasma in seven different gases where the RF power used to generate the plasma and the time period are controllable parameters. In our experiments, the plasma was generated in an Argon atmosphere to de-fluorinate the PVDF polymers [115, 116]. Ar gas was introduced in the DRIE chamber at 40sccm, and applying 100W to the bottom electrode generated the plasma. The time duration for the plasma exposure of the polymer film was 60 seconds. Figure 7.26 shows a schematic of the plasma exposing procedure. Due to the fluorine in P(VDF - TrFE), the LCs align with pretilt on the surface. Their alignment can be described as quasi-homeotropic. On exposure to Ar plasma, the surface is de-fluorinated [115,116]. LCs deposited on Ar plasma modified P(VDF - TrFE) films exhibit planar alignment, as shown in Figure 7.27. This image corresponds to LC alignment on a single film with a glass cover slip placed on top of the LC. The dashed white line is the divider between the virgin (unexposed) and

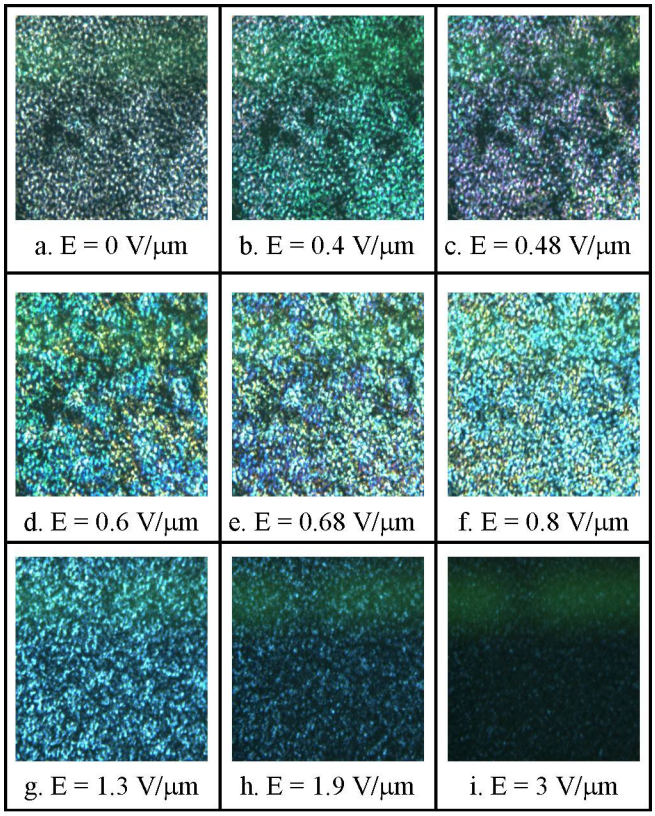

Figure 7.25: LC switching on the same film as shown in Figure 7.24. This area was not exposed to the corona discharge

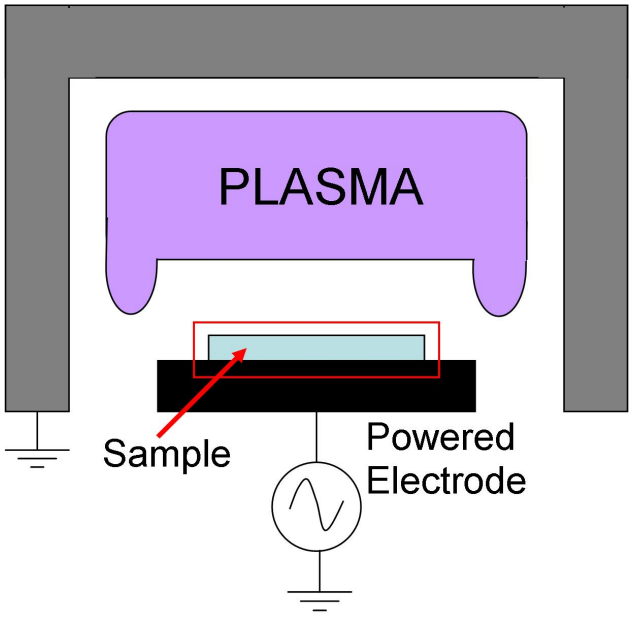

Figure 7.26: Schematic of the sample in the STS DRIE System

the exposed regions. The virgin area favors a quasi-homeotropic (or high pre-tilt) alignment due to the presence of fluorine on the surface. Hence on stage rotation, its colors do not change much as expected. The exposed regions are devoid of Fluorine, and hence a more planar alignment is favored. This explains why the black region shows more variations in color on stage rotation.

The LC alignment on these films is quite uniform as observed in Figure 7.28a. On complete switching a dark state is observed through the cell. A reduction of 90% in the transmission of white light as the field off voltage is observed at 0.6V/μm. This is a favorable operating field for most LCDs. Previous devices with rubbed P(VDF - TrFE) films as the alignment layer switched at 2V/μm [117]. The reason why the switching occurs at a lesser voltage is due to the lack of internal field in the polymer.

$$E_d = \frac{P_s}{\epsilon_0} \cdot \frac{w}{d} \tag{7.8}$$

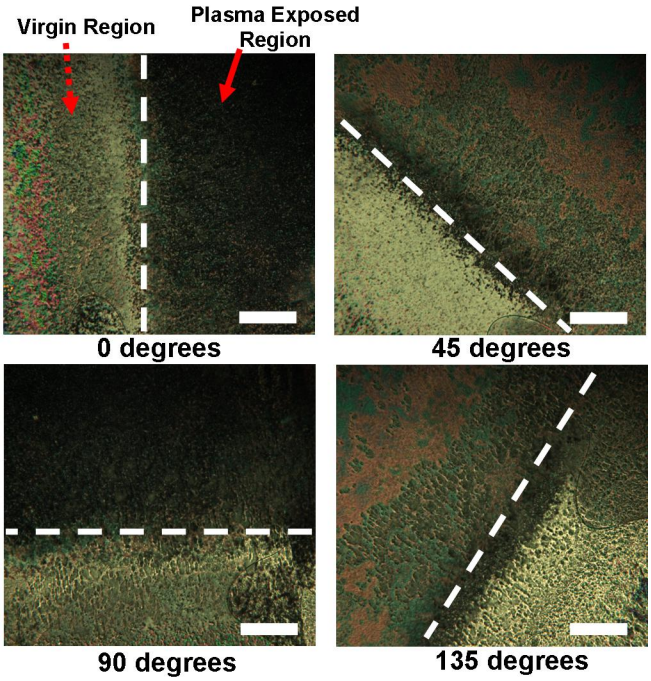

Figure 7.27: LC alignment on a P(VDF TrFE) film, which was selectively exposed to Ar plasma. On stage rotation, the colors in the virgin region remain relatively unchanged due to quasi-homeotropic alignment. Planar alignment in the plasma exposed region leads to color variations due to the azimuthal variations in perceived optical anisotropy. The images were observed through the crossed polarizers of the microscope and the scale bar corresponds to 200μm.

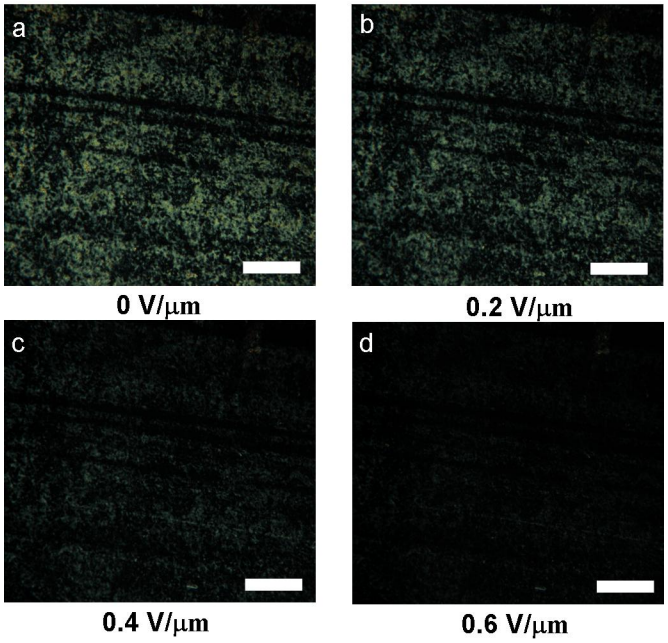

Figure 7.28: LC switching on Ar plasma modified P(VDF TrFE) film. The scale bar represents 200μm.

where E_d represents the internal electric field, P_s represents the internal polarization of the polymer, ϵ_0 is the free space permittivity, w is the polymer thickness, and d represents the thickness of the LC layer. Defluorination of the polymer leads to a very low value of the the surface polarization in the equation discussed earlier. As a result, the external electric field can easily change the orientation of the LC molecules. Hence, the switching field is reduced. Thus, plasma modification is a technique that can be used for the processing of alignment layers.

7.9 Modeling of LC Alignment on Ferroelectric Polymers

A basic model has been developed to understand the LC interaction with the polarization of PVDF. The model solves for equilibrium state of LC alignment, which is

governed by the energy represented as:

$$E = -\sum \cos 2(\theta_i - \theta_j) \tag{7.9}$$

where θ_n represents the angle associated with LC directors.

The system is minimized for different states of surface anchoring to provide visualizations of the alignment configurations. We use the simulated annealing algorithm explained in the previous chapter for the minimization. An alternating period of LC alignment was patterned on the surface. These surface directors were held fixed for the simulation. Figure 7.29 shows the initial state of the LC directors on such as surface and Figure 7.30 shows the most favorable alignment state. The patterned alignment on the surface is a thought-experiment of LC alignment on a sample polarization profile in the ferroelectric polymer. We are only plotting the LC layers and not the polymer. The vertical directors on the surface correspond to the LC on a corona poled or a strong polarized region in the polymer. The horizontal directors are the variables for our experiments. Their motion (or changes in orientation) corresponds to the influence of an external electric field, which is applied through the thickness of the cell (z-direction). Figures 7.31 to 7.33 show the change in the LC orientation as the surface molecules switch.

The order parameter of the LC directions is represented as a function of the variable angle of the surface LC directors. As we can see from the graph, there seems to be a threshold value after which the order parameter jumps. The threshold corresponds to the stronger forces the LC molecules face from the surface. Once they are overcome, the LC molecules are well-aligned, as indicated by the higher values of order parameter. We can compare this result with the color switching observed in 7.10 and 7.18. At low magnitudes of the field, the LC molecules will not completely follow the electric field but will align in intermediate positions corresponding to variations

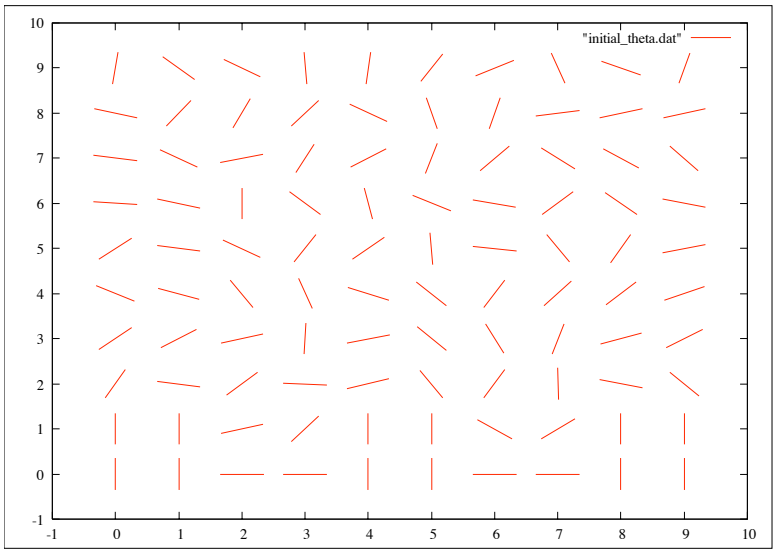

Figure 7.29: Initial state of LC alignment

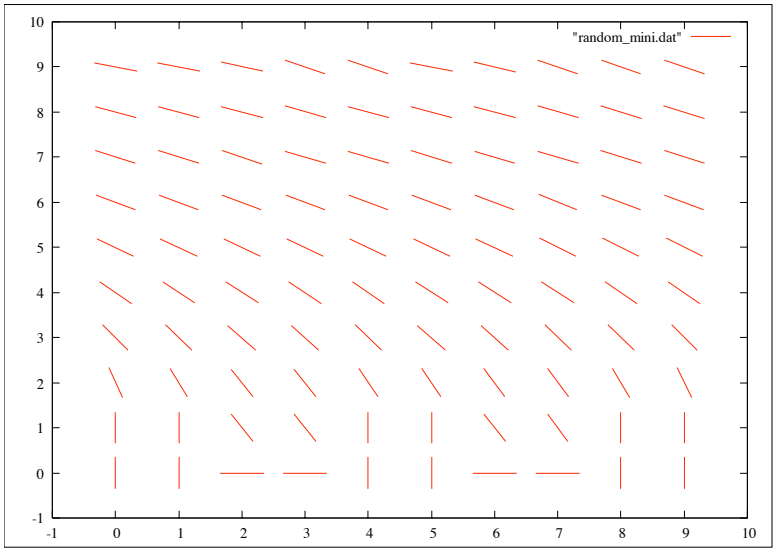

Figure 7.30: Final state of LC alignment after 1000 iterations.

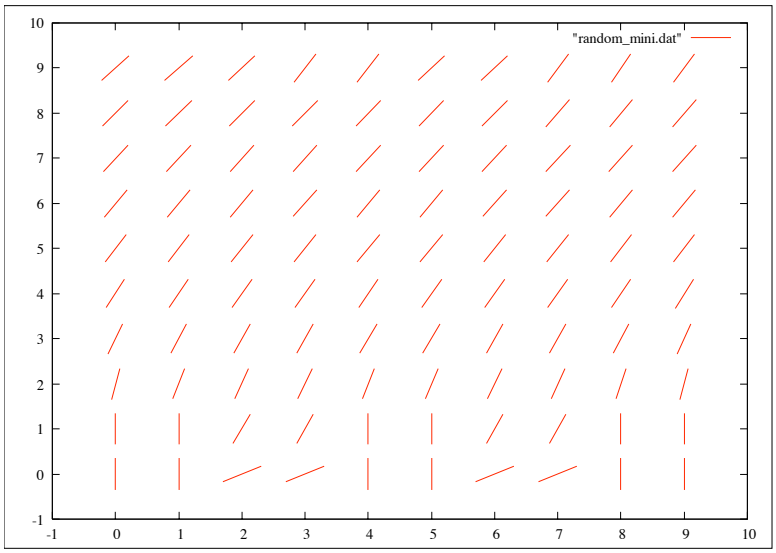

Figure 7.31: Final state of LC alignment for variable theta as 30 degrees

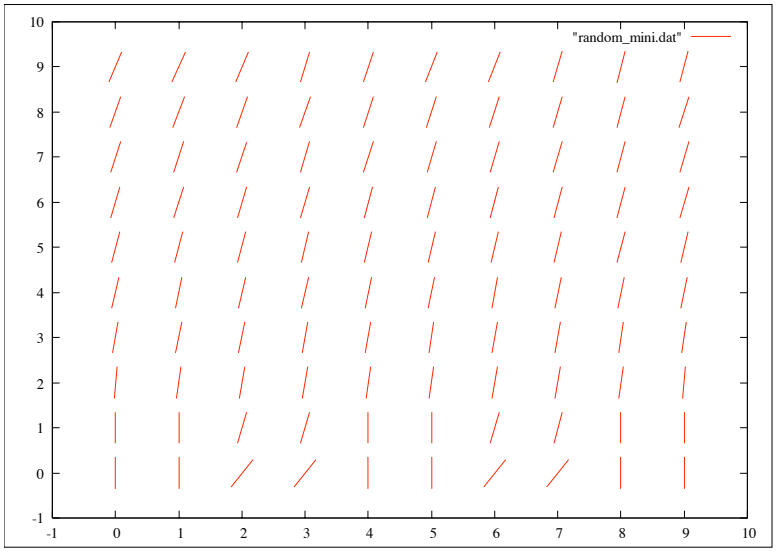

Figure 7.32: Final state of LC alignment for variable theta as 60 degrees

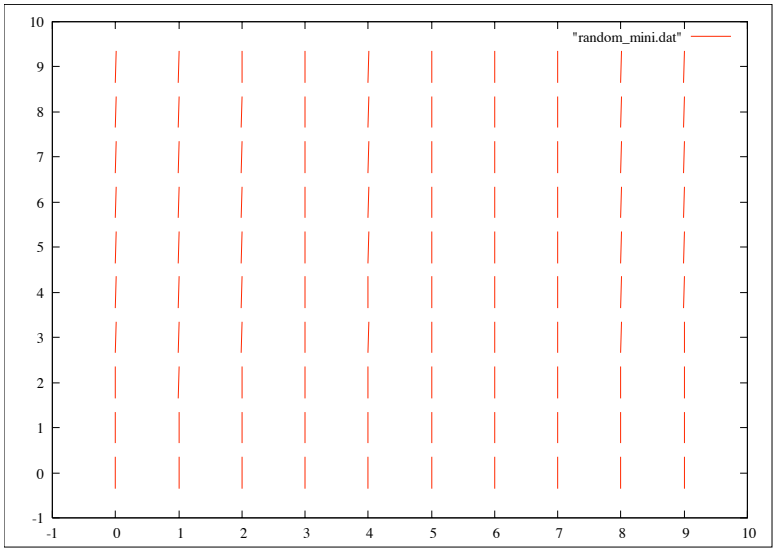

Figure 7.33: Final state of LC alignment for variable theta as 90 degrees

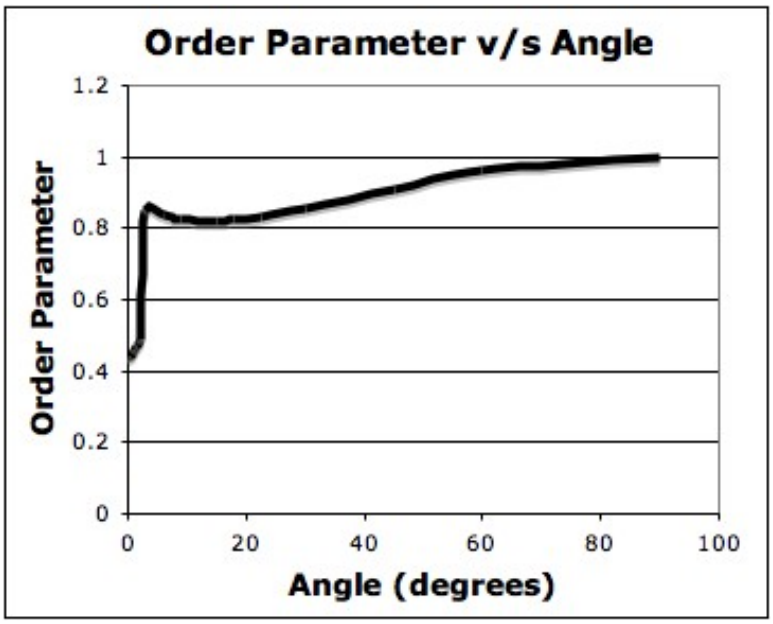

Figure 7.34: Order Parameter as a function of surface switchable directors

in ϕ as well as θ, the azimuth and elevation angles respectively. The variations result in a different value of phase delay experienced by the transmitting light leading to different colors. Even with a simple model, we have been able to understand the switching phenomenon. As we shall see in the next few pages, there is agreement of the order parameter variation with our spectrometry studies. However, for an exact match, we will need to consider other complex terms in the energy equation including field effects, long and short range LC interactions, and the complete Frank's equation of energy.

7.10 Conclusions

Using ferroelectric films as alignment layers for liquid crystals provides an approach to develop displays and optical data storage devices. Due to the interactions between the dipoles in the polymer and liquid crystal region, the displays exhibit a visible wavelength progression as a function of the applied electric field. As a result, simply varying the magnitude of the applied field can generate the desired color. Additionally, the transmitted wavelengths encompass the visible spectrum, an ideal property for this application. The PVDF - LC system can increase the display resolution by a factor of three when compared to the conventional method of using three pixels to generate one color. From a materials perspective, nanoclay doped PVDF films have shown the best response due to the switching efficiency. However, the aggregates of clay as observed through LC alignment could cause a problem in the generation of defects in a working device. The film, which is most applicable for use in the display industry is P(VDF- TrFE) films in a 65/35 ratio. These films have shown very uniform LC alignment, wavelength progression response, and switching efficiency [110]. The development of optical data storage devices is dependent on orienting the charge orientation within the polymer regions. Deposition of LCs on this substrate will map

the underlying dipole orientation providing an optical readout for the ferroelectric charge. Thus, the polymer can be used to record charges (data) with the LC layer providing the optical readout.

Corona poling was used to pattern charge distribution on the polymer films, and the liquid crystal layer provided the optical readout. These devices allow for ease of coupling data to optical systems used for next-generation computing and communication applications. In comparison to the corona poling procedure, RF plasma generated in Ar gas was utilized to change the surface chemical functionality of the polymer. After the plasma exposure, the polymer was de-fluorinated resulting in a loss of dipolar coupling for the LC layer. In this case, the external electric field did not have to overcome a large internal electric field corresponding to the polymer layer. The LC molecules readily responded to the external electric field; complete switching was observed at a low magnitude of $0.6\text{V}/\mu\text{m}$.

Chapter 8. Liquid Crystals and Carbon Nanotubes

Liquid crystals (LCs) are materials, which are used in a wide range of applications, which include displays (LCDs), electro-optic switches and imaging of biological cells. All of these devices typically contain an alignment or confining material to control the LC ordering. To improve the device operating parameters such as switching speed, diffraction efficiency, contrast ratio and switching voltage, the materials must be constantly improved. For LCs, the changes involve modification of the chemical groups, reduction or increase of the molecular length, and addition of dopants. One of the most active areas in improving LC devices is the development of LC - carbon nanotube (CNT) composites. Carbon nanotubes (CNTs) are very interesting materials for next-generation applications mainly due to their mechanical properties [118]. These are materials that are cylindrical shaped with the diameter on the order of single digit nanometers to a few hundred nanometers. The length is on the order of micrometers. Such a large aspect ratio between the length and the diameter give the CNTs large surface area. As a result, the mechanical properties including elastic modulus and hardness are much larger than that of bulk carbon. The temperature characteristics of these materials are also excellent, making them suitable for a variety of applications including those in biotechnology, display manufacturing (both liquid crystal and field emissive), and transport of fuel (liquid and gaseous). Additionally, they are also known to assemble in liquid crystalline phases depending on their concentration, which is a property of lyotropic LCs [119–121].

The discoveries in combining LCs and CNTs so far have only touched the surface of what might be found. CNTs can have different wall structures, sizes, and chemical functionalities. So far, majority of the work has considered commercially available single-walled and multi-walled CNTs. In general, these CNTs are, generally, not

straight but rather they form bundles. They have to be sonicated prior to use with LCs and their purification is also a problem. In this chapter, we will discuss the effects of straight and hollow CNTs, which have a diameter of 200nm on LCs. Such materials provide the opportunity to ask questions that include:

- What is the nature of LC alignment when these tubes are dispersed?
- Can the LC align such tubes?
- If the tubes are hollow, can they be used to study LC wetting and storage?
- If the chemical functionality of the tubes is changed, how does the LC respond?

This chapter aims to answer the above questions. First, we shall briefly discuss the formation of the CNTs and their physical properties. Following that, the formation of the CNT LC suspensions will be explained after which, the results of three different studies will be described; the interaction between the two materials, LCs and CNTs; LC wetting inside CNTs; and phase transition effects in LC CNT composites.

8.1 Interactions of LCs outside CNTs

To test the interaction of CVD CNTs with LC, they were suspended in ethanol and dried onto a glass microscope slide. Prior to any material deposition, the microslides were cleaned using methanol to remove any foreign particles or dust on the surface. The CNTs were left behind on the glass slide after the ethanol evaporated. A pipette was used to draw the LC in its nematic phase from the container. Only a single drop of LC was deposited on the substrate, and a glass cover slip was used to cover the sample and flatten out the LC. The placing of the cover slip caused the LC to flow along the area of the microscope slide, and uniformly disperse the CNTs. This effect was observed using polarizing optical microscopy (POM) on a Leica DMLP microscope. The 50x and 20x objectives were used in the polarized microscopy mode

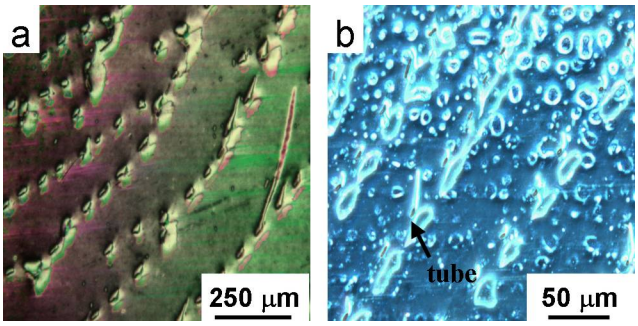

Figure 8.1: Alignment of carbon nanotubes using liquid crystals: a) Polarized optical microscopy image of CNP dispersed in liquid crystals; b) Phase contrast image of the area in a).

(cross-polarizers), and the 40x objective was used in the phase contrast mode. A CCD camera interfaced to a computer and suitable software (Magna Fire) was used to acquire the images.

8.1.1 Liquid Crystal Textures

The nematic order of the LCs aligns the CNTs periodically, as shown in Figure 8.1. The ordering of the CNTs is the highlight of the images. Figure 8.1a is the polarized optical microscope view of the dispersed CNTs in LCs. From Figure 8.1b, which shows the phase contrast images of the CNTs, it can be observed that the CNTs change the local orientation of the LC. Additionally, due to the spacing of the CNTs, their arrangement can be viewed as a periodic groove. This in turn leads to the alignment of LCs, and textures are observed on an ordinary glass microslide. The textures are shown in Figure 8.2. On a regular glass microslide, the alignment of the LCs is random and such textures are not observed, as shown in Figure 8.2(d). This indicates a two-way ordering effect of LCs on CNTs: the nematic LCs orders the CNTs and the CNT spacing leads to oriented textures of LCs. Additionally, these textures are observed in the bulk. Hence, it is not a cell-edge influenced phenomenon.

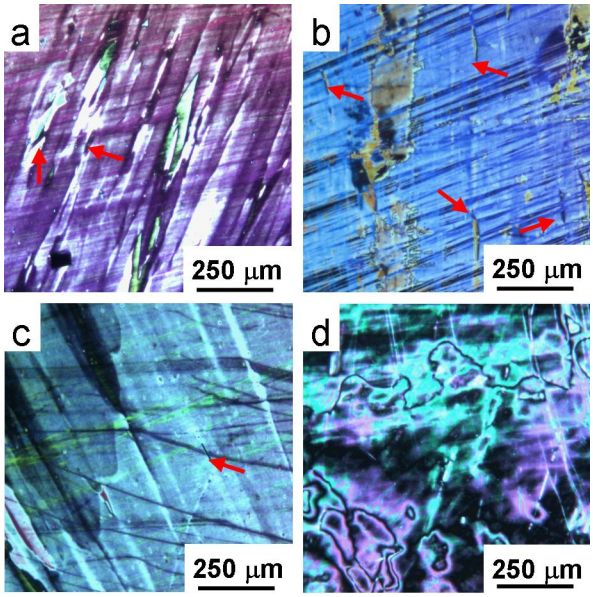

Figure 8.2: a-c)Liquid crystal textures due to carbon nanotube dispersion. The arrows show selected nanotube locations; e) Raman spectra of carbon nanotubes (top), liquid crystals (bottom) and CNP dispersed in LC (center); d) Liquid crystal textures without CNPs indicating lack of uniformity in alignment

The textures show uniform alignment domains and the color in each of these textures corresponds to the orientation of the LC molecules. This uniformity of colors and birefringence is absent without the dispersion of CNTs, as seen in Figure 8.2d.

In order to probe the type of interaction between the two materials, LCs and CNTs, were studied using Raman Spectroscopy. These results help us identify if the LC was chemically bonded to the CNT walls or whether the interaction is purely physical in nature. The Raman spectra shown in Figure 8.3 were recorded using a Raman spectrometer (Renishaw) with an Ar ion laser (514nm excitation wavelength). LC is characterized by a distinctive peak for C≡N stretching at 2226cm^{-1} and peaks at 1180cm^{-1} and 1605 cm^{-1} corresponding to in-plane C-H bending and C=C stretching in the ring structure of the 5CB, respectively11. The peak at 1285 cm^{-1} is attributed to the stretching of the biphenyl link and the broad band in the region 2900-3100 cm^{-1}

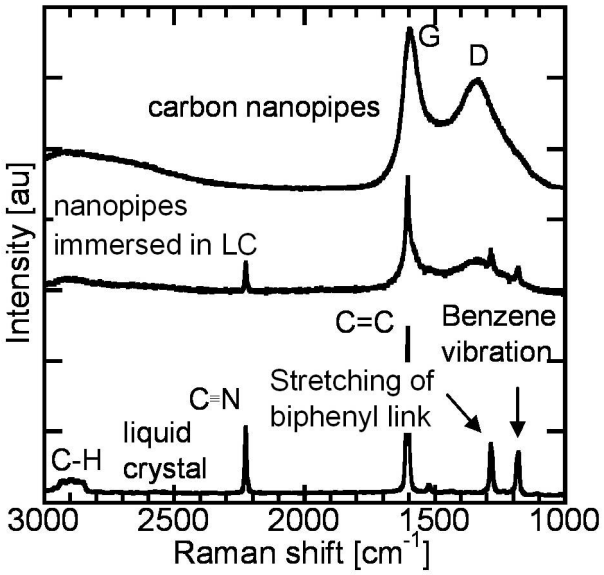

Figure 8.3: Raman spectra of carbon nanotubes (top), liquid crystals (bottom) and CNP dispersed in LC (center)

corresponds to C-H vibration in the linear hydrocarbon chains of the molecule. [122] The Raman spectrum of carbon nanotubes consists of a broad band around 1350cm^{-1}, which is a double resonance band common for carbon materials (D-band) and a slightly narrower one around 1600cm^{-1} related to in-plane vibrations of graphite (G-band). The spectrum collected from the suspension of carbon nanotubes in LC shows an overlapping of the spectra for the single phases. No additional Raman bands or changes in the CNT or LC peak positions have been observed. Thus, there is no chemical change in either material implying that the primary interaction between the materials is physical.

Due to the physical interaction between the two materials, we can model them as a solute-solvent interaction considering the LC as the solvent and the CNTs as the solute. The interfacial energy is given by: [108]

$$\gamma_{LC-CNT} = \gamma_{LC} + \gamma_{CNT} - 2\sqrt{\gamma_{LC}\gamma_{CNT}} = (\sqrt{\gamma_{LC}} - \sqrt{\gamma_{CNT}})^2 \qquad (8.1)$$

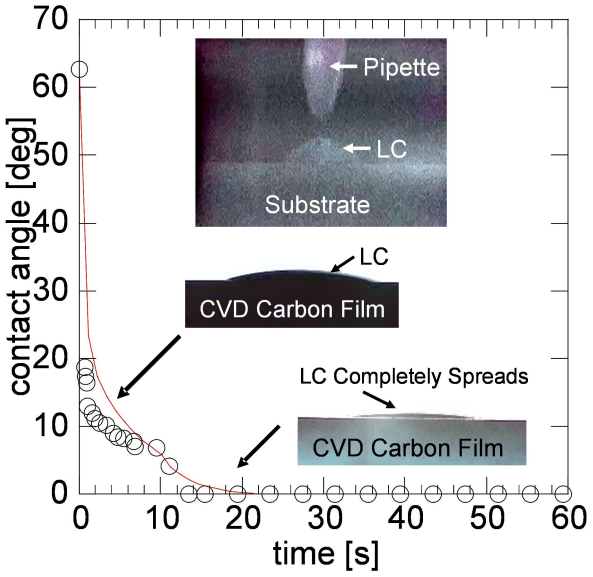

Figure 8.4: Contact angle measurements of LC on a film of CVD carbon that is identical in surface chemistry and structure to the carbon of which the CNPs are composed. The graph depicts the reduction in contact angle with respect to time as the droplet of LC begins to spread on the film.

where γ_{LC-CNP} is the interfacial energy, γ_{LC} and γ_{CNT} are the surface energies for LC and CNTs, respectively. The surface tension for the CNTs, γ_{CNT}, is ~41mN/m[10] and that of 5CB, γ_{LC}, ranges from 30 to 40mN/m [123]. Thus, the net interfacial energy can be calculated to give an upper value of 0.857mN/m (γ_{LC}=30mN/m) and a lower value of 0.006mN/m (γ_{LC}=40mN/m). These low values of interfacial energies explain the free flow of the LC within the CNTs and indicate complete wetting. Using the Sessile drop method, complete wetting of LC droplets on CNT films was observed within 20seconds, as shown in Figure 8.4. For this experiment, a CVD carbon film was deposited on a polished silicon wafer and treated with NaOH. This treatment ensures that the film is chemically and structurally identical to the wall structure of the CNTs used in this study [81].

As we understood in the previous section, the LC - CNT suspension is characterized by low values of interfacial energies. This explains the free flow of the CNTs in

the LC medium. However, due to repulsive forces, the CNTs are forced to remain in the dispersed state. Hence, the association or clustering of tubes in LCs is not preferred over the dispersed state in the LC used. This is observed in the POM images of CNTs mixed with LCs at room temperature, which is in the nematic temperature range of the LCs. It was suggested by Lynch et al. [72] to use the order parameter of the LCs to align the CNTs. The ordering of the nematics exerts a torque on the CNTs, forcing them to align as per the direction of the molecules, as shown in Figure 8.1.

8.1.2 Switching the LC - CNT Suspension Using an Electric Field

For these experiments, CNT-LC suspensions were prepared by ultra-sonication of CNTs dispersed in LCs. As shown in Figure 8.5, a 10μm sandwich cell was created using glass slides coated with Indium Tin Oxide (ITO), a transparent and conductive coating. The ITO-glass slides were separated using 10μm fiber spacers and glued using an optical adhesive, leaving openings to fill the empty cell. The CNT-LC suspension was introduced in the cell using capillary action. An electric field was applied across the thickness of the cell to observe the motion of the CNTs in response to an external force.

Due to the dielectric anisotropy of the LCs, it is possible to manipulate them using electric fields. For LCs with a positive dielectric anisotropy, the long-axis of the molecules aligns parallel to the direction of the applied electric field. The application of an electric field exerts a torque on the LC molecules, thus orienting them parallel to the field direction. Beyond a threshold magnitude of the electric field, $\sim$1.0V/μm for a 10μm cell, the molecules are oriented parallel to the applied field direction. As the molecules rotate, they are fixed in their position as long as the field is applied, with their orientation minimizing the free energy of the LC system. The free energy

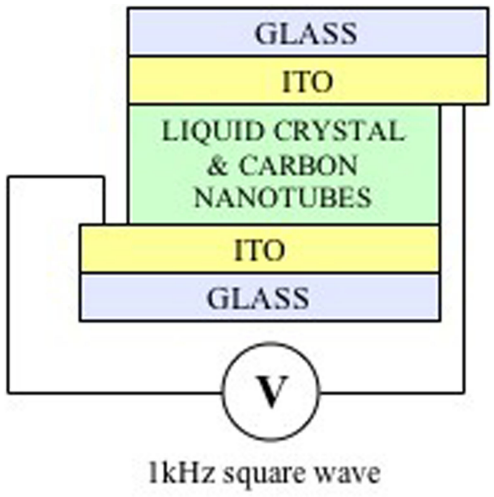

Figure 8.5: Schematic of the CNT - LC sandwich cell

in the case of a LC system depends on the order parameter of the LCs, and the minimum energy corresponds to the ordered LCs [12]. The influence of an external field is dominant in respect to the LC-LC forces, and the molecules rotate collectively along the field, increasing the LC order. Figure 8.6(a) shows the CNTs in a LC region before a voltage is applied across the cell. The LC molecules in the dark regions are aligned parallel to the polarizer or analyzer. As we increase the magnitude of the applied field to a value greater than 1.0V/μm, the LC and CNTs rotate. With an increase in magnitude of the electric field, the CNTs are slowly rotated out of plane. The dynamics of the CNT motion is shown in Figure 8.6(a)-(e). For an electric field greater than 1.5V/μm, the CNTs are oriented out-of-plane, as shown in Figure 8.6(d) and 8.6(e). As the CNTs rotate out-of-plane, the surrounding LC molecules now have a different orientation, deviating from the aligned state of the rest, which are in parallel with the field direction. This leads to the formation of defects in the LC region, which are observed as the bright spots in the dark background. The background does not change, remaining dark, indicating that the LC is perfectly aligned parallel to the field. This out-of-plane alignment of the LC is referred as

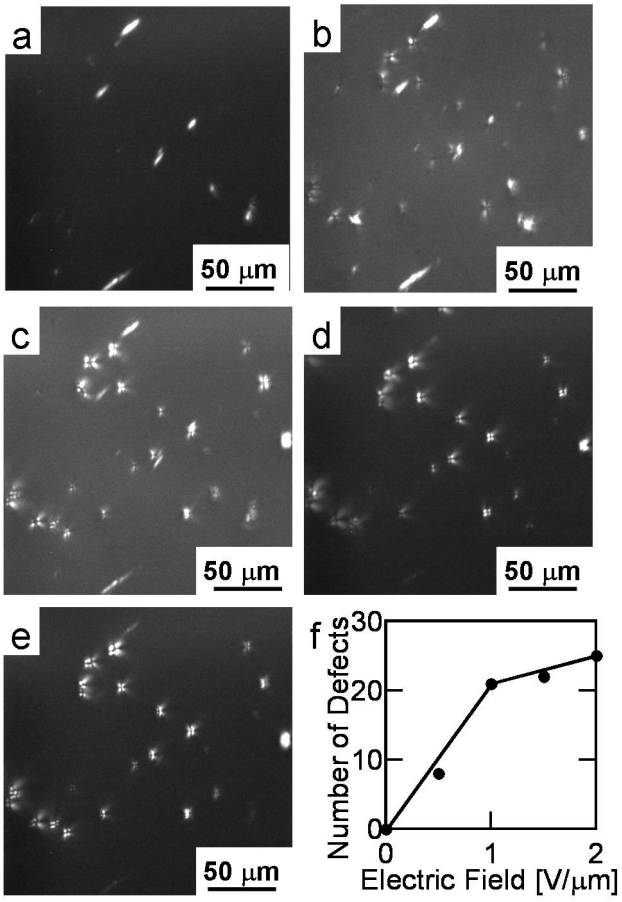

Figure 8.6: Manipulation of carbon nanotubes due to electric field: a) Electric field = 0 V/μm; b) Electric field = 0.5V/μm; c) Electric field = 1.0V/μm; d) Electric field = 1.5V/μm; e) Electric field = 2.0V/μm; f) number of defects as a function of the applied electric field.

homeotropic alignment. The LC defects induced by the out-of-plane rotation of the CNTs are interesting from a surface interaction viewpoint. One of the main causes for the defects in this system is the possible flow of LCs inside the open-ended tubes. Another possible reason is the surface roughness of the CNTs. Although the CNTs used in our experiments have straight walls, a variation at the order of angstroms is enough to change the local orientation of the LC molecules. Again, this signifies that the wetting of the LC with the carbon nanotubes is very high. The variations in the size and shape of defects could be due to the length, diameter, and thickness of walls as well as surface roughness of the CNTs. Although the walls of the CNTs are smooth, variations on the order of angstroms could lead to a change in the orientation of LCs. It can be assumed that the area spanned by the defect is dependent on the smoothness of the CNTs. This is an important fact to consider for manufacturing of LCDs using a mixture of CNTs and LCs as the switchable elements. Though the switching characteristics may be better compared to using only LCs, the defects may harm image generation. Thus, the resolution and the quality of the image generated may be compromised. Another point to consider is that the nanotubes used in these experiments are open from both ends. Upon switching, the LC is able to flow inside the CNTs. This problem could be eliminated if the CNTs were closed from both ends, leading to a better display with good switching response. Also, the defects are a ready method of characterizing vertically aligned CNTs. Vertically-aligned CNTs have been used in the development of field emission displays. The SEM and AFM are the only methods of characterizing the manufactured tubes. Though the resolution is excellent in both methods, they are time consuming. Polarized light microscopy of the defects LCs deposited over manufactured tubes provides imaging over a much larger area in a short time. Also, the LCs are non-chemically active with the tubes. After imaging, they can be easily washed away using solvents including methanol and ethanol. Also, from the equilibrium energy point of view, this is an interesting system

where high-energy states of defects are allowed to overcome the aligning forces of the electric field. The energy surrounding a defect is always high, and is an expense to the system. In a system consisting of LC molecules only, the defects are attributed to surface variations, and presence of foreign particles including dust. The tendency of the molecules in such a system is to orient themselves till the lowest energy state of the system is achieved. The presence of defects in this case would correspond to irresolvable alignment imparted on the LCs by the surface or foreign bodies. On application of an electric field, these forces are overcome, and the LC molecules align uniformly parallel to the applied field. However, for the LC-CNT system, the defects occur when the CNTs rotate out-of-plane on the application of the electric field. This again signifies the excellent interaction between the LCs and CNTs.

Thus, we have seen a two-way effect of aligning carbon nanotubes using liquid crystals and inducing liquid crystal textures due to the presence of CNTs. Due to the physical interaction defects in the LC are observed, when electric fields larger than Fredericks transition threshold are applied. The defects result because of the out-of-plane rotation of CNTs in response to the force exerted by LC molecules and electric field.

8.1.3 Phase Transition in LC - CNT Suspensions Due to Joule Heating

So far, we have discussed phenomenon for as-produced CNTs on LCs. The favorable interaction between the two materials permits the LCs to easily flow inside the hollow CNTs for confinement studies. The interaction also helps in using the CNTs as materials for LC alignment. Now, we shall consider the effects of changing the properties of CNTs in terms of conductivity and wall structure on LC behavior. Specifically, we will now consider LCs doped with CNTs that are conductive in nature and observe the changes in switching behavior. To improve the switching speed and the

alignment in devices, doping of LCs with additives has been extensively studied. The additives include chiral dopants inducing a twist through the cell thickness, different particles such as carbon solids, ferroelectric particles, and photosensitive particles for lasing applications [62,64,69,124]. The heat conductive properties of CNTs have been exploited for nematic elastomers or polymers to be used as electromechanical actuators [125]. Recently, LC elastomers doped with carbon black demonstrated length variations due to Joule heating caused by an external electric field [126].

To our knowledge, no complete phase transition from the nematic phase to the isotropic phase in LCs has been observed through the addition of dopants. Phase transition relies on providing sufficient thermal energy to the system, which usually requires a heating source. In our experiments, have observed a nematic-to-isotropic transition in LC - CNT suspensions uniquely due to the electric field. Such an effect highlights the possibility of using CNTs for applications including electronic phase changing materials and annealing materials at the sub-micrometer scale.

8.1.3.1 Results

Figure 8.7a shows the texture of a LC - CNT suspension as observed through the crossed polarizers of a microscope. The majority of the textures suggest partial alignment of the LC suspension. On application of the electric field, the LC molecules rotate, reducing the perceived birefringence (Figure 8.7b). On holding the electric field across the cell, after some time isotropic domains (black spots) are observed as shown in Figure 8.7b. These domains flicker on and off over time (Figure 8.7c) and eventually, the domains expand in size and over the entire cell in a curtain-like fashion (Figure 8.7d - 8.7o). This is the final state of the LC - CNT suspension, and holding the field does not cause any other effects. On removal of the electric field, a reverse transition from isotropic to nematic state is observed as shown in Figure 8.8.

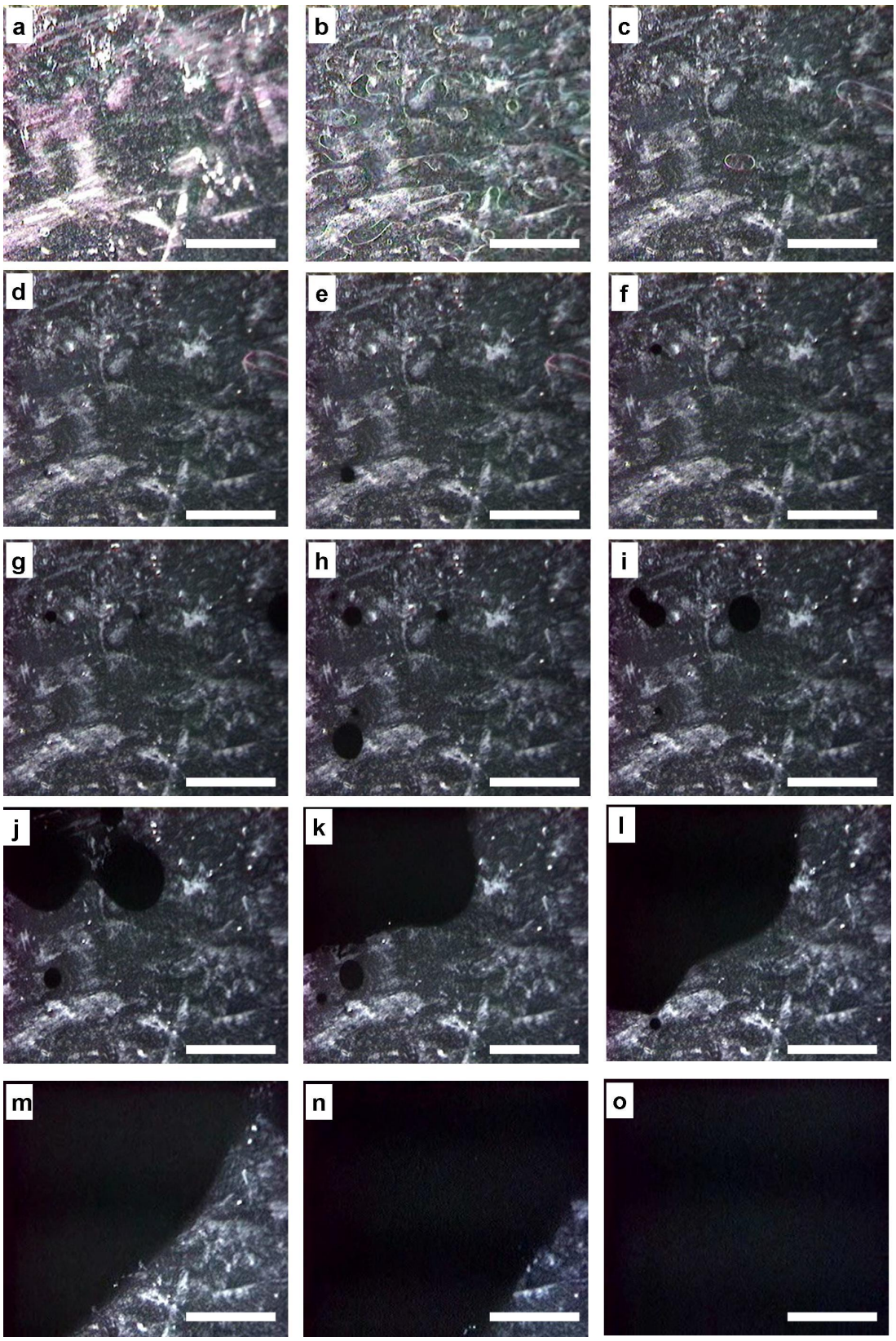

Figure 8.7: Nematic to Isotropic transition observed on application of a 1 kHz square wave, $20V_{pp}$ to the cell. The images show snapshots at different time intervals a) Initial, b) after 5 secs, c) 20 secs, d) 36.20 secs, e) 37.73 secs, f) 40.53 secs, g) 54.07 secs, h) 58.13 sec, i) 1.10 min, j) 1.18 min, k) 1.22 min l) 1.25 min, m) 1.30 min, n) 1.34 min, and o) 1.38 min

The black state persists for a few seconds following which a fast transition of colors is observed (Figures 8.8 b - o). This progression of colors is identical to the isotropic - nematic transition observed in LCs when using a heating stage. Figure 8.7 shows the same effect, where the cause of transition was the electric field. The switching process was not observed for the as-produced (670°C) nanotubes, which have about 3 orders of magnitude lower electrical conductivity than the CNTs annealed at 2000°C [82]. In Figure 8.8 b - o, white threads can be seen in as the liquid front proceeds to settle into the nematic phase. The threads are a result of the LC flow from the state of complete disorder (isotropic) to a more ordered nematic phase. The final state in Figure 8.8o is identical to the initial state in Figure 8.7a. This state corresponds to the minimal state of energy for the LC and is strongly influenced by the surface impurities and roughness, as can be clearly seen.

Analysis of switching times for increasing concentration of CNTs in LCs for nanotubes annealed at 1200°C have shown a concentration threshold at about 0.04% wt for switching to occur (Figure 8.9). Below the threshold value, the low concentration of annealed CNTs was able to produce only local isotropic droplets. Above the threshold value, a linear dependence of switching time to concentration is observed (Figure 8.9). In order to compare the switching times between CNT-LC samples with CNTs annealed at different temperatures and, hence, having different conductivities, it was necessary to normalize the concentrations for the different samples. The procedure is as follows: The concentration values for nanotubes annealed at different temperatures in LC were normalized to the concentration of the samples containing as-produced (670°C) nanotubes. Subsequently, the switching time for each sample was divided by the corresponding normalized concentration. This is possible due to the linear relation between switching time and concentration observed for the 1200°C annealed sample (Figure 8.9). Finally, the normalized switching time was plotted against the conductivity values for nanotubes annealed at different temperatures [82].

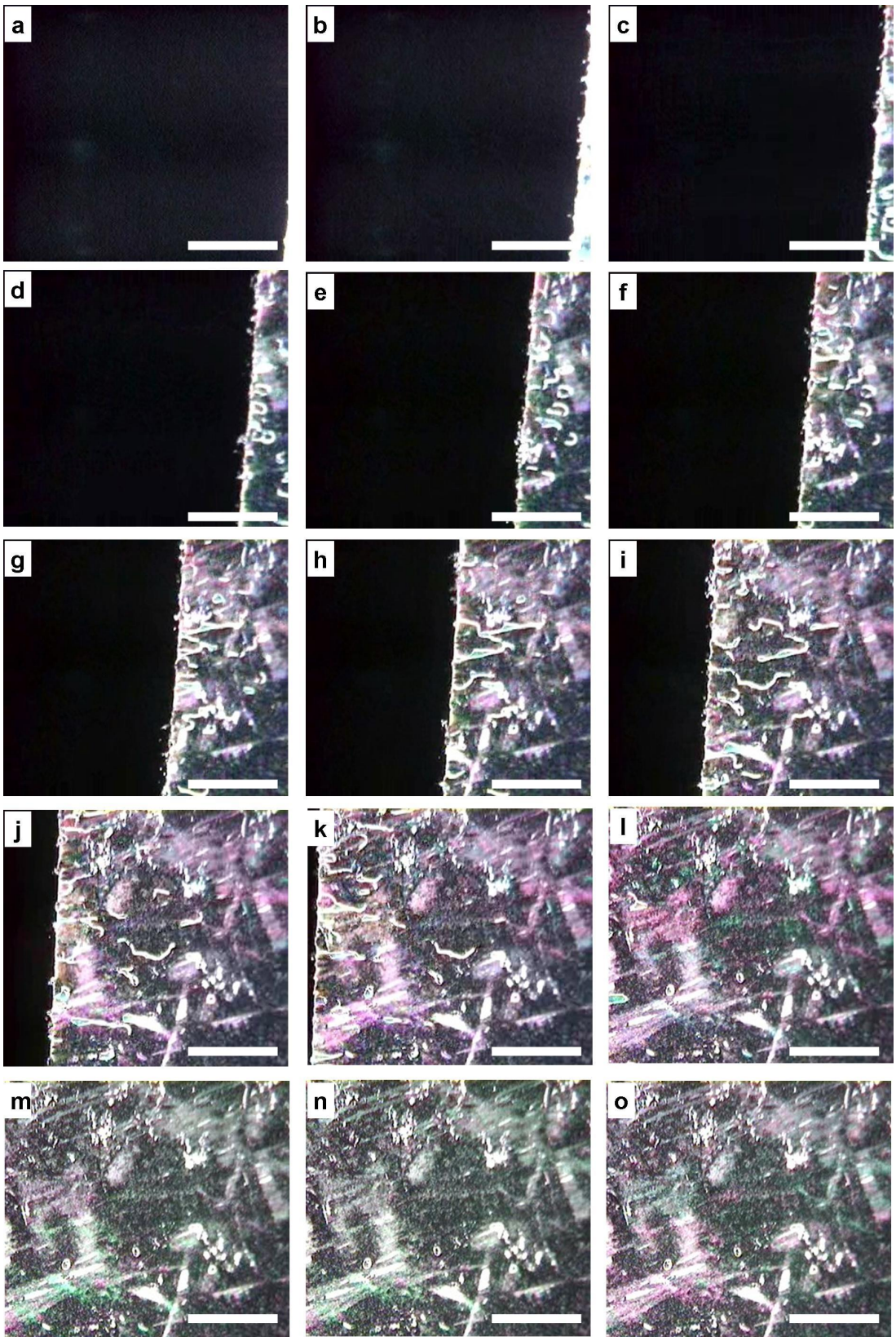

Figure 8.8: Nematic to Isotropic transition observed on removal of the electric field in the cell. The images show snapshots at different time intervals a) after 5.53 secs, b) 5.73 secs, c) 5.87 secs, d) 6.13 secs, e) 6.47 secs, f) 6.73 secs, g) 7.07 secs, h) 7.40 secs, i) 8 secs, j) 8.67 secs, k) 9.27 secs l) 11 secs, m) 19 secs min, n) 22 secs, and o) 1 min

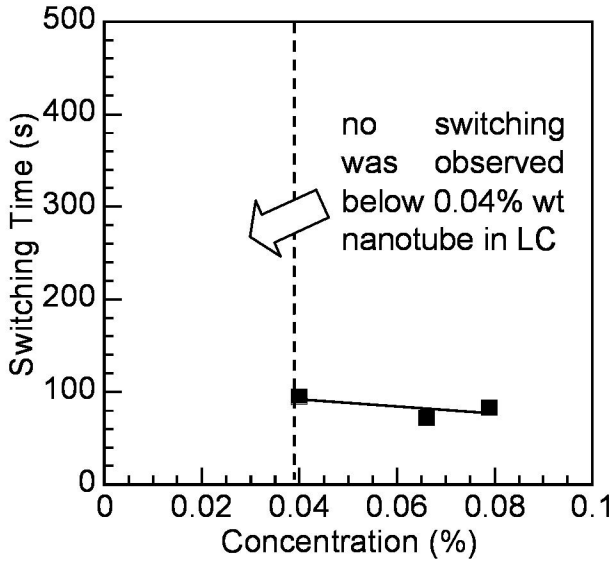

Figure 8.9: Switching time as a function of nanotube concentration in liquid crystal in the cell for CNTs annealed at 1200°C. Below 0.04 % wt of CNTs in LC, no switching occurs

No switching was observed for the as-produced sample, while switching time appears to be almost independent of annealing temperature and conductivity (Figure 8.10). The change in conductivity with annealing temperature is due to the graphitization of the as-produced nanotubes, whose wall structure is shown in the TEM image in the left inset in Figure 8.10. The wall is made of turbostratic graphite, consisting of small (∼2-3 nm) graphite crystallites patched together during CVD. As a result, the conductivity is about 1-2 orders of magnitude lower than for the ordered structure attained after annealing at 2000°C (right inset, Figure 8.10), with conductivity close to that of graphite [82].

The presence of a conductivity threshold for the switching phenomena to occur suggests that Joule heating in the CNTs might raise locally the temperature enough for the phase transition to occur. The length of the CNTs manufactured after the CVD process is 60μm, which is reduced by sonication and physical contact with lab

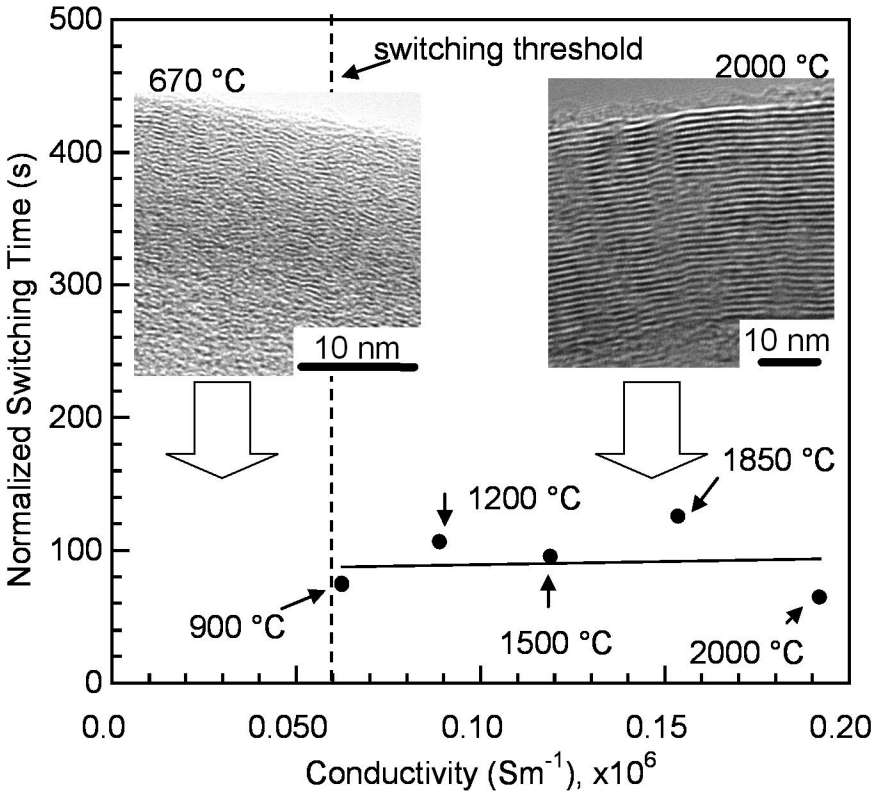

Figure 8.10: Normalized switching time (switching time/normalized concentration) vs. CNT conductivity. No switching occurs for the as-produced (670°C) nanotubes. The insets show TEM micrographs of the walls of as-produced (left) and 2000°C annealed (right) nanotubes.

equipment including tweezers and pipettes. Thus, within the LC - CNT suspension, the length of CNTs varies from 5μm to 60μm indicating that most of the CNTs are longer than the thickness of the sandwich cell (5μm). On application of a field much larger than the Fredericks transition threshold, the LCs as well as CNTs rotate out-of-plane to align parallel to the field direction [73]. On rotation, the longer CNTs simultaneously touch both the ITO electrodes of the cell. Due to the conductivity of the CNTs, a current is able to flow between the electrodes through the CNTs. The current flow through the conductor (CNT) results in a local increase of the temperature according to the Joule heating phenomenon.

Figure 8.11 provides a schematic of the LC - CNT interaction under local temperature increases by Joule heating. Initially, the higher temperature disturbs the nematic order of the molecules near the long tubes. After a certain threshold temperature increase, the nematic phase transitions into the isotropic phase (as seen by the bubble appearance in Figure 8.7). By holding the field constant over time, the disorder and temperature spread to the entire cell due to diffusion. Repeated experiments have revealed the presence of tubes at the center of the isotropic bubbles observed in Figure 8.7. The CNTs act as nucleation sites for the nematic to isotropic phase transition. Scalia et al., have reported that the nucleation of nematics occurs at CNTs when reducing the temperature from the isotropic phase [127]. Our studies are indicating a reverse effect of nucleation of isotropic domains at CNTs. In our case, the temperature is increased by having current flow through the CNTs leading to Joule heating.

8.1.3.2 Explanation of the Effect

Recently, Mottram et al. [128] have reported on electric field induced phase transition in a system having domains of both nematic and isotropic phases. Depending on

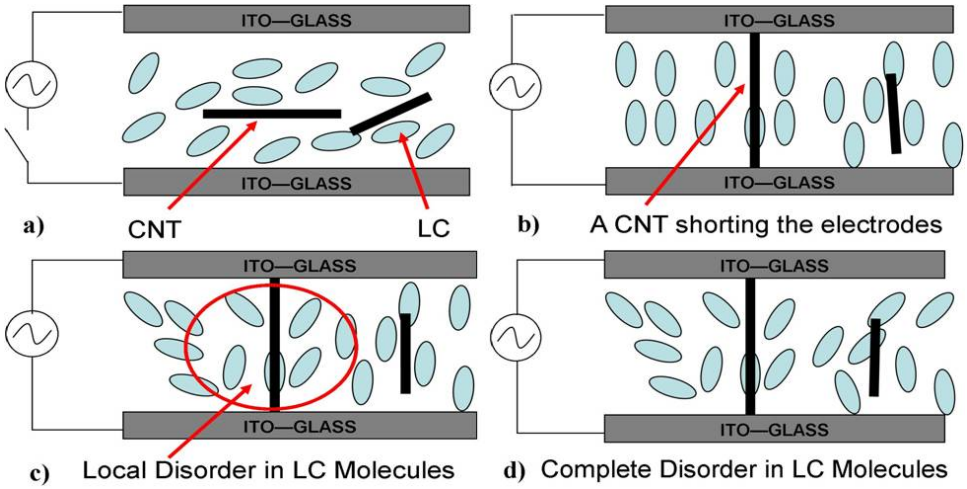

Figure 8.11: Schematic of the nematic-to-isotropic LC transition upon application of the electric field in presence of annealed nanotubes: a) Initial Nematic phase; b) Upon application of the electric field across the cell, the CNTs rotate out of plane, short circuiting the cell. c) Local phase transition from nematic to isotropic occurs close to shorting CNTs, due to Joule heating; d) The nematic-to-isotropic phase transition extends to the whole cell sue to diffusion.

the domain size of the components and the magnitude of the electric field either the nematic phase or the isotropic phase is favored. The above statement holds true only if the temperature within the system guarantees a meta-stable nematic phase. Typically, this temperature is slightly above the nematic to isotropic transition temperature. For 5CB, this temperature is $\sim$40°C.

The free energy in the system is given by:

$$F = F_t + F_d + F_e + F_i \tag{8.2}$$

where F_t represents the thermotropic free energy, F_d is the elastic energy associated with nematic LCs, F_e is the electrostatic energy, F_i and is the interfacial energy. The

total free energy per area of the cell is then given by:

$$F = [d^*(\sigma(S_N) - \sigma(S_I)) + d\sigma(S_I)] - \frac{1}{2}\frac{\epsilon_0\epsilon_I\epsilon_N^2}{d^*(\epsilon_I - \epsilon_N) + d\epsilon_N} + \gamma(S_N - S_I)^2 \qquad (8.3)$$

where d^* is the nematic domain size, $\sigma(S_N)$ represents the entropic contribution of the nematic phase, $\sigma(S_I)$ denotes the entropic contribution of the isotropic phase, ϵ_0 is the permittivity of free space, ϵ_N is the permittivity of the nematic medium, ϵ_I is the permittivity of the isotropic phase, γ is the interfacial energy, and S_N and S_I represent the order parameters of the nematic and isotropic phase, respectively. Since an electric field is applied while isotropic domains are formed, the order in the isotropic phase has to be accounted for.

Also by minimizing the free energy, a phase diagram can be constructed, which illustrates the field-dependent transition phenomenon. The phase transition depends on the voltage applied and the temperature within the cell. In our work, initially, the cell is covered with the nematic phase. After the electric field is applied, the LC and CNTs rotate out-of-plane to result in a net homeotropic (perpendicular) alignment. Due to the joule heating caused by the CNTs, small isotropic domains are formed in addition to rise in the temperature within the cell. Holding the voltage across the cell leads to a steady current flow resulting in an increase of the temperature in the cell. The phenomenon shown in Figure 8.7 follows a path identical to the phase diagram shown by Mottram et al. [128]. The cell has reached a critical point where for any fixed temperature after T_{NI}, for a minimum voltage, not even a strong nematic region (near the surface) will be able to prevent a transition of the cell into the isotropic phase.

8.1.3.3 Attraction between the Isotropic Droplets

A model describing the interaction between colloidal particles at the nematic-isotropic interface can be also used to explain the isotropic domain growth in our system [129]. Their system consisted of a colloidal particle, which could be a liquid particle, near a nematic-isotropic interface. The system minimized the Landau-de Gennes free energy to predict the merging of the particle into the isotropic region. Also, the isotropic region covered a larger area of the cell after submerging the colloidal particle. In our system, we can consider the presence of isotropic domains as colloidal particles near a large nematic-isotropic interface. One such visualization is provided in Figure 8.7i. The interaction between the two isotropic domains will be always attractive in a nematic medium [108]. Once a smaller isotropic domain is near the larger one, the two merge with the larger interface bulging towards the smaller one. Eventually, the larger domain engulfs the smaller domain covering a larger area of the cell. Eventually, the entire cell area is covered with the isotropic region.

The system considered by such experiments involves placing the cell between two ovens, one hot and the other cold, to cause a phase separating domain line between the nematic and isotropic phases. Our system shows the same results, however, with a very simple experimental set-up albeit with a change in the material set.

8.1.3.4 Verification of Switching Under Different Temperatures

In order to verify that the CNTs produce a temperature increase due to Joule heating, a switching study was performed with the sandwich cell kept under different external temperatures. Under these conditions, if Joule heating is the reason for such a phenomenon, a decrease in the phase transition time should be observed with an increase in external temperature. An increase of temperature in the samples external environment introduces a degree of disorder from the nematic phase. As a result,

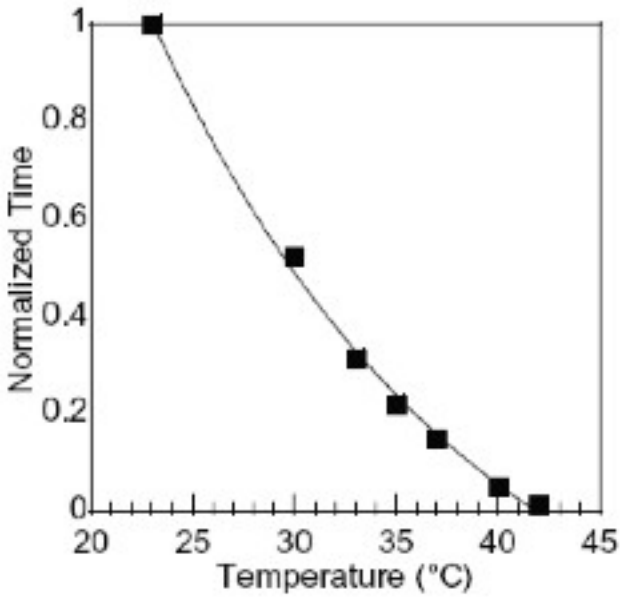

Figure 8.12: Normalized switching time of the cell with LC and CNTs annealed at 1200°C for increasing external applied temperature.

when an electric field is applied to the LC - CNT cell, the phase transition proceeds at a faster rate when compared to the time at room temperature, as shown in Figure 8.12. This verifies our claim that the CNTs contribute towards increasing the system temperature.

This phenomenon is exciting for the development of devices where conductive CNTs can be used to provide localized melting of materials including liquids and biological cells. Some applications of liquid crystals such polymer-dispersed liquid crystals rely on matching one refractive index of the LC with the polymer whereas the other index should be quite different for maximum device efficiency. A LC - CNT composite used in this work can provide the best application for the index mismatch because of the wide difference in refractive index between the nematic and isotropic states of the LC.

In order to verify that the CNTs produce a temperature increase due to Joule

heating, a switching study was performed with the sandwich cell kept under different external temperatures. Under these conditions, if Joule heating is the reason for such a phenomenon, a decrease in the phase transition time should be observed with an increase in external temperature. An increase of temperature in the samples external environment, introduces a degree of disorder from the nematic phase. As a result, when an electric field is applied to the LC - CNT cell, the phase transition proceeds at a faster rate when compared to the time at room temperature. This verifies our claim that the CNTs contribute towards increasing the system temperature.

This phenomenon is exciting for the development of devices where conductive CNTs can be used to provide localized melting of materials including liquids and biological cells. Some applications of liquid crystals such polymer-dispersed liquid crystals rely on matching one refractive index of the LC with the polymer whereas the other index should be quite different for maximum device efficiency. A LC - CNT composite used in this work can provide the best application for the index mismatch because of the wide difference in refractive index between the nematic and isotropic states of the LC.

We have observed a reversible phase transition in liquid crystal - carbon nanotube (LC - CNT) composites induced by electric field. The CNTs used for the experiments are conductive in nature. On switching the composite, the CNT rotation shorts the electrodes of the sandwich cell permitting current to flow. This leads to Joule heating within the medium causing localized temperature increase in the cell and nematic-to-isotropic transition in the LC surrounding the CNTs, which ultimately covers the entire sample area. From an applications viewpoint, CNTs filled with LCs could be used to realize nanoscale optical switches based on polarized light reflection from CNTs filled with LCs. For this device, the LC alignment state is responsible for the polarization rotation of the reflected light to generate OFF (dark state) or ON (bright states). Transitions between the ON and OFF states would be regulated by suitable

electro-magnetic fields. Another application is for removal of defects in liquid crystal displays (LCDs). Line and point defects in the LC can be impossible to remove leading to dead pixels. However, if the LC consists of a dispersion of these conductive tubes, the defects could be removed by thermal annealing. In this case, an electric field will be applied to cause a phase transition leaving the LC in the isotropic state. On field removal, the defects should vanish unless they are due to a physical impurity such as a dust particle. The phase transition should not limit the working of LCDs because the switching time corresponding to the frame rate is much lesser than the time required for electric-field induced phase transition.

8.2 Liquid Crystals inside CNTs

Now we shall probe the wetting of LCs inside CNTs. One of the applications being heavily investigated is the study of fluid transport through carbon nanotubes. The results of such a study apply to the field of drug delivery. The success of this project will allow for delivery of pico to atto-liters of drugs to a patient. This is based on the idea that, for example, a patient suffering from diabetes will respond to minute but multiple doses of insulin spread throughout the day rather than one or two large shots of insulin in the same period [130]. A possible configuration for such a device is shown in Figure 8.2 where a CNT is shown to connect a drug reservoir with a cell reservoir. In the schematic, electric field is used to drive the drug to the cell body. The principle can be extended to driving the drug through any other external field including magnetic fields. Early investigations have revealed the presence and wetting of water within the walls of a CNT [131–133]. Eventually, flow studies of glycerol and fluorescent particles were performed within CNTs [134]. However, these are relatively simpler fluids compared to drugs. Most drugs are a mixture of chemicals with complex structures and possible multiple phase characteristics. In order to really

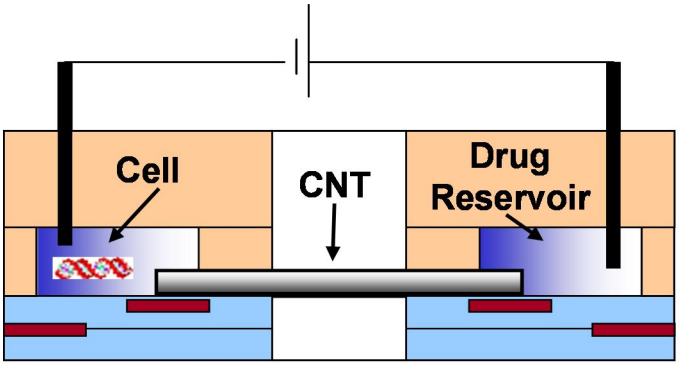

Figure 8.13: CNTs for drug delivery. From Proc. of NATO-ASI, Nanoengineered Nanofibrous Materials; Guceri, S., Gogotsi, Y., Kutsnetzov, V., Eds. Kluwer: The Netherlands, 2004, 407

understand how medical drugs can be transported through CNTs, it is necessary to use them (CNTs) to study the wetting of complex fluids. The complex fluids category encompasses materials including colloids, emulsions, suspensions, and liquid crystals.

LCs are exciting materials for the study of complex fluids through CNTs for multiple reasons: they are often a blend of several chemicals, they exhibit multiple phases, and they can mimic biological cells and their interactions. On the other hand, CNTs provide a suitable material set for the study of confinement on LC alignment. LC alignment in confined geometries is a topic of much research and still unsolved visualizations about the arrangement of molecules within polymeric cavities for PDLC based devices. The principal tasks for such a study can be broken down into the following parts:

1. Shortlisting of possible microscopy techniques

2. Demonstration of the wetting

3. Verification of LC wetting inside CNTs

Each of these tasks shall be explained in the following pages.

8.2.1 Microscopy Technique to image LC alignment within CNTs

An accurate study of LC wetting in a confined medium requires keeping the LC in its active state without touching it. Due to the scale of the confining medium (CNTs), using optical microscopy even with the highest objectives will not be able to resolve the configurations within the CNTs. The task requires microscopy techniques that are useful at the nanometer scale. These techniques include Scanning Electron Microscopy (SEM), Atomic Force Microscopy (AFM), transmission electron microscopy (TEM), and Near field Scanning Optical Microscopy (NSOM).

LC alignment is very sensitive even to surface variations on the level of angstroms. If a probe touches it, at least the local alignment is subject to change giving an inaccurate picture. NSOM requires probing of a material using an optical fiber that delivers and collects light from the sample. The probe has to be stuck inside the liquid. These rule out NSOM for the task. Also, so far, NSOM has not been used to study the wetting of any liquid within a confined medium at the scale of a CNT.

AFM suffers from the drawback that it cannot penetrate a CNT and provide a description of the confined material. If one were to really use only an AFM, it would have to be done with a special mode including the electrostatic force microscopy (EFM) where the imaging is performed with a field applied either to the AFM tip or the sample. In this case, the force curves need to be extrapolated to understand how the LC inside a CNT affects the electrostatic interactions. This is a tedious task and the accuracy of the results cannot be guaranteed. Additionally, the AFM is a slow instrument requiring hours of operation and set-up time for a single sample, especially for real-time imaging of the LC [135].

TEM is a technique that provides nanoscale imaging based on the electrons obtained after transmission through a sample. Since the technique relies on diffraction of electron beams by the sample, this poses limitations to the materials that can be

used for microscopy. Imaging liquids is not possible because the sample cannot be mounted onto special TEM grids. Also, if the liquid falls anywhere in the chamber, it will damage the instrument. All these limitations virtually ruled out TEM as a possible technique for our project.

SEM in its conventional mode cannot be applied to a nonconductive system like a LC - CNT suspension. An effect called as charging, which leads to presence of a surface charge due to the electron beam, hampers proper imaging. The surface charge repels all further electron beams leading to intense scattering to the detector. Consequently, the image appears washed in white limiting feature resolution. Also, due to the liquid nature of LC, it cannot be properly coated with a conductive layer to enable imaging. However, some SEMs have a special mode known as the environmental mode, which makes possible the imaging of liquids and non-conductive materials without experiencing the charging effect. In the environmental mode, water vapor is dispersed in the SEM chamber during the imaging under low pressures. Due to the vapor, any surface charge on the sample by the electron beam is neutralized. As a result, the electron beams do not experience repulsion, and they can penetrate the sample. Using the environmental scanning electron microscope (ESEM), water was imaged within CNTs of similar dimensions in our study [133].

8.2.1.1 Environmental Scanning Electron Microscopy (ESEM)

An FEI XL30 Environmental Scanning Electron Microscope (ESEM) was employed to observe the LC menisci inside the CNTs. The ESEM is a special mode available in certain SEMs that allows the imaging of non-condutive materials without the requirement of a conductive coating. This is best suited for materials including polymers and especially liquids allowing them to be imaged in their natural state without any alteration.

The experiments were performed by maintaining the ESEM chamber at 3 - 5Torr, and using a Gaseous Secondary Electron Detector at voltages ranging from 10 - 30kV. A LC-CNT suspension was prepared and a droplet of this suspension was placed on the sample holder and washed with methanol to remove excess LC. In case a large quantity of LC is placed over the CNTs, imaging through the ESEM becomes difficult because the electron beam cannot penetrate the thick LC layer and reach the CNTs.

In some of our experiments, using the ESEM we tried to image the flow of LCs inside the CNTs. The Peltier cooling stage was used to control the phase of 5CB. On one end of the sample holder, a droplet of CNTs dispersed in ethanol was deposited. After the ethanol evaporated, a droplet of LC was deposited on the other end of the holder, and the ESEM chamber was closed. Using the Peltier stage, the sample was kept at 4°C. At this temperature, the LC is in the solid, crystalline phase. The CNTs were located using the electron beam following which the temperature of the Peltier stage was increased to 21°C. The LC begins to melt at this temperature, and starts to flow. Because the flow velocity was not appreciable, the sample stage was tilted in such a way that the LC fluid approached the CNTs. Images were taken at different instances related to the LC proximity near the CNTs.

8.2.2 Observations

First, we will discuss LC wetting inside CNTs. As mentioned earlier, the LC and CNTs placed on the sample holder were washed with methanol to remove excess LC. As a result, some of the LC remained trapped within the CNTs and could be observed in the ESEM. The entire methanol is evaporated by the time the ESEM chamber achieves low pressure. In order to image liquids inside the CNTs, generally, a voltage of 10kV or higher is necessary so that the beam can penetrate through the CNT walls. Using the Kanaya-Okayama Depth Penetration Formula, we can estimate

Table 8.1: Penetration Depth of the Electron Beam in the ESEM

Voltage (kV)	$\mathbf{R}_{DisorderedCarbon}\mu\mathbf{m}$	$\mathbf{R}_{Graphite}\mu\mathbf{m}$
5	0.47	0.44
10	1.5	1.39
15	2.95	2.73
20	4.77	4.92
25	6.92	6.41
30	9.39	8.70

the depth of the electron beam in a material: [85]

$$\mathbf{R} = \frac{0.0276\mathbf{A}\mathbf{E}^{1.67}}{\mathbf{Z}^{0.89}\rho} \tag{8.4}$$

where $\mathbf{R}$ is the penetration depth in μm, $\mathbf{A}$ is the atomic weight in grams/mol, $\mathbf{E}$ is the electron beam energy in kV, $\mathbf{Z}$ is the atomic number, and ρ is the density in grams/cm^3.

As we can see from Table 8.1, the penetration depth in disordered carbon at beam strengths greater than 5kV is greater than 300nm, which is the thickness of the CNTs. Also, the wall structure of the CNTs is disordered carbon ensuring that the beam sufficiently penetrates the material. As a result, any material present within the CNTs will be easily imaged.

Before we discuss how LC appears inside CNTs, it is important to show a few images regarding how empty CNTs appear when imaged using the ESEM. As shown in Figure 8.14, the CNTs appear transparent to the electron beam. In Figure 8.14, the substrate morphology can be clearly seen through the CNT. However, liquid inclusions inside the CNTs tend to block the electron beam causing these regions to appear lighter in color than the parts of the CNT that are empty. In Figure 8.15, therefore, the lighter phase represents the LC residue within the CNTs forming a low contact angle meniscus, while the darker phase is the part of the CNT that is not

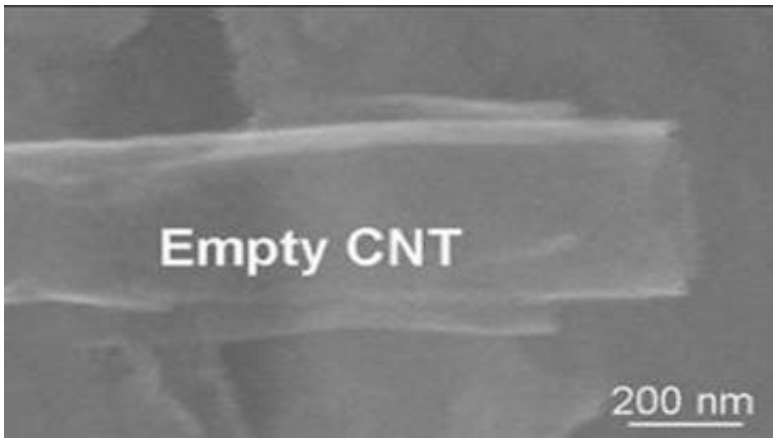

Figure 8.14: ESEM image of an empty CNT

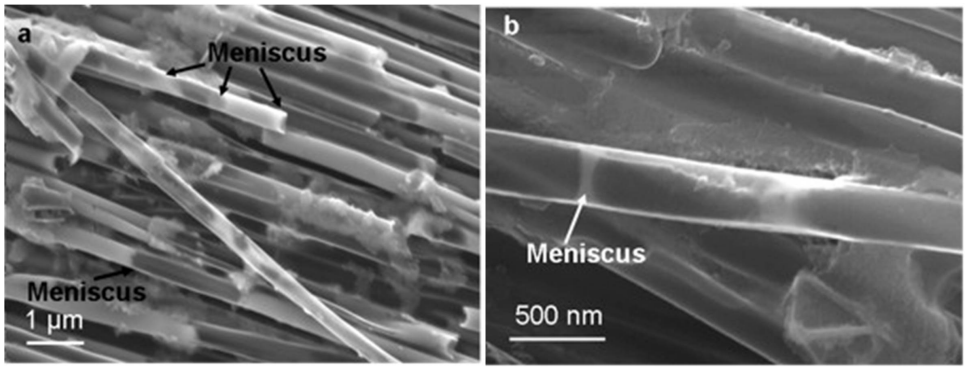

Figure 8.15: (a) ESEM image of LCs inside an agglomerate of CNPs. (b) ESEM image of menisci inside an individual CNP. The lighter phase is the LC plug, while the darker phase is the empty part of the CNP.

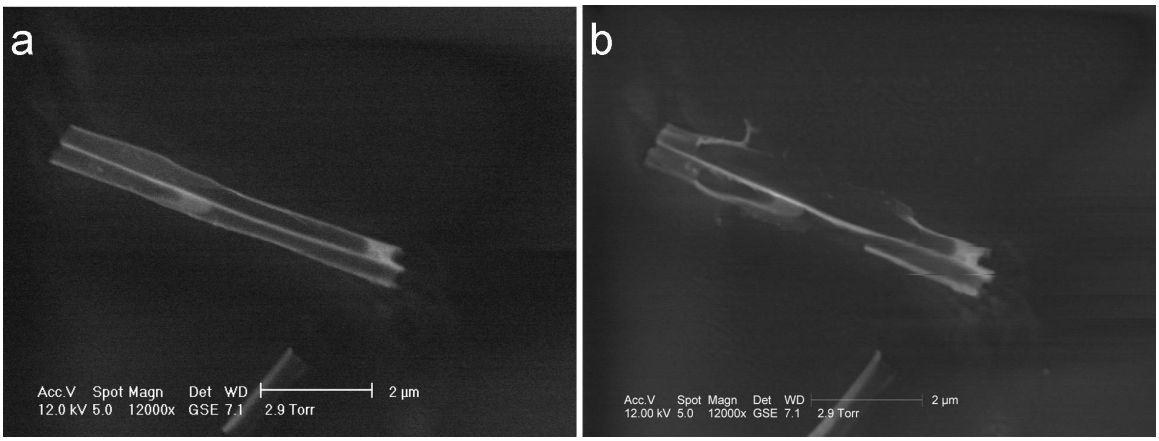

Figure 8.16: a).LC wetting in two adjacent tubes and b). LC outflow on melting the CNT walls using the electron beam

filled with LC.

LC wetting has been observed in tubes of different configurations. For the case of Figure 8.16, the electron beam was focused on the tube walls at a high beam strength (30 kV), which resulted in intense heating. When the tube walls melted away, the LC flowed out as shown in Figure 8.16b. We have also observed a nematic ordering of the tubes in the ESEM as shown in Figure 8.17

While performing ESEM with LCs and CNTs, the microscopist often encounters coated tubes. These refer to the CNTs, which are covered with a sufficient amount of LC to prevent the electron beam from penetrating further. One examples of these tubes is shown in Figure 8.18. In such cases, on keeping the electron beam over the tubes for an extended time, around a couple of minutes, the LC starts to melt because of the heat imparted by the beam. Surprisingly, the molten LC does not show as a uniform film but rather as stripes over the CNTs. This is shown in Figure 8.19. In addition to the LC stripes, condensation of the LC droplets is also observed as shown in Figure 8.20. The exact reason for this is not known. However, the CNTs can be thought to influence nucleation sites for the LC where growth and melting have

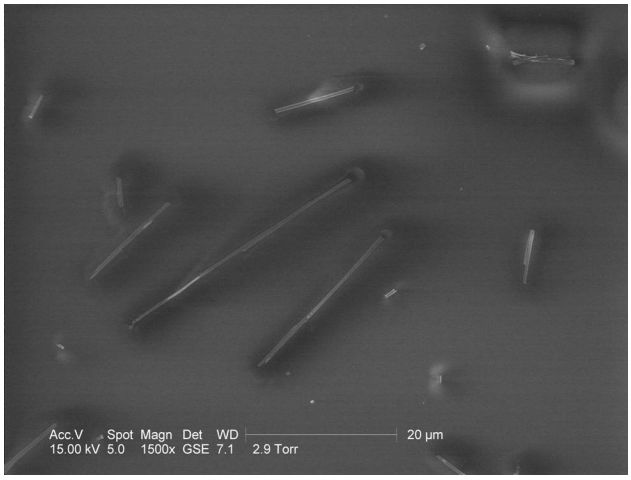

Figure 8.17: Nematic ordering of the CNTs as observed using the ESEM

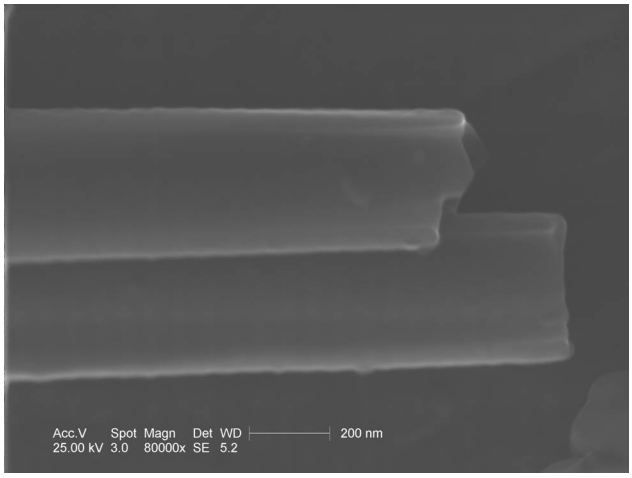

Figure 8.18: LC coated on the CNT surface

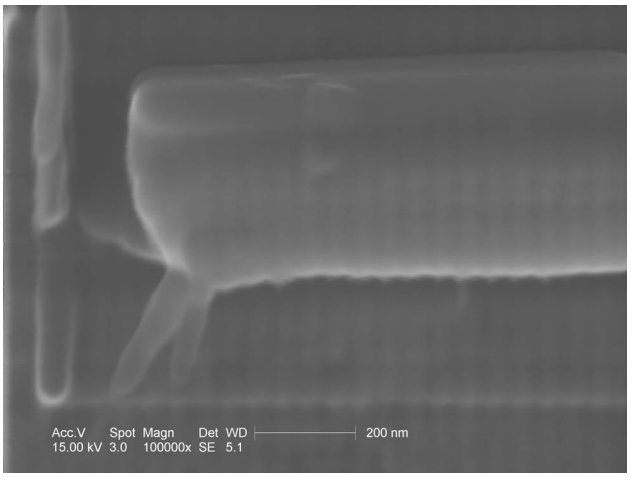

Figure 8.19: Melting of LC on the CNT walls using the electron beam of the ESEM

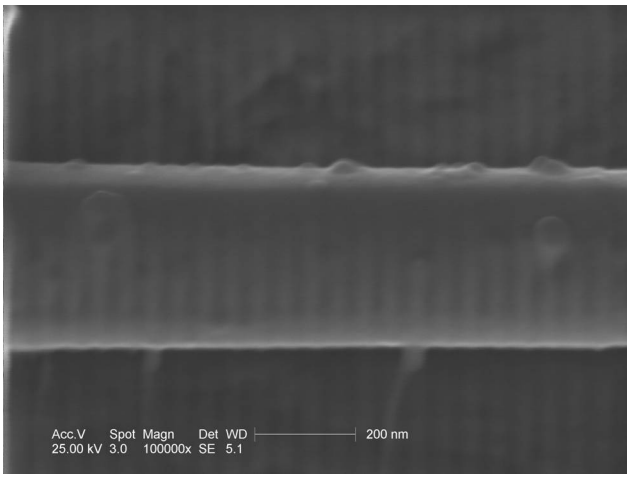

Figure 8.20: Condensation of LC droplets on the CNT walls

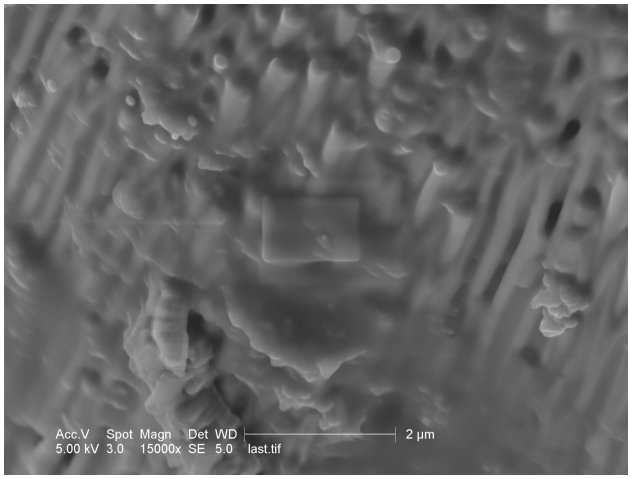

Figure 8.21: LC wetting on Alumina membrane, in which the CNTs are grown

preferred states [127]. The LC coating is also found in case of alumina membranes in which the CNTs are grown. For these experiments, after the CNTs were formed, the alumina was not dissolved in NaOH. The images of LC wetting are shown in Figures 8.21 and 8.22.

Now we shall discuss the results of the experiments where we tried to flow the LCs inside the CNTs by using the Peltier heat stage. First, we tried to image LCs in their active state. The goal of the experiments was to probe the limits of the ESEM to image individual nematic domains and/or nematic molecules. However, because of the fluid nature of the LC, imaging is difficult and the experiments of flowing 5CB into CNTs resulted in similar images as shown in Figure 8.23. Raman spectroscopy: In order to verify that the LC was confined within the CNTs, they were probed using Raman spectroscopy. A droplet of the LC-CNT suspension was placed on a polished silicon wafer and analyzed. Subsequently, the excess liquid crystals were removed by washing with methanol and a single nanotube, not surrounded by liquid crystals, was analyzed. A LC signal was observed only in the center of the nanotube and not at the two ends, as shown in the schematic in Figure 8.24, thus verifying the hypothesis that

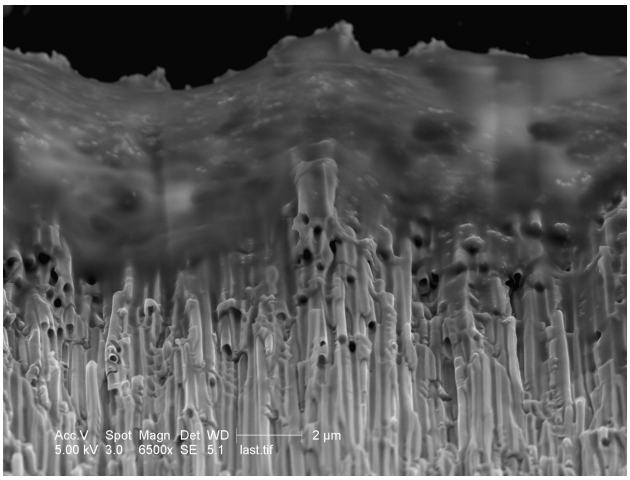

Figure 8.22: LC wetting on Alumina membrane, in which the CNTs are grown

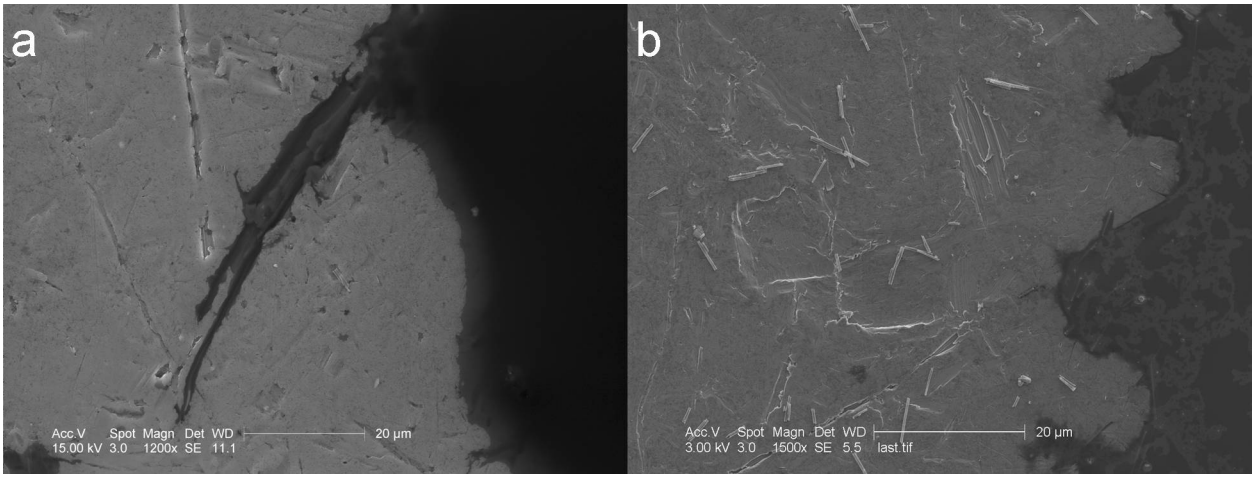

Figure 8.23: ESEM of LC flowing towards the CNTs

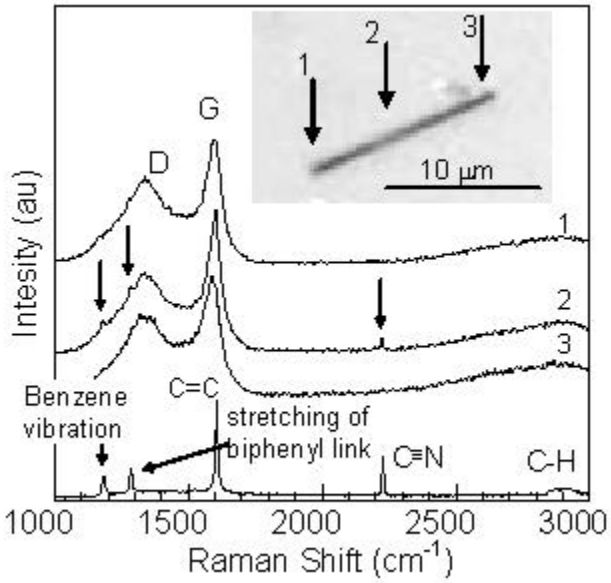

Figure 8.24: Raman Spectroscopy of LC confined in a CNT

LC remained inside the nanotube after the ethanol wash. Thus, we have described a microscopy technique, which can be used to image LCs in their live state without sample destruction. Different menisci for the LC wetting were observed in varying tube configurations.

8.3 Conclusions

A two-way effect of aligning carbon nanotubes using liquid crystals and inducing liquid crystal textures due to the presence of CNTs is presented. A theory describing the dispersion of carbon nanotubes and liquid crystals is also discussed. Using electric fields, the liquid crystals can be switched from an in-plane orientation to the out-of-plane orientation. This leads to an out-of-plane rotation of the CNTs, signifying that in addition to the external fields, the nanotubes experience torques due to the alignment of liquid crystals. However, when the CNTs are aligned out-of-plane, they cause a local deviation in the liquid crystal orientation, which is observed as defects on

the polarized optical microscope. The generation of defects is an important parameter to consider the use of CNT-LC mixtures in LCDs as it could hamper image generation.

We have observed a reversible phase transition in liquid crystal carbon nanotube (LC - CNT) composites induced by electric field. The CNTs used for the experiments are conductive in nature. On switching the composite, the CNT rotation shorts the electrodes of the sandwich cell permitting current to flow. This leads to Joule heating within the medium causing localized temperature increase in the cell and nematic-to-isotropic transition in the LC surrounding the CNTs, which ultimately covers the entire sample area.

Also, we have reported the filling and observation of liquid crystals inside carbon nanotubes using the ESEM. Due to low interfacial energies between the materials, LC is able to flow freely within the nanotubes. As verified by Raman spectroscopy, the primary interaction between these two materials is physical in nature.

Chapter 9. Applications

My research has always been geared towards the development of applications. Devices, and in a way, end products have motivated me to start different projects. In this chapter, I will explain some possible applications of my research discoveries.

9.1 Patterned polymers:

Patterned substrates are attractive for the development of liquid crystal displays (LCDs) with multiple stable states. Such displays allow for a huge saving in power consumption because if the LCD is in one of its preferred state, it can maintain it without application of electric field. In these cases, the field needs to be applied only while switching from one state to the other.

For LC research, our patterns are interesting for fundamental studies of LC confinement. LC devices requiring dispersion in polymer layers are typically confined within rough, spherical cavities. The patterns in our polymers are developed using the MTS NanoIndenter by scratching the diamond tip into the surface with a constant load applied. Consequently, the patterns have a rough inside, which can approximate the internal morphology of the polymer cavities. Since the patterns are on top of the surface, LC alignment and deposition can be studied through optical microscopy. The sample configuration is also compatible with demands placed by major spectroscopy techniques to allow for a more detailed study.

The image analysis algorithms applied to our microscopy images are very simple in their operation. Virtually, any grayscale image can be analyzed to observe variations in intensity across pixels. For my study, the intensity variations are directly correlated to the LC alignment and minute variations in LC alignment were more

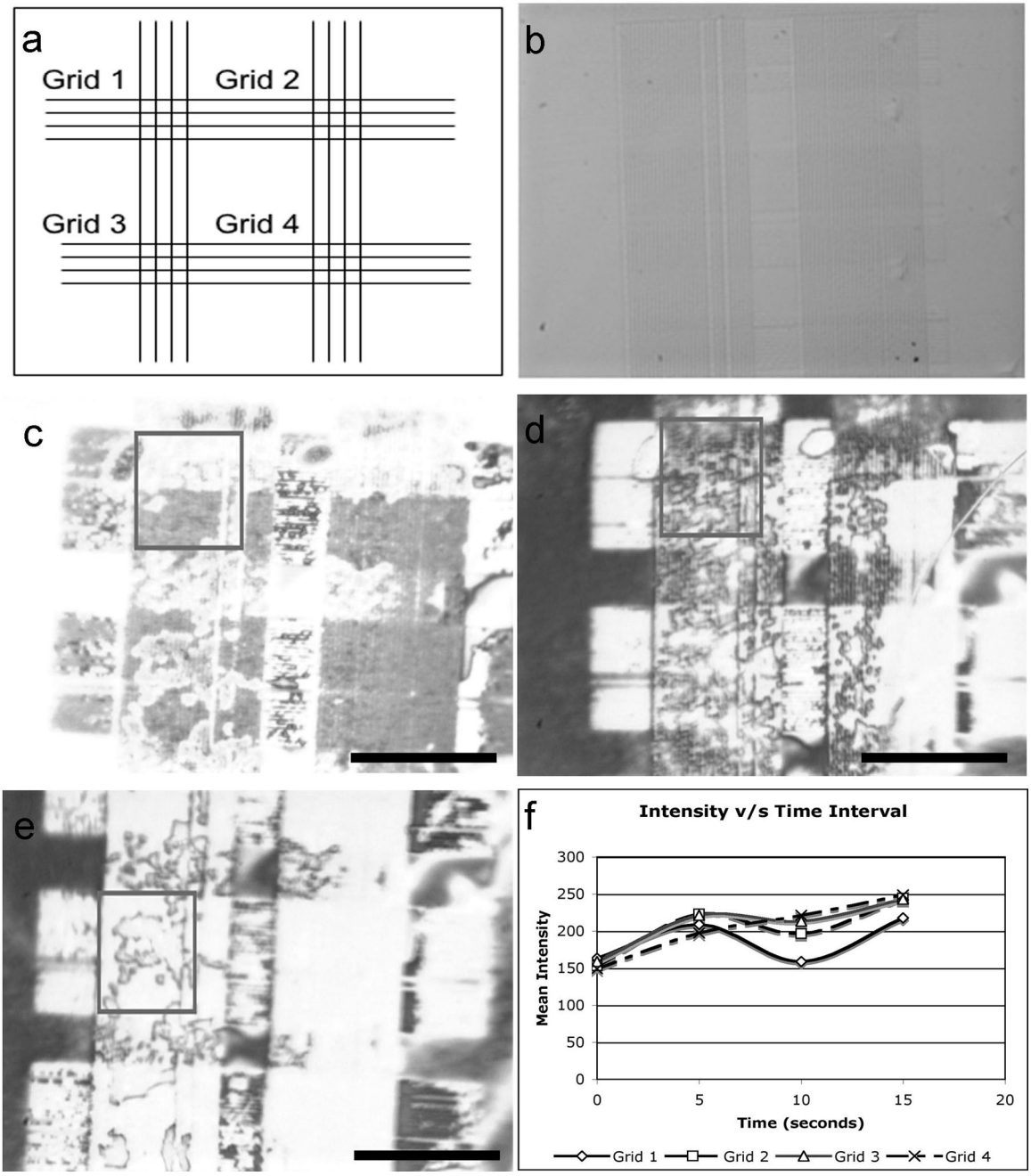

Figure 9.1: POM images of the LC alignment within the nano-patterned PMMA surface. The square box in the images can be used track changes for images in a-d; a) Schematic of the patterned grid, b) Without LC Deposition, c) LC alignment 5 seconds after deposition, d) LC alignment after stabilization (time = 10 seconds), e) Final state of LC (time = 15 seconds), and f) Time variation of the intensity

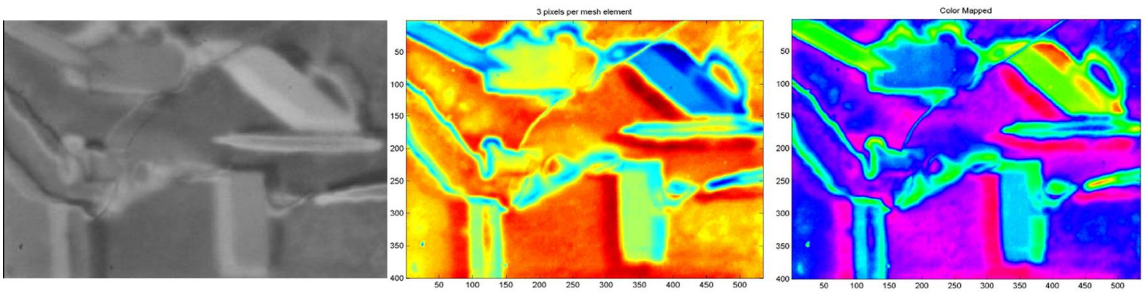

Figure 9.2: Image Analysis Results; a) POM of LC on patterned PMMA, b) Color mapped pixilated intensities of image a, c) Gradient analysis of image b

clearly observed after image analysis. The same technique can be applied to any field or applications dealing with images.

9.2 Ferroelectric polymers

Ferroelectric polymers are touted as one of the most suitable materials for next generation electronics, especially for data storage. The reasons include their ability to record polarization states, ease of forming thin films down to monolayers, low temperatures for annealing, and simple materials processing. We are one of the very few groups to combine ferroelectrics and liquid crystals. For ferroelectric polymers and liquid crystals, we are the second group to undertake this study. Of the many possible applications and research directions available to these two materials, we have undertaken some. The applications of this material set that we can surely claim are as follows:

- **Liquid crystal displays (LCDs):** The LCDs developed by using ferroelectric polymer as an alignment layer exhibit a voltage-controlled wavelength progression. This is a fascinating observation for LCD manufacturers because it allows them to generate a single color through every pixel. Typically, require three pixels to generate an effective color. Under these conditions, manufacturing

costs increase because not only they have to provide three times the actual number of observed pixels but also they need to purchase other materials such as color filters. The methods of adding the color filter layer to each pixel are also sophisticated and time-consuming. Instead, using our material set allows for the possibility of using one pixel for every visible wavelength without color filters.

- **Active color filters:** Optical telecommunication links require filtering of wavelengths over the fiber-optic links. The wavelength progression in our devices can be applied in these systems as an active color filter where the desired wavelength to be transmitted is set by holding a fixed voltage across the device. Over time, if a different wavelength is to be filtered, all that needs to be changed is the magnitude of the applied voltage. One concern is that the switching speeds of our devices is ∼3msec. However, this is with a basic nematic LC. A LC customized to the device parameters can provide faster switching.

- **Optical data storage:** Since ferroelectric polymers allow for storage of polarization, they can be coupled to LCs for developing optical data storage devices. Due to the morphology and polarization in the polymer, the LC has preferred states of alignment. Changing the polarization state through poling results in a change of LC alignment. For optical data storage, this phenomenon can be utilized by representing the data through polarization in the polymer with the LC providing optical readout. The principal concern here is the switching speed of the LCs, which will limit the application for high-speed memory devices.

- **Plasma modification of materials:** Affecting the polymer surface layers by plasma exposure has opened the doors to using semiconductor technology for display manufacturing. Typically, plasma is used for cleaning of glass in a display manufacturing business. The treatment of alignment layers is usually

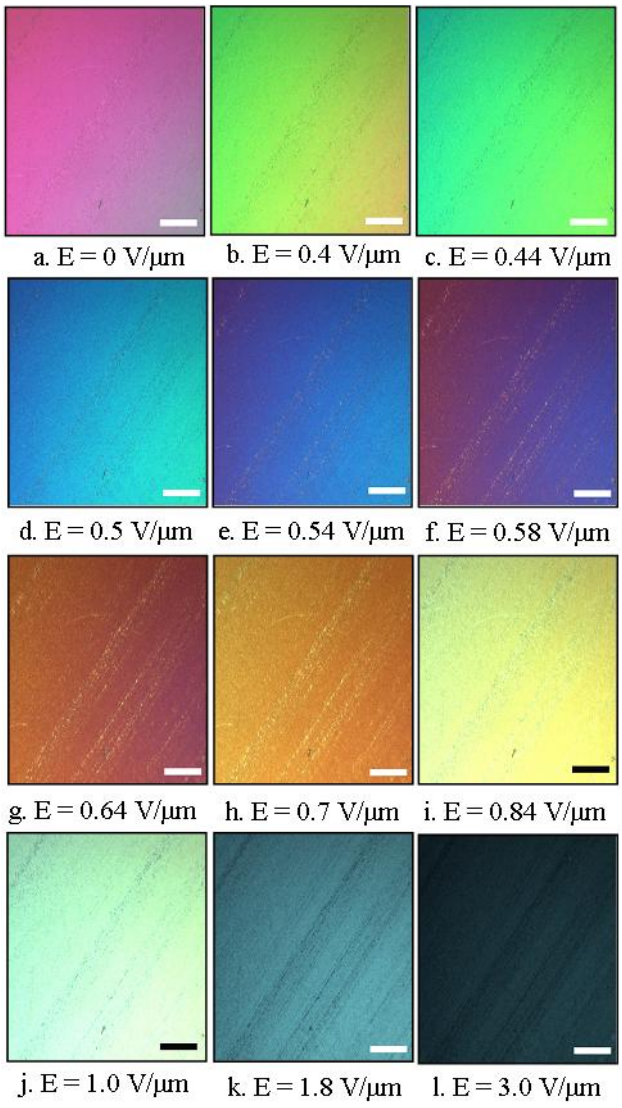

Figure 9.3: Visible wavelength progression due to liquid crystal switching on rubbed P(VDF TrFE) films. Scale bar represents 200μm

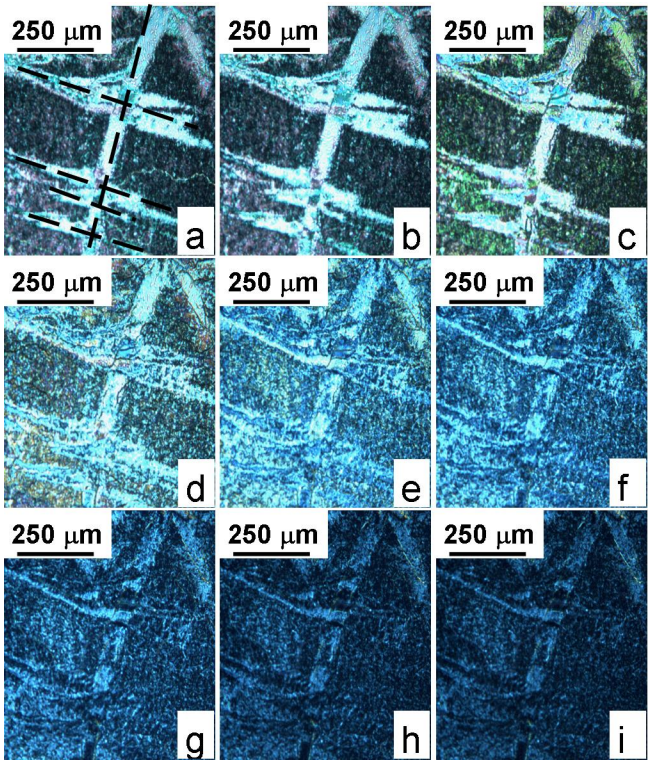

Figure 9.4: Switching Transition of LCs on a charge patterned line. a: 0V/μm, b: 1V/μm, c: 1.2V/μm, d: 1.6V/μm, e: 2V/μm, f: 2.4V/μm, g: 3V/μm, h: 3.6V/μm, i: 4 V/μm

performed through contact-based techniques such as rubbing. Currently, plasma alignment for alignment layers is provided through an angled plasma beam, which is time consuming when considering large display sizes. Our observations suggest the use of isotropic plasma for treatment of alignment layers. For display manufacturers, this is exciting because their existing glass cleaning system can be used for a non-contact alignment technique.

9.3 Liquid Crystals and Carbon Nanotubes

Carbon nanotubes (CNTs) are one of the most widely investigated materials for applications in the field of nanotechnology. Their intended uses range from drug delivery to gas storage to electronic devices. Combining them with LCs was an open-ended goal with two questions to guide us:

- Can we flow LCs inside CNTs?
- How do the CNTs affect LC switching?

The CNTs used in our studies are different from commercially available tubes in several aspects: open-ended (resembling nanopipes), straight walls, ease of dispersion in organic solvents, and no aggregation. Our discoveries in these fields can be applied as follows:

- **Fluid transport:** Previous studies had shown the flow of basic liquids such as water and glycerol in CNTs. The wetting of LC on the inside opens the door to studies of flow in complex fluids at the nanoscale. Depending on their type, LCs can mimic biological cells, especially lipids. Our results can encourage further studies of LC confinement in CNTs.
- **Nano electro-optic devices:** Since LCs allow for electro-optic switching, it is possible to switch them within the CNT walls. This configuration can be

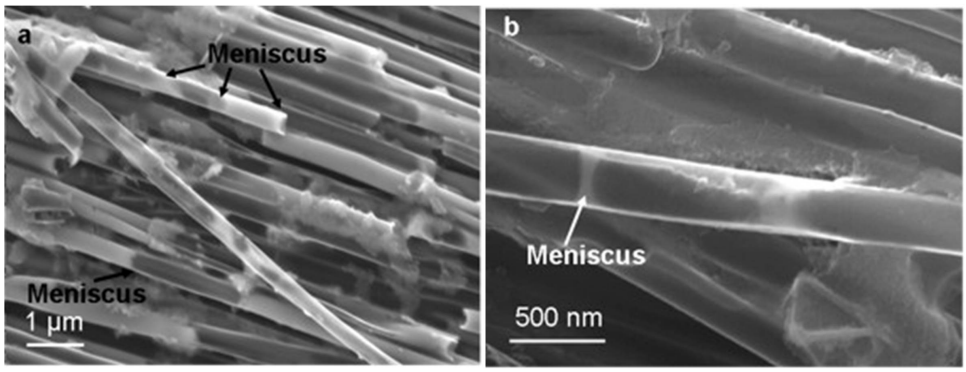

Figure 9.5: (a) ESEM image of LCs inside an agglomerate of CNPs. (b) ESEM image of menisci inside an individual CNP. The lighter phase is the LC plug, while the darker phase is the empty part of the CNP.

applied for developing nanoscale electro-optic switches. We were limited by experimental equipment including microscope limitations, and fabrication of suitable switching pads. Hopefully, future researchers can build up from our observations and demonstrate a working device.

- **Alignment material for LCDs:** The dispersion of CNTs has resulted in aligned textures of the CNTs. The reason for this is attributed to the well-spaced distribution of CNTs due to Van der Walls interactions. For use as alignment materials in display applications, a method of aligning and distributing CNTs on substrates is required. Also, the CNTs should be surface stabilized and well-anchored otherwise switching the LCD could lead to defects. With advent of inkjet printing of CNTs, this application does seem promising.

- **Annealing materials:** Our observation of Joule heating mediated phase-transition in LC-CNT suspensions highlights another future application for CNTs: as nano-heaters. The current flow through CNTs leads to heat dissipation, which caused a phase transition from the nematic phase to the isotropic phase in the LC. For LC devices, this phenomenon is useful for removal of de-

fects in the LC. Defect removal is typically hard to perform for large devices since it requires heating the material to the isotropic phase and cooling it down to the nematic phase. For small devices, this may not be a problem but it is hard to find ovens that will fit a larger sample. For LC-CNT materials, defect removal can be performed by the application and holding of an electric field for a time long enough for the phase transition to occur. Once the LC is in the isotropic phase, field removal will let the system cool down to the nematic phase. For non-LC applications, CNTs can be used for localized annealing or melting purposes.

Most of my projects were inter-disciplinary and I learned a lot through them. Some of these observations were not expected but thats how science is, I guess. I have been fortunate in the discovery of many exciting phenomenon. The exact nature for some of those is not known at the time of writing but I hope that they will inspire future work. Learning is a never ending process, and I will continue to search for answers as I move along in my career.

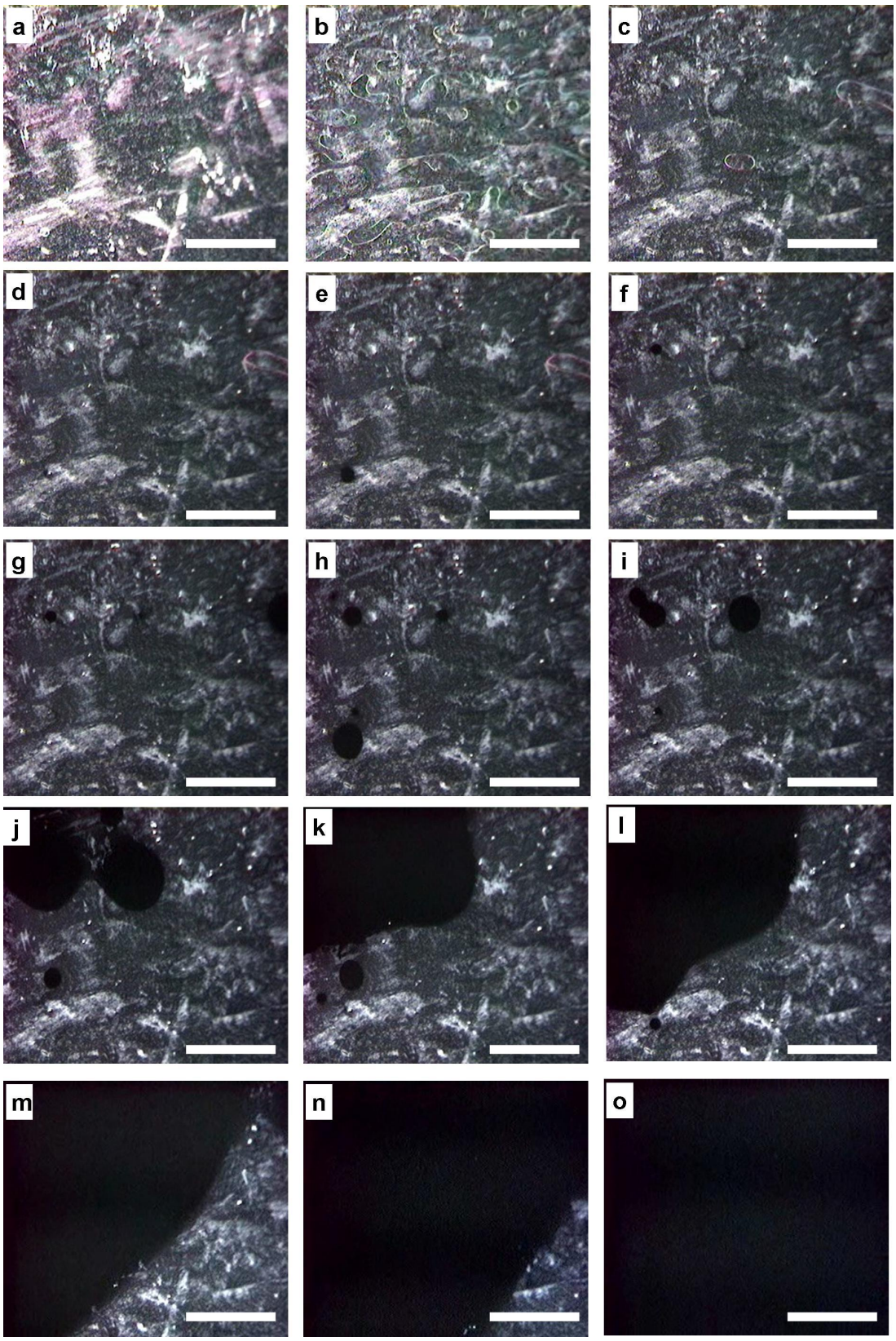

Figure 9.6: Nematic to Isotropic transition observed on application of a 1 kHz square wave, $20V_{pp}$ to the cell. The images show snapshots at different time intervals a) Initial, b) after 5 secs, c) 20 secs, d) 36.20 secs, e) 37.73 secs, f) 40.53 secs, g) 54.07 secs, h) 58.13 sec, i) 1.10 min, j) 1.18 min, k) 1.22 min l) 1.25 min, m) 1.30 min, n) 1.34 min, and o) 1.38 min

Chapter 10. Conclusions

As we have seen so far, liquid crystal (LC) alignment depends strongly on the interface with the substrate. The principal parameters of the surface from the perspective of LC alignment are the surface morphology and the surface charge. Through this thesis, we have seen the influence of a patterned surface, a surface with charge distribution, and materials with a large aspect ratio on LC alignment.

For patterned surfaces, we studied LC alignment on a grid structure that was inscribed onto the surface using the MTS NanoIndenter. By performing a time analysis study of the LC alignment using the polarized light microscope, we were able to observe the influence of the surface patterns. The patterns included parallel lines at different angles in addition to the grid structures. After LC deposition, we observed the difference in the light intensities between the patterns indicating the influence of the substrate morphology. Image analysis allowed us to observe these variations at a resolution, which was three times higher than the one provided by microscopy images. Thus, minor variations were also easily observed. These variations were also verified through a basic finite difference model developed to visualize LC alignment on patterned surfaces.

Ferroelectric polymers are exciting materials that provide a ready, controllable distribution of charges. In addition these polymers can easily form stable, transparent films making them suitable for display applications, especially flexible displays. Using ferroelectric polymers as alignment layer, we have demonstrated a voltage controlled wavelength progression in liquid crystal displays (LCDs). This progression is attributed to the dipolar interactions between the polymer and the LC molecules. The polymers were modified through addition of copolymers, dopants, plasma processing and rubbing to improve the alignment and switching response of the LCs.

Apart from displays, we have also demonstrated a proof-of-concept optical data storage device using ferroelectric polymer and LCs. Polarization patterns were written on the polymer using corona discharge technique, and the LC alignment provided the readout. By improving the resolution (area) of the charge patterns, stable submicron scale optical data storage devices can be easily produced for mass-manufacturing.

Finally, we have studied the interactions between carbon nanotubes (CNTs) and LCs. CNTs are materials that have a lot of promise for next-generation electronic devices and especially for nanoscale fluid delivery and transport. Their interactions with LCs were studied at two scales: internal and external. For the first time, LC wetting was observed within open-ended CNTs using a non-invasive microscopy technique, environmental scanning electron microscopy (ESEM). Due to extremely low interfacial energies between these two materials, it is possible to observe excellent wetting of LCs. The physical interaction was also verified using Raman Spectroscopy. For the external effects, LC - CNT suspensions were prepared for study of electro-optic characteristics. A two way alignment effect was observed where the addition of CNTs results in well-aligned LC textures whereas the nematic order of the LC is also transferred to the CNTs. The modification of the conductivity in the CNTs through annealing results in a field-induced phase transition from the nematic phase to the isotropic phase for the LC. This phenomenon results to Joule heating, which is attributed to the engineering of the sandwich cell.

Thus, we have studied LC alignment at three different interfaces, which were engineered in different aspects related to morphology, charge, and aspect ratio.

10.1 Contributions of this Dissertation

Liquid crystals (LCs) are fascinating materials, which can be used to develop electro-optic applications that include displays, imaging of biological cells, wavelength filters,

and temperature sensors. If one had to pinpoint one factor that plays a critical role in the optimum working conditions of the above devices, it would be surface alignment of LC molecules. The interface of LCs with the substrate is critical in imparting order (or disorder) in the medium. Ordering of LCs is critical since it plays a role in providing the necessary anisotropy to the material. Anisotropy in LCs exists in its optical properties (birefringence) and electro-magnetic properties (electric and magnetic anisotropy). Uniform alignment helps in providing uniformity in the perceived optical and electro-magnetic anisotropies. Since electro-optic applications require switching of the LC molecules from an OFF state to the ON state or vice-versa, uniformity in LC alignment leads to a clear distinction between the two states. In applications that require multiple states of LC alignment such as displays where gray scale variations in intensities are required, alignment is even more critical.

There are many ways to control LC alignment, which can be divided into two categories: surface variations and liquid crystal material. Within each of these there are multiple approaches, of which I have considered a total of three methods: surface morphology, surface polarization and doping the LC with carbon nanotubes.

The influence of surface morphology such as undulations on LC alignment is a known fact for decades. A process known as rubbing involves passing a polymer film in contact with a cloth rotating at a high speed. The resulting friction leads to grooves on the surface and when LCs are deposited, they align in a direction parallel to the rubbing direction. This procedure is implemented throughout the LC display manufacturing industry even today. However, rubbing does not lead to uniform undulations on the surface questioning the net influence of surface morphology on LC alignment. One method to answer this question is to study LC alignment on patterned surfaces. The patterns, which we have considered in this thesis are grids formed by the intersection of horizontal and vertical scratches on a polymer surface. Such a structure allows for the study of LC alignment in isolated grooves as well as

within intersection regions where LCs are sandwiched between the two competing directions imparted by the surface morphology. This thesis discusses experimental techniques and the results of observing the alignment variations in different patterns. The LC alignment was studied using polarized light microscopy, which is a great tool to measure differences in optical anisotropy of materials. However, depending on the microscope objectives (lens), there is a size limit to the resolution at which alignment variations can be observed. Image analysis of the microscopy images allows us to improve the resolution in addition to observing minute variations. A finite-difference model has also been developed to predict LC alignment on patterned substrates. [136]

Significance of LC alignment on patterned substrates:

- Until this date, no investigation has covered LC alignment in a 3D confined region at the length scale of 500nm x 500nm x 100nm. A recent publication discussed LC alignment in grid structures at length scales which are 100 times larger than ours. [90]

- The patterns were developed using an unconventional instrument for patterning, the MTS NanoIndenter, a material hardness-testing tool. Our technique for patterning has proven to be reliable, repeatable, and can be developed faster than most patterning techniques including lithography or an Atomic Force Microscope for fabrication. [91]

- Through a simple image analysis technique implemented in MATLAB, we have demonstrated better observation of alignment variations in microscopy images. The algorithm can be applied to systems other than liquid crystals since it can be implemented on any image. Due to its simplicity, the algorithm is fast, consumes less computing power, and can be run efficiently on a standard microcomputer. [137]

- The model we have developed for observing LC alignment is based on simulated annealing. This technique has the drawback of consuming more time compared to other minimization techniques. However, its simplicity and ease of coding make it very advantageous. Through our models, we have observed the variations of LC alignment on a patterned substrate. In addition to observing LC directors, the code is great at visualizing defect interaction. The visualization was implemented by a minor change to the code and plotting program to allow for real-time snapshots as the system settles into its state of equilibrium. [136]

The next approach to control LC alignment is through surface polarization where we have used ferroelectric polymers as the alignment layer for developing LC displays (LCDs). These polymers are characterized with a ready distribution of dipoles, which can be oriented using a variety of experimental techniques. Depending on the surface morphology, polymer composition, and polarization, the LC alignment can be controlled. The application of electric fields to a LCD where the alignment layers are ferroelectric polymers leads to a voltage-controlled wavelength transmission. LC alignment is represented by two angles, θ and ϕ, which correspond to azimuth and elevation. The resulting birefringence in the LC leads to a phase delay in the transmitted light causing selected wavelengths to be observed. At this point, the exact reason for such a phenomenon is not known due to the relative complexity of the system. The principal contributors are the surface morphology and polarization. Surface morphology is attributed to the natural assembly of the polymer chains, rubbing, and addition of dopants such as copolymers and nanoparticles. The polarization is controlled by addition of the mentioned dopants and by external fields through a poling process. I have tried to develop a comprehensive study of all these parameters towards the development of electro-optic devices. This chapter considers the effect of polymer composition on its morphology and the LC alignment. Development of

LCDs requires a controllable switching response. In our studies, we have found the combination of rubbing and certain material compositions to demonstrate controlled wavelength progression over a large surface area (1mm×1mm). Surface functionality of the polymers also plays an important role in LC alignment. Using Argon plasma, we have modified the surface of the polymer layers to develop LCDs, which operate at very low voltages. We have also demonstrated the writing of polarization states in the polymer using corona poling. This process leads to a build-up of a large internal field, which locks the LC alignment. Such a phenomenon is useful for the development of optical data storage devices.

Significance of controlling LC alignment through polarization in ferroelectric polymers:

- We have demonstrate a new LC device where the transmitted wavelength can be controlled through magnitude of the applied electric field. These devices allow for improving the resolution of current displays by 300%. Conventional LCDs generate color by the addition of intensities from red, green, and blue pixels. In order to manufacture a display with 1000 pixels, effectively 3000 pixels need to be manufactured. The wavelength progression phenomenon allows bypassing the manufacturing of red, green, and blue pixels saving production costs and improving the resolution with a given number of pixels. This is the first time such a phenomenon has been observed with a very simple nematic LC. [110, 117, 138]

- Another application for this phenomenon is to use the wavelength progression for the deign of light filters for optical communication. Lightwave technology requires filtering of select wavelengths over the transmission lines. Our devices allow for a tunable filtering through voltage variation.

- Locking the LC alignment by patterned poling of the ferroelectric polymer can

be used to develop optical data storage devices. The data in these devices is written through the polymer by poling whereas the LC layer provides the optical readout. [40]

- Through plasma modification of ferroelectric polymers, we have shown an improved performance of LCDs. Typically, directional plasma ion beams are used to control the LC alignment on regular alignment materials such as polyimide. Ferroelectric polymers provide a wonderful system to control the LC alignment using isotropic plasma. This method and material set are adaptable for large-scale manufacturing of displays. [40]

The thesis also explores the interaction between carbon nanotubes (CNTs) and liquid crystals. CNTs are exciting materials for next-generation electronics because of their ability to be used as materials for nanoscale transport as well as for their electrical characteristics. Previous studies have used the orientational order in the LCs to align CNTs. In our work, we have used CNTs, which are open-ended on both sides to study LC wetting. The nanotubes provide a means to study the effect of LC confinement at the submicron scale. We have observed LC wetting within the CNT walls using the environmental scanning electron microscopy (ESEM), a non-invasive microscopy technique. For the first time, LCs were imaged in their natural state within a variety of CNTs. We also verified that the interaction between these two materials is physical in nature i.e. without chemical bonding through Raman spectroscopy. A second part of this project involved the use of CNTs to influence LCs. Changing the conductivity of the CNTs gives us a system where we can disperse conductors in LC. On application of a large electric field to the LC-CNT suspension, CNTs as well as LCs rotate out-of-plane to align parallel to the field. If the CNTs are longer than the cell gap, an out-of-plane rotation shorts the electrodes through which the field is applied. In the case of conductive CNTs, a current will flow through

them giving rise to Joule heating. Over time, the heat dissipates in the surrounding LC medium causing a local phase transition to the isotropic phase. The isotropic phase will cover the entire cell if there are enough CNTs dispersed throughout the cell. This is an exciting phenomenon of annealing the LC without using an external heating source. Applications of this phenomenon include local heating through CNTs, and defect removal for LC devices.

Significance of carbon nanotubes on LC wetting and switching:

- For the first time, LCs were imaged real-time in a scanning electron microscope (SEM). Usually, SEM prohibits the imaging of liquids and for LC-based devices a freeze fracturing procedure is required. As a result, the sample is no longer imaged in its natural state and virtually all information regarding the LC is lost. For confined LCs, the closest estimates involve using nuclear magnetic resonance or electron spin resonance techniques. Both of these give LC information in terms of spectra, which have to be analyzed in order to understand LC wetting. In our work, we have a direct visualization of the LC wetting within the CNT walls. [139]

- Raman Spectroscopy was performed on LCs confined within the walls of the CNTs. This procedure not only allowed us to verify the physical interaction i.e. no chemical bonding between the materials but also was also able to locate the LC within the tubes. Though the Raman spectroscopy results were mainly used as a verification technique for our experiments, it can be applied to other confined LC systems such as polymer-dispersed liquid crystals (PDLCs).

- We are the first group to observe the two-way alignment effect in CNTs dispersed in LCs. In addition to ordered CNTs, we have also observed aligned textures of LC. This was in a cell without any alignment layer indicating that the CNTs were responsible for the LC alignment. The CNT ordering is due to the nematic

order of LCs. These results do suggest the suitability of using surface-stabilized CNTs as an alignment layer for LCDs. However, the implications on switching and long-term stability need to be studied in greater detail.

- The phase transition effect observed in LC - CNT suspensions is an exciting effect that allows annealing without an external heat source. Through conductive CNTs, localized heat spots may be created to remove defects in the material. This phenomenon is also attractive for materials such as LCs, where cooling down from the isotropic phase leads to minimal defects. The CNTs can be used to drive the system into the isotropic phase. LC theorists have demonstrated through thought experiments an electrically controlled phase transition from the nematic to isotropic phase starting with a phase boundary. Hopefully, our results will give them some joy by our practical verification of their theories.

Bibliography

[1] S. Chandrasekhar, *Liquid Crystals*, Cambridge University Press, 1993.

[2] A. J. Lovinger, "Ferroelectric polymers," *Science*, vol. 220, pp. 1115, 1983.

[3] F. Reinitzer, "Contributions to the understanding of cholesterol," *Monatshefe fur Chemie (Wien)*, vol. 9, pp. 421, 1888.

[4] M. Schadt and W. Helfrich, "Voltage-dependent optical activity of a twisted nematic liquid crystal," *Applied Physics Letters*, vol. 18, pp. 127, 1971.

[5] R. R. Shah and N. L. Abbott, "Principles for measurement of chemical exposure based on recognition-driven anchoring transitions in liquid crystals," *Science*, vol. 293, no. 5533, pp. 1296–1299, Aug. 2001.

[6] J. Fang, W. Ma, J.V. Selinger, and R. Shashidhar, "Imaging biological cells using liquid crystals," *Langmuir*, vol. 19, no. 7, pp. 2865–2869, 2003.

[7] Timothy J. Sluckin, David A. Dunmur, and Horst Stegemeyer, *Crystals that Flow: Classic papers from the history of liquid crystals*, Taylor and Francis, 2004.

[8] Ch. Mauguin, "On the liquid crystals of lehmann," *Bulletin de la Societe francaise de Mineralogie*, vol. 34, pp. 71, 1911.

[9] Ch. Mauguin, "Orientation of liquid crystals by a magnetic field," *Comptes rendus de l'Academie des Sciences*, vol. 152, pp. 1680, 1911.

[10] F. Grandjean, "The orientation of anisotropic liquids on crystals," *Bulletin de la Societe francaise de Mineralogie*, vol. 39, pp. 164, 1916.

[11] Peter J. Collings, *Liquid Crystals: Nature's Delicate Phase of Matter*, Princeton University Press, 2002.

[12] P. G. de Gennes and J. Prost, *The Physics of Liquid Crystals*, Oxford University Press, 1995.

[13] Bing Wen and Charles Rosenblatt, "Planar nematic anchoring due to a periodic surface potential," *Journal of Applied Physics*, vol. 89 (9), pp. 4747, 2001.

[14] A. Rastegar, M. Skarabot, B. Blij, and Th. Rasing, "Mechanism of liquid crystal alignment on submicron patterned surfaces," *Journal of Applied Physics*, vol. 89 (2), pp. 960, 2001.

[15] A. J. Pidduck, S. D. Haslam, G. P. Bryan-Brown, R. Bannister, and I. D. Kitely, "Control of liquid crystal alignment by polyimide surface modification using atomic force microscopy," *Applied Physics Letters*, vol. 71 (20), pp. 2907, 1997.

[16] Kohki Takatoh, Masaki Hasegawa, Mitsuhiro Koden, Nobuyuki Itoh, Ray Hasegawa, and Masanori Sakamoto, *Alignment Technologies and Applications of Liquid Crystals*, CRC, 2004.

[17] P. Chatelain, "The orientation of liquid crystals by polished surfaces," *Bulletin de la Societe francaise de Mineralogie*, vol. 66, pp. 105, 1943.

[18] D. W. Berreman, "Alignment of liquid crystals by grooved surfaces," *Molecular Crystals Liquid Crystals*, vol. 23, pp. 215, 1973.

[19] D.W. Berreman, "Solid surface shape and the alignment of an adjacent nematic liquid crystal," *Physical Review Letters*, vol. 28, pp. 1683, 1972.

[20] M. Barmentlo, R. W. J. Hollering, and N. A. J. M. van Aerle, "Correlations between surface and bulk liquid-crystal alignment observed with optical second-harmonic generation," *Phys. Rev. A*, vol. 46, pp. R4490, 1992.

[21] K.-Y. Han and T. Uchida, "A study of the relation between surface alignment of polymers and liquid-crystal pretilt angle," *Journal of the SID*, vol. 3, pp. 15, 1995.

[22] J. H. Kim, S. Kumar, and Sin-Doo Lee, "Alignment of liquid crystals on polyimide films exposed to ultraviolet light," *Physical Review E*, vol. 57, pp. 5644, 1996.

[23] Y. Reznikov, O. Ostroverkhova, K.D. Singer, J-H. Kim, S. Kumar, O. Lavrentovich, B. Wang, and J.L. West, "Photoalignment of liquid crystals by liquid crystals," *Phys. Rev. Lett.*, vol. 84 (9), pp. 1930, 2000.

[24] Yea-Feng Lin, Ming-Chao Tsou, and Ru-Pin Pan, "Alignment of liquid crystals by ion etched grooved glass surfaces," *Chinese Journal of Physics*, vol. 43 (6), pp. 1066, 2005.

[25] M. Ruetschi, P. Grutter, J. Funfschilling, and H.-J. Guntherodt, "Creation of liquid crystal waveguides with scanning force microscopy," *Science*, vol. 265 (5171), pp. 512, 1994.

[26] H-Y. Chen, W. Lee, and N. A. Clark, "Faster electro-optical response characteristics of a carbon-nanotube-nematic suspension," *Applied Physics Letters*, vol. 90, pp. 033510, 2007.

[27] Jong-Hyun Kim, Makoto Yoneya, and Hiroshi Yokoyama, "Tristable namatic liquid crystal device using micropatterned surface alignment," *Nature*, vol. 40 (6912), pp. 159, 2002.

[28] Hideo Fujikake, Masashi Kuboki, Takeshi Murashige, Hiroto Sato, Hiroshi Kikuchi, and Taiichiro Kurita, "Alignment mechanism of liquid crystal in a stretched porous polymer film," *Journal of Applied Physics*, vol. 94, no. 5, pp. 2864–2867, 2003.

[29] Dae-Shik Seo and Shunsuke Kobayashi, "Preliminary communication generation of pretilt angles in a nematic liquid crystal by transcription alignment on polyimide surfaces," *Liquid Crystals*, vol. 24 (3), pp. 473, 1998.

[30] L. M. Blinov, R. Barberi, S. P. Palto, M. P. De Santo, and S. G. Yudin, "Switching of a ferroelectric polymer langmuir-blodgett film studied by electrostatic force microscopy," *Journal of Applied Physics*, vol. 89, no. 7, pp. 3960, 2001.

[31] Ch. Ghwiller, "Temperature dependence of flow alignment in nematic liquid crystals," *Phys. Rev. Lett.*, vol. 2, pp. 1554, 1972.

[32] A. V. Zakharov and Ronald Y. Dong, "Flow alignment in a shearing nematic liquid crystal near a charged surface," *Phys. Rev. E*, vol. 65, pp. 052701, 2002.

[33] Jin Seog Gwag, Chul Gyu Jhun, Jae Chang Kim, Tae-Hoon Yoon, Gi-Dong Lee, and Seong Jin Cho, "Alignment of liquid crystal on a polyimide surface exposed to an ar ion beam," *Journal of Applied Physics*, vol. 96, no. 1, pp. 257–260, 2004.

[34] Jong Bok Kim, Kyung Chan Kim, Han Jin Ahn, Byoung Har Hwang, Dong Choon Hyun, and Hong Koo Baik, "Variable liquid crystal pretilt angles on various compositions of alignment layers," *Applied Physics Letters*, vol. 90, no. 4, pp. 043515, 2007.

[35] J. Stohr, M. G. Samant, J. Luning, A. C. Callegari, P. Chaudhari, J. P. Doyle, J. A. Lacey, S. A. Lien, S. Purushothaman, and J. L. Speidell, "Liquid crystal alignment on carbonaceous surfaces with orientational order," *Science*, vol. 292, no. 5525, pp. 2299–2302, 2001.

[36] P. Chaudhari, James Lacey, James Doyle, Eileen Galligan, Shui-Chi Alan Lien, Alesandro Callegari, Gareth Hougham, Norton D. Lang, Paul S. Andry, Richard John, Kei-Hsuing Yang, Minhua Lu, Chen Cai, James Speidell, Sampath Purushothaman, John Ritsko, Mahesh Samant, Joachim Stohr, Yoshiki Nakagawa, Yoshimine Katoh, Yukito Saitoh, Kazumi Sakai, Hiroyuki Satoh, Shuichi Odahara, Hiroki Nakano, Johji Nakagaki, and Yasuhiko Shiota, "Atomic-beam alignment of inorganic materials for liquid-crystal displays," *Nature*, vol. 411, no. 6833, pp. 56–59, May 2001.

[37] Vinay K. Gupta and Nicholas L. Abbott, "Design of surfaces for patterned alignment of liquid crystals on planar and curved substrates," *Science*, vol. 276, no. 5318, pp. 1533–1536, June 1997.

[38] M.J. Escuti and G.P. Crawford, ," in *Materials Research Society Symposium*, 2002, vol. 709, pp. 293–298.

[39] M. Sutkowski, T. Grudniewski, R. Zmijan, J. Parka, and E. Nowinowski-Kruszelnicki, "Optical data storage in lc cells," *Opto-Electronics Review*, vol. 14 (4), pp. 335, 2006.

[40] H. J. Shah, D. Delaine, and A. K. Fontecchio, "Plasma modification of fluoropolymers for aligning liquid crystals," *in press for IEEE/OSA Journal of Display Technology*.

[41] Scott Woltman and Gregory Crawford, "Two-dimensional color array for emissive color-filter technology," in *26th International Display Research Conference*, 2006.

[42] M. F. Moreira, I. C. S. Carvalho, W. Cao, C. Bailey, B. Taheri, and P. Palffy-Muhoray, "Cholesteric liquid-crystal laser as an optic-fiber based temperature sensor," *Applied Physics Letters*, vol. 85, pp. 2691, 2004.

[43] T. J. Bunning, L. V. Natarajan, V. P. Tondiglia, and R. L. Sutherland, "Holographic polymer-dispersed liquid crystals (h-pdlcs)," *Annu. Rev. Mater. Sci.*, vol. 30, pp. 83, 2000.

[44] A. K. Fontecchio, J. Qi, M. J. Escuti, I. Amimori, G. P. Crawford, and S. Faris, "Diffuse renditions of spatially pixelated and temporally multiplexed h-pdlcs for full color reflective displays," *SID Digest of Technical Papers XXXII*, vol. 31, pp. 348, 2001.

[45] M. Vilfan, B. Zalar, A. K. Fontecchio, M. Vilfan, M. J. Escuti, G. P. Crawford, and S. Zumer, "Deuteron nmr study of molecular ordering in a holographic polymer dispersed liquid crystal," *Physical Review E*, vol. 66, pp. 021710, 2002.

[46] Jong-Hyun Kim, Makoto Yoneya, Jun Yamamoto, and Hiroshi Yokoyama, "Nano-rubbing of a liquid crystal alignment layer by an atomic force microscope: a detailed characterization," *Nanotechnology*, vol. 13 (2), pp. 133, 2002.

[47] Jong-Hyun Kim, Makoto Yoneya, Jun Yamamoto, and Hiroshi Yokoyama, "Surface alignment bistability of nematic liquid crystals by orientationally frustrated surface patterns," *Applied Physics Letters*, vol. 78 (20), pp. 3055, 2001.

[48] E.H. Lay, A. Kirakosian, J.L. Lin, D.Y. Petrovykh, J.N. Crain, F.J. Himpsel, R.R. Shah, and N.L. Abbott, "Alignment of liquid crystals on stepped and passivated silicon templates prepared in ultrahigh vacuum," *Langmuir*, vol. 16, pp. 6731–6738, 2000.

[49] C. J Newsome, M. O'Neill, Farley R. J., and G. P. Bryan-Brown, "Laser etched gratings on polymer layers for alignment of liquid crystals," *Applied Physics Letters*, vol. 72, pp. 2078, 1998.

[50] Xuemin Lu, Qinghua Lu, Zikang Zhu, Jie Yin, and Zongguang Wang, "Liquid crystal alignment on periodic microstructure induced by single-beam 532 nm polarized laser illumination on poly(urethane-imide) film," *Chemical Physics Letters*, vol. 377 (3 - 4), pp. 433, 2003.

[51] Baoshe Zhang, Fuk Kay Lee, Ophelia K. C. Tsui, and Ping Sheng, "Liquid crystal orientation transition on microtextured substrates," *Phys. Rev. Lett.*, vol. 91, pp. 215501, 2003.

[52] T. J. Reece, S. Ducharme, A. V. Sorokin, and M. Poulsen, "Nonvolatile memory element based on a ferroelectric polymer langmuir-blodgett film," *Applied Physics Letters*, vol. 82, no. 1, pp. 142, 2003.

[53] H.S. Nalwa, *Ferroelectric polymers: chemistry, physics, and applications*, Marcel-Dekker, 1995.

[54] J. F. Hubbard, H. F. Gleeson, R. W. Whatmore, C. P. Shaw, and Q. Zhang, "Coupling of the remanent polarisation in thin film oxide ferroelectrics with nematic liquid crystals," *Journal of Materials Chemistry*, vol. 9, pp. 375, 1998.

[55] L. M. Blinov, S. P. Palto, S. V. Yakovlev, and D. G. Sikharulidze, "Asymmetric electro-optical switching of a nematic cell controlled by a corona poled ferroelectric polymer layer," *Applied Physics Letters*, vol. 72, no. 25, pp. 3377–3379, 1998.

[56] A. R. Geivandov and S. P. Palto, "The influence of ferroelectric polymer alignment layer on electrooptical properties of nematic lc cell," *Molecular Crystals And Liquid Crystals*, vol. 433, pp. 155–164, 2005.

[57] Hui-Yu Chen and Wei Lee, "Suppression of field screening in nematic liquid crystals by carbon nanotubes," *Applied Physics Letters*, vol. 88, pp. 222105, 2006.

[58] W. Lee, J.-S. Gau, and H.-Y. Chen, "Electro-optical properties of planar nematic cells impregnated with carbon nanosolids," *Applied Physics B: Lasers and Optics*, vol. 81 (2 - 3), pp. 171, 2005.

[59] Natalie Kamanina and Igor Denisyuk, "Switching of optical response in fullerene-doped liquid crystal compounds," *Optics Communications*, vol. 235 (4 - 6), pp. 361, 2004.

[60] E. Ouskova, O. Buchnev, V. Reshetnyak, and Yu. Reznikov, "Dielectric relaxation spectroscopy of a nematic liquid crystal doped with ferroelectric $sn_2p_2s_6$ nanoparticles," *Liquid Crystals*, vol. 30, pp. 1, 2003.

[61] Yurii Reznikov, Olexander Buchnev, Olexander Tereshchenko, Victor Reshetnyak, Anatoliy Glushchenko, and John West, "Ferroelectric nematic suspension," *Applied Physics Letters*, vol. 82 (12), pp. 1917, 2003.

[62] Fenghua Li, Oleksandr Buchnev, Chae Il Cheon, Anatoliy Glushchenko, Victor Reshetnyak, Yuri Reznikov, Timothy J. Sluckin, and John L. West, "Orientational coupling amplification in ferroelectric nematic colloids," *Physical Review Letters*, vol. 97, pp. 147801, 2006.

[63] O. Buchnev, C. I. Cheon, A. Glushchenko, Yu. Reznikov, and J. L. West, "New non-synthetic method to modify properties of liquid crystals using micro and nano-particles," *Journal of the SID*, vol. 13/9, pp. 749, 2005.

[64] M. Talarico, G. Carbone, R. Barberi, and A. Golemme, "Fullerenes surface gratings for liquid crystal alignment," *Applied Physics Letters*, vol. 85, no. 4, pp. 528, 2004.

[65] W. Lee, H.Y. Chen, and S.L. Yeh, "Surface-sustained permanent gratings in nematic liquid crystals doped with carbon nanotubes," *Optics Express*, vol. 10, no. 11, pp. 482, 2002.

[66] Wei-Lee and Yuan-Lin Wang, "Evidence for holographic image storage in a fullerene-doped liquid-crystal film," *Chinese Journal of Physics*, vol. 39 (4), pp. 295, 2001.

[67] Wei Lee and Chi-Shen Chiu, "Observation of self-diffraction by gratings in nematic liquid crystals doped with carbon nanotubes," *Optics Letters*, vol. 26 (8), pp. 521, 2001.

[68] I. C. Khoo, "Orientational photorefractive effects in nematic liquid crystal films," *IEEE Journal of Quantum Electronics*, vol. 32 (3), pp. 525, 1996.

[69] W. Lee and S.L. Yeh, "Optical amplification in nematics doped with carbon nanotubes," *Applied Physics Letters*, vol. 79, no. 27, pp. 4488, 2001.

[70] W. Lee and H. C. Chen, "Diffraction efficiency of a holographic grating in a liquid-crystal cell composed of asymmetrically patterned electrodes," *Nanotechnology*, vol. 14, no. 9, pp. 987–990, Sept. 2003.

[71] Wei Lee and Yuan-Lin Wang, "Voltage-dependent orientational photorefractivity in a planar c60-doped nematic film," *J. Phys. D: Appl. Phys.*, vol. 35, pp. 850, 2002.

[72] M. D. Lynch and D. L. Patrick, "Organizing carbon nanotubes with liquid crystals," *Nano Letters*, vol. 2, no. 11, pp. 1197–1201, 2002.

[73] I. Dierking, G. Scalia, and P. Morales, "Liquid crystal-carbon nanotube dispersions," *Journal of Applied Physics*, vol. 97, no. 4, pp. 044309, 2005.

[74] I. Dierking, G. Scalia, P. Morales, and D. LeClere, "Aligning and reorienting carbon nanotubes with nematic liquid crystals," *Advanced Materials*, vol. 16, no. 11, pp. 865, 2004.

[75] C. Da Cruz, P. Launois, and M. Veber, "Original magnetic alignment of a nematic phase containing single-walled nanotubes," *Journal of Nanoscience and Nanotechnology*, vol. 4 (1 - 2), pp. 86, 2004.

[76] Joete M. Russell, Soojin Oh, Issac LaRue, Otto Zhou, and Edward T. Samulski, "Alignment of nematic liquid crystals using carbon nanotube films," *Thin Solid Films*, vol. 509, pp. 53, 2006.

[77] M. Wegener, W. Kunstler, K. Richter, and R. Gerhard-Multhaupt, "Ferroelectric polarization in stretched piezo- and pyroelectric poly(vinylidene fluoride-hexafluoropropylene) copolymer films," *Journal of Applied Physics*, vol. 92, no. - 12, pp. 7447, 2002.

[78] M. Wegener and R. Gerhard-Multhaupt, "Electric poling and electromechanical characterization of 0.1-mm-thick sensor films and 0.2-mm-thick cable layers from poly(vinylidene fluoride-trifluroethylene)," *IEEE Transactions on Ultrasonics, Ferroelectrics and Frequency Control*, vol. 50, no. 7, pp. 921, 2003.

[79] L. Priya and J. P. Jog, "Intercalated poly(vinylidene flouride)/clay nanocomposites: structure and properties," *Journal of Polymer Science, Part B (Polymer Physics)*, vol. 41, no. 1, pp. 31, 2003.

[80] Younghoon Kim, James L. White, and Solvay Solexis, *SOLEF (R) Technical Manual for Polyvinylidene Fluoride*, vol. 3, Society of Plastics Engineers, Chicago, IL., United States.

[81] D. Mattia, H. Bau, and Y. Gogotsi, "Wetting of cvd carbon films by polar and non-polar liquids and implications for carbon nanopipes," *Langmuir*, vol. 22, no. 4, pp. 1789, 2006.

[82] D. Mattia, M. P. Rossi, B. H. Kim, G. Korneva, H. H. Bau, and Y. Gogotsi, "Effect of graphitization on the wettability and electrical conductivity of cvd carbon nanotubes and films," *Journal of Physical Chemistry B*, vol. 110, no. 20, pp. 9850, 2006.

[83] H.O. Pierson, *Handbook of Carbon, Graphite, Diamond and Fullerenes*, Noyes, 1993.

[84] I Dierking, *Textures of Liquid Crystals*, Wiley-VCH, 2003.

[85] Maria Pia Rossi, *Environmental scanning electron microscopy study of the interaction of carbon nanotubes with fluids*, Ph.D. thesis, Drexel University, 2006.

[86] P. J. Hendra, "How does ftir work?," *International Journal of Vibrational Spectroscopy*, vol. 5 (5), pp. 2, 2001.

[87] Frank Settle, Ed., *Handbook of Instrumental Techniques for Analytical Chemistry*, Prentice Hall, 1997.

[88] Michael L. Ermold and Adam K. Fontecchio, "Electrically switchable holographic parabolic mirrors," *Journal of Applied Physics*, vol. 99, pp. 093111, 2006.

[89] Lay Min Lee, Hye J. Kwon, Joo H. Kang, Ralph G. Nuzzo, and Kenneth S. Schweizer, "Anchoring and electro-optical dynamics of thin liquid crystalline films in a polyimide cell: Experiment and theory," *J. Chem. Phys*, vol. 125, pp. 024705, 2006.

[90] Youngwoo Yi, Michi Nakata, Alexander R. Martin, and Noel A. Clark, "Alignment of liquid crystals by topographically patterned polymer films prepared by nanoimprint lithography," *Applied Physics Letters*, vol. 90, pp. 163510, 2007.

[91] Hemang J. Shah and Adam K. Fontecchio, "Nano-patterned polymer structures for h-pdlcs," in *The International Symposium on Optical Science and Technology: SPIE's 48th Annual Meeting Proceedings, Section 5225: Physical Chemistry and Interfaces II*, 2003.

[92] C M Care and D J Cleaver, "Computer simulation of liquid crystals," *Reports on Progress in Physics*, vol. 68, pp. 2665, 2005.

[93] M. R. Wilson, "Atomistic simulations of liquid crystals," *Struct. Bond.*, vol. 94, pp. 42, 1999.

[94] M. P. Allen and D. J. Tildesley, *Computer simulation of liquids*, Clarendon Press, 1988.

[95] R. Berardi, M. Ricci, and C. Zannoni, "Ferroelectric and structured phases from polar tapered mesogens," *Ferroelectrics*, vol. 309, pp. 3, 2004.

[96] D. L. Cheung, S. J. Clark, and M. R. Wilson, "Calculation of the rotational viscosity of a nematic liquid crystal," *Chem. Phys. Lett.*, vol. 356, pp. 140, 2002.

[97] D. L. Cheung, S. J. Clark, and M. R. Wilson, "Calculation of flexoelectric coefficients for a nematic liquid crystal by atomistic simulation," *J. Chem. Phys*, vol. 121, pp. 9131, 2004.

[98] Kerson Huang, *Statistical Mechanics*, Wiley, 1987.

[99] William H. Press, Brian P. Flannery, Saul A. Teukolsky, and William T. Vetterling (Author), *Numerical Recipes in C: The Art of Scientific Computing*, Cambridge University Press, 1992.

[100] S. Kirkpatrick, C. D. Gelatt, and M. P. Vecchi, "Optimization by simulated annealing, science," *Science*, vol. 220 (4598), pp. 671, 1983.

[101] B. Xu, Y. Ovchenkov, M. Bai, A. N. Caruso, A. V. Sorokin, S. Ducharme, B. Doudin, and P. A. Dowben, "Heterojunction diode fabrication from polyaniline and a ferroelectric polymer," *Applied Physics Letters*, vol. 81, no. 22, pp. 4281, 2002.

[102] M. Date, T. Furukawa, T. Yamaguchi, A. Kojima, and I. Shibata, "Opto-ferroelectric memories using vinylidene fluoride and trifluoroethylene copolymers," *1988 6th International Symposium on Electrets, 1-3 Sept. 1988*, vol. 24, no. 3, pp. 537, 1989.

[103] A. V. Bune, V. M. Fridkin, S. Ducharme, L. M. Blinov, S. P. Palto, A. V. Sorokin, S. G. Yudin, and A. Zlatkin, "Two-dimensional ferroelectric films," *Nature*, vol. 391, no. 6670, pp. 874, 1998.

[104] Atitsa Petchsuk, *Ferroelectric terpolymers, based on semicrystalline VDF/TrFE/chloro-containing termonomers synthesis, electrical properties, and functionalization reactions*, Ph.D. thesis, Pennsylvania State University, 2003.

[105] L. Priya and J. P. Jog, "Polymorphism in intercalated poly(vinylidene fluoride)/clay nanocomposites," *Journal of Applied Polymer Science*, vol. 89, no. 8, pp. 2036, 2003.

[106] L. Priya and J. P. Jog, "Poly(vinylidene fluoride)/clay nanocomposites prepared by melt intercalation: crystallization and dynamic mechanical behavior studies," *Journal of Polymer Science, Part B (Polymer Physics)*, vol. 40, no. 15, pp. 1682, 2002.

[107] D. R. Dillon, K. K. Tenneti, C. Y. Li, F. K. Ko, I. Sics, and B. S. Hsiao, "On the structure and morphology of polyvinylidene fluoride - nanoclay composites," *Polymer*, vol. 47, pp. 1678–1688, 2006.

[108] Jacob N. Israelachvili, *Intermolecular and Surface Forces: With Applications to Colloidal and Biological Systems*, Academic Press, London, second edition, 1991.

[109] E. M. Inc, "Technical data sheet, lcg k15, product no. 058300," Tech. Rep.

[110] H. J. Shah and A. K. Fontecchio, "Low-voltage color switching in liquid crystal displays," in *26th International Display Research Conference*, Kent, Ohio, 2006, p. 315.

[111] J. A. Giacometti, P. A. Ribeiro, M. Raposo, J. N. Marat-Mendes, J. S. Carvalho Campos, and A. S. DeReggi, "Study of poling behavior of biaxially stretched poly(vinylidene fluoride) films using the constant-current corona triode," *Journal of Applied Physics*, vol. 78, no. 9, pp. 5597–603, 11/01 1995, M1: Copyright 1995, IEE.

[112] D. K. Das-Gupta and K. Doughty, "Corona charging and the piezoelectric effect in polyvinylidene fluoride," *Journal of Applied Physics*, vol. 49, no. 8, pp. 4601–3, 08/ 1978, M1: Copyright 2005, IEE.

[113] Y. Bormashenko, R. Pogreb, O. Stanevsky, E. Bormashenko, A. V. Bune, V. M. Fridkin, S. Ducharme, L. M. Blinov, S. P. Palto, A. V. Sorokin, S. G. Yudin, and A. Zlatkin, "Two-dimensional ferroelectric films," *Polymer Testing*, vol. 391, no. 6670, pp. 874, 1998.

[114] C. J. L. Constantino, A. E. Job, R. D. Simoes, J. A. Giacometti, V. Zucolotto, O. N. Oliveira, G. Gozzi, and D. L. Chinaglia, "Phase transition in poly(vinylidene fluoride) investigated with micro-raman spectroscopy," *Applied Spectroscopy*, vol. 59, no. 3, pp. 275–279, 2005.

[115] E. T. Kang and Y. Zhang, "Surface modification of polymers via molecular design," *Advanced Materials*, vol. 12, pp. 1481, 2000.

[116] Y. W. Park and N. Inagaki, "A new approach for selective surface modification of fluoropolymers by remote plasmas," *Journal of Applied Polymer Science*, vol. 93, pp. 1012, 2004.

[117] H. J. Shah and A. K. Fontecchio, "Influence of ferroelectric polymer layers on liquid crystal alignment," *Abstracts Of Papers Of The American Chemical Society*, vol. 230, pp. U3504–U3504, 2005.

[118] Peter J. F. Harris, *Carbon Nanotubes and Related Structrures*, Cambridge University Press, 1999.

[119] W. H. Song, I. A. Kinloch, and A. H. Windle, "Nematic liquid crystallinity of multiwall carbon nanotubes," *Science*, vol. 302, no. 5649, pp. 1363, 2003.

[120] M. S. P. Shaffer, X. Fan, and A. H. Windle, "Dispersion and packing of carbon nanotubes," *Carbon*, vol. 36 (11), pp. 1603, 1998.

[121] Wenhui Song, Ian A. Kinloch, and Alan H. Windle, "Nematic liquid crystallinity of multiwall carbon nanotubes," *Science*, vol. 302, pp. 1363, 2003.

[122] G. W. Gray and A. Mosley, "The raman spectra of 4-cyano-4'-pentylbiphenyl and 4-cyano-4'-pentyl-d/sub 11/-biphenyl," *Molecular Crystals and Liquid Crystals*, vol. 35, no. 1-2, pp. 71, 1976.

[123] J. Cognard, ," *Mol. Cryst. Liq. Cryst. Supp.*, vol. 78, pp. 1, 1982.

[124] W. Lee, C.Y. Wang, and Y.C. Shih, "Effects of carbon nanosolids on the electro-optical properties of a twisted nematic liquid-cry," *Applied Physics Letters*, vol. 85, no. 4, pp. 513–515, 2004.

[125] S. Courty, J. Mine, A. R. Tajbakhsh, and E. M. Terentjev, "Nematic elastomers with aligned carbon nanotubes: New electromechanical actuators," *Europhysics Letters*, vol. 64, pp. 654, 2003.

[126] Martin Chambers, Bostjan Zalar, Maja Remskar, Slobodan Zumer, and Heino Finkelmann, "Actuation of liquid crystal elastomers reprocessed with carbon nanoparticles," *Applied Physics Letters*, vol. 89, no. 24, pp. 243116, 2006.

[127] G. Scalia, J. P. F. Lagerwall, M. Haluska, U. Dettlaff-Weglikowska, F. Giesselmann, and S. Roth, "Effect of phenyl rings in liquid crystal molecules on swcnts studied by raman spectroscopy," *Physica Status Solidi (b)*, vol. 243, no. 13, pp. 3238–3241, 2006.

[128] N. Mottram, C. M. Care, and D. J. Cleaver, "Control of the nematic-isotropic phase transition by an electric field," *Physical Review E*, vol. 74, pp. 041703, 2006.

[129] D. Andrienko, M. Tasinkevych, P. Patricio, and M. M. Telo da Gama, "Interaction of colloids with a nematic-isotropic interface," *Physical Review E*, vol. 69, pp. 021706, 2004.

[130] P. F. Semple, C. White, and W. G. Manderson, "Continuous intravenous infusion of small doses of insulin in treatment of diabetic ketoacidosis," *British Medical Journal*, vol. 2 (5921), pp. 694, 1974.

[131] N. Naguib, H. Ye, Y. Gogotsi, A. G. Yazicioglu, C. M. Megaridis, and M. Yoshimura, "Observation of water confined in nanometer channels of closed carbon nanotubes," *Nano Letters*, vol. 4, pp. 2237–2243, 2004.

[132] M. P. Rossi and Y. Gogotsi, "Environmental sem studies of nanofiber-liquid interactions," *Microscopy and Analysis (The Americas Edition)*, vol. 18, no. 4, pp. 9–11, 2004.

[133] M. P. Rossi, H. Ye, Y. Gogotsi, S. Babu, P. Ndungu, and J.C. Bradley, "Environmental scanning electron microscopy study of water in carbon nanopipes," *Nano Letters*, vol. 4, pp. 989–993, 2004.

[134] B. M. Kim, S. Qian, and H. H. Bau, "Filling carbon nanotubes with particles," *Nano Letters*, vol. 5, no. 5, pp. 873–878, 2005.

[135] Klemen Kocevar, *Study of Ordering and Forces in Liquid Crystal-Solid Interfaces*, Ph.D. thesis, University of Ljubljana, 2001.

[136] Hemang J. Shah and Adam K. Fontecchio, "Modeling and experimental studies of lc alignment induced by nanopatterned substrates," in *The International Symposium on Optical Science and Technology: SPIE's 49th Annual Meeting Proceedings, Section 5518: Liquid Crystals VIII*, 2004.

[137] H. J. Shah, M. L. Ermold, and A. K. Fontecchio, "Image analysis to study lc alignment on patterned substrates," *Molecular Crystals and Liquid Crystals*, vol. 438, pp. 291, 2005.

[138] Hemang J. Shah, David Delaine, and Adam K. Fontecchio, "Tailored liquid crystal alignment using ferroelectric polymers," *Journal of Society for Information Display*, vol. 15 (8), pp. 579, 2007.

[139] H. J. Shah, A. K. Fontecchio, M. P. Rossi, D. Mattia, and Y. Gogotsi, "Imaging of liquid crystals confined in carbon nanopipes," *Applied Physics Letters*, vol. 89, no. 4, pp. 043123, 2006.

Vita

Hemang J. Shah

Education

Ph.D. Electrical Engineering, Drexel University, Philadelphia, PA, USA, 2007
M.S. Electrical/Telecom Engineering, Drexel University, Philadelphia, PA, USA, 2004
B.E. Electronics and Telecommunications Engineering, University of Mumbai, Mumbai, India, 2002
Diploma Electronics and Telecommunications Engineering, Board of Technical Education, Mumbai, India, 2002

Professional Experience

- **PhD Research Fellow**, Drexel University, 09/2002 - 09/2007
- **Graduate Teaching Assistant**, Drexel University, 09/2003 - 09/2007
- **Graduate Fellow**, National Institute of Standards and Technology, 06/2003 - 09/2003

Awards

1. Chairmans Fund - Grant for the Gordon Research Conference on Liquid Crystals, 2007
2. Research Excellence Award, Drexel University, 2007
3. George Hill, Jr. Fellowship by the College of Engineering - Drexel University 2005
4. Sigma Xi Societys Grants-in-Aid of Research Award, 2004

Selected Publications

1. H. J. Shah, D. Delaine, and A. K. Fontecchio, "Plasma Modification of Fluoropolymers for Aligning Liquid Crystals," *accepted for IEEE/OSA Journal of Display Technology*.
2. H. J. Shah, D. Delaine, and A. K. Fontecchio, "Tailored Liquid Crystal Alignment using Ferroelectric Polymers," *Journal of the Society for Information Display* **15**, 579 (2007).
3. H. J. Shah, M. P. Rossi, D. Mattia, Y. Gogotsi, and A. K. Fontecchio, "Imaging of Liquid Crystals Confined in Carbon Nanopipes," *Applied Physics Letters* **89**, 043123 (2006).
4. H. J. Shah and A. K. Fontecchio, "Low-Voltage Color Switching in Liquid Crystal Displays," *IDRC 2006 Digest Society for Information Display* **P-27** (2006).
5. H. J. Shah and A. K. Fontecchio, "Influence of Ferroelectric Polymer Layers on Liquid Crystal Alignment," *Preprints of the Polymer Materials Science and Engineering Division - American Chemical Society* **93** (2005).
6. H. J. Shah, M. L. Ermold, and A. K. Fontecchio, "Image Analysis to Study LC alignment on Nanopatterned Substrates," *Molecular Crystals and Liquid Crystals* **438**, 1855 (2005).
7. H. J. Shah and A. K. Fontecchio, "Modeling and Experimental Studies of LC Alignment Induced by Nanopatterned Substrates," *The International Symposium on Optical Science and Technology: SPIE's 49th Annual Meeting Proceedings* **Section 5518**, 1855 (2004).
8. H. J. Shah and A. K. Fontecchio, "Nano-patterned Polymer Structures for H-PDLCs," *The International Symposium on Optical Science and Technology: SPIE's 48th Annual Meeting Proceedings* **Section 5525**, 1855 (2003).